

# Fractal superconductivity near localization threshold

M. V. Feigel'man<sup>a,b</sup>, L. B. Ioffe<sup>c,d,a</sup>, V. E. Kravtsov<sup>e,a</sup>, E. Cuevas<sup>f</sup>

<sup>a</sup>*L. D. Landau Institute for Theoretical Physics, Kosygin st. 2, Moscow 119334, Russia*

<sup>b</sup>*Moscow Institute of Physics and Technology, Moscow 141700, Russia*

<sup>c</sup>*Department of Physics and Astronomy, Rutgers University, Piscataway, NJ 08854, USA*

<sup>d</sup>*CNRS and Université Paris-Sud, UMR 8626, LPTMS, Orsay Cedex, F-91405 FRANCE*

<sup>e</sup>*Abdus Salam International Center for Theoretical Physics, Trieste, Italy*

<sup>f</sup>*Departamento de Física, Universidad de Murcia, E-30071 Murcia, Spain*

---

## Abstract

We develop a semi-quantitative theory of electron pairing and resulting superconductivity in bulk "poor conductors" in which Fermi energy  $E_F$  is located in the region of localized states not so far from the Anderson mobility edge  $E_c$ . We assume attractive interaction between electrons near the Fermi surface. We review the existing theories and experimental data and argue that a large class of disordered films is described by this model.

Our theoretical analysis is based on analytical treatment of pairing correlations, described in the basis of the exact single-particle eigenstates of the 3D Anderson model, which we combine with numerical data on eigenfunction correlations. Fractal nature of critical wavefunction's correlations is shown to be crucial for the physics of these systems.

We identify three distinct phases: 'critical' superconductive state formed at  $E_F = E_c$ , superconducting state with a strong pseudogap, realized due to pairing of weakly localized electrons and insulating state realized at  $E_F$  still deeper inside localized band. The 'critical' superconducting phase is characterized by the enhancement of the transition temperature with respect to BCS result, by the inhomogeneous spatial distribution of superconductive order parameter and local density of states. The major new feature of the pseudo-gaped state is the presence of two independent energy scales: superconducting gap  $\Delta$ , that is due to many-body correlations and a new "pseudogap" energy scale  $\Delta_P$  which characterizes typical binding energy of localized electron pairs and leads to the insulating behavior of the resistivity as a function of temperature above superconductive  $T_c$ . Two gap nature of the pseudogapped superconductor is shown to lead to specific features seen in scanning tunneling spectroscopy and point-contact Andreev spectroscopy. We predict that pseudogaped superconducting state demonstrates anomalous behavior of the optical spectral weight. The insulating state is realized due to presence of local pairing gap but without superconducting correlations; it is characterized by a hard insulating gap in the density of single electrons and by purely activated low-temperature resistivity  $\ln R(T) \sim 1/T$ .

Based on these results we propose a new "pseudospin" scenario of superconductor-insulator transition and argue that it is realized in a particular class of disordered superconducting films. We conclude by the discussion of the experimental predictions of the theory and the theoretical issues that remain unsolved.

**Keywords:** Superconductivity, Disorder Superconductor-Insulator transition,

## Contents

<b>1</b>	<b>Introduction</b>	<b>3</b>
1.1	Theoretical models . . . . .	4
1.1.1	Coulomb blockade versus Superconductivity in Josephson junction arrays. . . . .	5
1.1.2	Coulomb suppression of $T_c$ in uniformly disordered thin films. . .	7
1.1.3	Localization versus Superconductivity. . . . .	9
1.2	Experimental results on S-I transitions. . . . .	10
1.3	Main features of the fractal pseudospin scenario. . . . .	16
<b>2</b>	<b>Model</b>	<b>17</b>
2.1	BCS Hamiltonian for electrons in localized eigenstates. . . . .	17
2.1.1	Ultra-small metallic grain. . . . .	18
2.1.2	Vicinity of the mobility edge. . . . .	19
2.2	Fractality and correlations of the wave functions near the mobility edge. . .	21
2.2.1	Wavefunction correlations at the mobility edge: algebra of multifractal states. . . . .	22
2.2.2	Scaling estimates for matrix elements: mobility edge. . . . .	26
2.2.3	Scaling estimates for matrix elements: multifractal insulator. . . .	33
2.2.4	Scaling estimates for matrix elements: multifractal metal. . . . .	34
2.2.5	Matrix elements of the off-critical states beyond the multifractal frequency domain. . . . .	35
<b>3</b>	<b>Insulating state.</b>	<b>37</b>
<b>4</b>	<b>Cooper instability near the mobility edge: the formalism.</b>	<b>44</b>
4.1	Modified mean-field approximation. . . . .	45
4.2	Ginzburg - Landau functional. . . . .	49
4.2.1	Transition temperature: coefficient $a(T)$ . . . . .	51
4.2.2	Quartic term: coefficient $b$ . . . . .	52
4.2.3	Gradient term: coefficient $C$ . . . . .	53
4.2.4	Mesoscopic fluctuations: coefficient $W$ . . . . .	56
4.2.5	Ginzburg parameters for thermal and mesoscopic fluctuations . .	58
4.3	Pseudo-spin Hamiltonian. . . . .	59
4.4	Virial expansion method. . . . .	60

---

*Email address:* feigel@landau.ac.ru (M. V. Feigel'man)

<b>5</b>	<b>Superconducting state very close to mobility edge.</b>	<b>64</b>
5.1	Pairing in the modified mean-field approximation. . . . .	64
5.2	Comparison of $T_c$ values obtained in three different approximations. . . .	66
5.3	Pairing amplitude in the real space . . . . .	67
5.4	Low-temperature density of states. . . . .	70
5.5	Superfluid density and critical current. . . . .	71
<b>6</b>	<b>Superconductivity with a pseudogap.</b>	<b>72</b>
6.1	Transition temperature and insulating gap as functions of Fermi energy.	72
6.2	Tunneling conductance. . . . .	80
6.2.1	Tunneling in a normal state. . . . .	80
6.2.2	Tunneling in a superconductor. . . . .	83
6.2.3	Point contact tunneling. . . . .	85
6.3	Andreev contact conductance at low temperatures. . . . .	89
6.4	Spectral weight of high-frequency conductivity and superconducting density. . . . .	91
<b>7</b>	<b>Summary of results and unsolved problems.</b>	<b>96</b>
<b>Appendix A</b>	<b>Virial expansion in pseudospin subspace</b>	<b>101</b>
<b>Appendix B</b>	<b>Virial expansion including single-occupied states</b>	<b>104</b>
Appendix B.1	One-orbital problem . . . . .	104
Appendix B.2	Two-orbital problem . . . . .	104
Appendix B.3	Three-orbital problem . . . . .	106

## 1. Introduction

The purpose of this paper is to develop the semi-quantitative extension of the BCS theory of superconductivity that describes strongly disordered conductors which normal state is a weak Anderson insulator [1] or a very poor metal. The paper focuses on the case of "uniformly disordered" materials, which do not contain morphological structures such as grains coupled by tunnel junctions. Below in this section we briefly review the existing theoretical models of the superconductor-insulator transition (SIT), compare them with the results of the experimental studies of the uniformly disordered films and choose the appropriate model for the superconductor-insulator transition in these materials. The conclusion of this introductory part is that this quantum transition in uniformly disordered films can be described by BCS pairing of electrons which single-particle states are close to the mobility edge of Anderson localization [1]. Because BCS pairing is most relevant for electrons close to the Fermi surface, the transition occurs when Fermi-level  $E_F$  is located in the region of localized single-electron states but close to the mobility edge. In the vicinity of the transition localization length is longer than typical distance between carriers while the relevant single electron states have the statistical properties of "critical wavefunctions". Section 2 formulates the model in more detail and discusses the issue of *wavefunction fractality*, which turns out to be very important for the theory of superconductor-insulator transition developed in this work.

The important difference between our approach and many other works on superconductor-insulator transition is neglect of the effects of Coulomb interaction but consistent treatment of moderately strong disorder. In this respect our work is the extension of the approaches developed originally by Ma and Lee [2], Kapitulnik and Kotliar [3], Bulaevskii and Sadovskii [4], and more recently by Ghosal, Trivedi and Randeria [5] that have considered competition of superconducting pairing and Anderson localization without explicit account for Coulomb interaction. We give detailed arguments which justify applicability of our approach to disordered films such as amorphous  $\text{InO}_x$  and  $\text{TiN}$  on both phenomenological and microscopic levels below in subsection 1.2. Briefly, one should distinguish two possible effects of the Coulomb interaction: suppression of pairing interaction between individual fermions which occurs at short scales and enhancement of the phase fluctuations of the order parameter at large scales. The first would lead to a gap suppression in a direct contradiction with data while the second would lead to the phenomenology similar to that of Josephson junction arrays which display markedly different behavior. Our theory can be also applied to the cold atoms in optical and magnetic lattices with a controlled disorder. In such systems interaction is always attractive and effectively short-range. Moreover, it is tunable by magnetic field due to the Feshbach resonance [6] which would allow to test directly the detailed predictions of the developed theory.

The important consequence of the wave function fractality is the formation of the strongly bound electron pairs which survive deep in the insulating regime. In this situation the pairing interaction reduces the mobility of individual electrons leading to "superconductivity-induced" insulator. We discuss this behavior in section 3. Theory of Cooper pairing of electrons populating critical fractal states is developed in section 4. Here we develop three different approximations for the computation of the superconducting transition temperature and other properties. Section 5 gives the physical properties of the superconductor in this regime. We show that three different approximations developed in section 4 agree with each other and predict parametrically strong enhancement of  $T_c$  with respect to its value given by the "Anderson theorem". Another distinguishing feature of the emerging superconducting state is extremely strong spatial inhomogeneity of superconducting order parameter and the presence of a well-defined global  $T_c$ .

Section 6 presents the theory of superconductivity coexisting with a strong pseudogap. Here we show that superconductivity survives when  $E_F$  is located much deeper in the localized band than it was previously expected. In this regime the superconductivity develops against the background of the pseudogap and, thus, is characterized by a number of unconventional properties. We present the specific results for the tunneling density of states and tunneling conductance, Andreev point-contact conductance, and spectral weight of high-frequency conductivity in this pseudogap superconductive state. Finally, section 7 reviews the main results and discusses a number of open problems. The Appendices present technical details of virial expansion that was used as the one of methods for the determination of  $T_c$ .

### 1.1. Theoretical models

Quantum phase transitions from superconducting to insulating state in disordered conductors and artificial structures were studied intensively since mid-1980s, for review see e.g. [7, 8, 9]. A number of theoretical models describing such transitions were proposed and studied but a fully coherent theoretical picture of this phenomena has

not been established. We believe that such transitions might be driven by different mechanisms in different materials and thus belong to different universality classes which should be described by different models. Below in this section we briefly review the alternative mechanisms and the theoretical methods employed for their description (see also short review [10]). To avoid confusion, we note that the first and the second of the mechanisms described below will not be studied in the main part of our paper. We describe them in some detail mostly because we need these details in order to argue below in this section that they are not relevant for the superconductor-insulator transition in homogeneous amorphous films.

#### 1.1.1. Coulomb blockade versus Superconductivity in Josephson junction arrays.

Macroscopic conductor that looks homogeneous at a macroscopic scale might be in fact composed of small grains or islands of a good superconducting metal with transition temperature  $T_{c0}$ . These grains are coupled to each other via low-transparency insulating tunnel barriers [7, 9], characterized by dimensionless tunnel conductances  $G_{ij} = h/(2e)^2 R_{ij}$ . The transition is due to the competition of the charging and Josephson energies. Exactly the same physics is realized in the artificial Josephson junction arrays, the only difference between the inhomogeneous films and artificial array is that the number of neighbors and of plaquette areas in the former are random. The simplest model describing this physics is given by effective Hamiltonian written in terms of phases  $\phi_j$  and charges  $Q_j$  assigned to grains:

$$H_1 = \frac{(2e)^2}{2} \sum_{ij} C_{ij}^{-1} N_i N_j - \sum_{ij} E_J^{ij} \cos(\phi_i - \phi_j) \quad (1)$$

where  $N_j = Q_j/2e$  is the number of Cooper pairs on the  $j$ -th grain,  $C_{ij}$  is the matrix of mutual capacitances, and  $E_J^{ij}$  is the Josephson coupling energy, correspondingly. The model is often further simplified by assuming that  $E_J^{ij} = E_J$  is a non-zero constant only for nearest-neighboring grains while the capacitance matrix is diagonal,  $C_{ij} = C_0 \delta_{ij}$ . This model neglects the effects of the quasiparticles which might be (sometimes) justified for small grains at low temperatures  $T \ll T_{c0}$ , due to exponentially small density of normal electrons. The key parameter of the problem is the energy ratio  $x = E_J/E_C$  where  $E_C = (2e)^2/2C_0$  is the Coulomb charging energy due to  $2e$  charge transfer. As was shown in the paper [11] the ground-state of the Hamiltonian (1) is insulating at  $x \ll 1$  and superconducting at  $x \gg 1$ , thus a phase transition(s) takes place at  $x \sim 1$ . An essence of this phase transition is the Mott-Hubbard localization of Cooper pairs, taking place when tunneling matrix element of a pair ( $E_J$ ) is much less than on-site repulsion  $E_C$ .

However, the model (1) is unlikely to describe correctly the physics of superconductor-insulator transition in Josephson arrays or granular materials, especially in its simplified version with diagonal capacitance matrix. It has two important deficiencies.

First, realistic Josephson junction arrays and disordered films are poorly described by the model of diagonal capacitance matrix  $C_{ij} = C_0 \delta_{ij}$  because normally the charging effects are controlled by capacitances of junctions  $C \gg C_0$ , not by the ground capacitances of the islands (see Ref. [9]). It is in fact impossible to have a capacitance matrix dominated by the ground capacitance in the arrays which dimensionless normal state conductance is  $G = h/[(2e)^2 R_T] \gtrsim 1$  because in these arrays the capacitance of the

junctions cannot be small. The reason for this is that apart from purely geometrical contribution  $C_{\text{geom}} = 4\pi S/d$ , junction capacitance  $C = C^{\text{geom}} + C^{\text{ind}}$  contains additional induced term  $C_{\text{ind}} = \frac{3}{16}Ge^2/\Delta$ , (this expression is valid at  $T \ll \Delta$ ). This induced contribution is due to virtual electron transition across the gap [12, 13]. As a result, the charging energy can not be made arbitrary large (equivalently capacitance cannot be small):  $E_C \leq 32\Delta/3G$ . Josephson energy of the symmetric junction at low temperatures is  $E_J = G\Delta/2$ , thus the condition  $E_C \geq E_J$  cannot be realized at large  $G$ . Furthermore, at temperatures above the parity effect threshold  $T^*$ , (see [14]) an additional contribution to the screening of Coulomb interaction between Cooper pairs comes from single-electron tunneling. Thus, in all cases the effect of capacitance renormalization is that the ratio  $x = E_J/E_C$  in granular arrays is controlled by the dimensionless conductance  $G$  in such a way that Coulomb effects are always weak at  $G \geq 1$ . Ground capacitance larger than the junction capacitance thus implies that the transition into the insulating state would occur in the arrays characterized by very small  $G \ll 1$ . Such behavior was never observed experimentally in Josephson arrays (see section 1.2).

More realistic model involves the capacitance matrix that is dominated by the junctions capacitances with a small contribution from the ground capacitance of each grain. In this case the arguments of preceding paragraph show that the transition between the insulating and superconducting state should occur at  $G_c \sim 1$ . [15] Moreover, deep in the insulating phase the electrostatic interaction between the charges in 2D Josephson array becomes logarithmic in distance, similar to the one between the vortices in the superconducting phase. Assumption of the full duality between vortices in the superconducting state and charges in the insulating state allows one to make a number of predictions. [16, 17] For instance, because the current of vortices generates voltage while the current of pairs implies the electrical current one expects that superconducting-insulator transition is characterized by the universal value of  $G_c = 1$ . [17]

Unfortunately, despite a significant experimental effort the universal value of the resistance was never experimentally confirmed for Josephson arrays and for most disordered films. Moreover, in non-zero magnetic field the Josephson arrays often show a large regime of the temperature-independent resistance. The reason for this is likely to be due to the important physical effects missed by the model (1), namely the presence of random induced charge on the superconducting islands. As was shown in a number of Josephson junction studies (see e.g. [18]) the induced charge on each island exhibits very slow random fluctuations and is therefore inherently random variable. Most likely the time dependence of these fluctuations can be neglected and the induced charge can be regarded as a quenched random variable  $q_i$  that should be added to the Hamiltonian (1):

$$H_1 = \frac{(2e)^2}{2} \sum_{ij} C_{ij}^{-1} (N_i - q_i)(N_j - q_j) - \sum_{ij} E_J^{ij} \cos(\phi_i - \phi_j) \quad (2)$$

The properties of the model (2) are not currently well understood; in particular, it seems likely (see [19]) but was not proven that insulating state has many glassy features responsible for intermediate 'normal' phase. It is, however, clear that in this model the transition, or a series of transitions occurs at  $E_J/E_C \sim 1$ , which corresponds to  $G \sim 1$  in the normal state. Near the critical point the gapless excitations correspond to collective modes build of electron pairs while the electron spectrum remains fully

gapped. In analogy with spin glasses, one expects that effective frustration introduced by random charges and magnetic field leads to a large density of low energy states. This might explain the observed temperature independent resistance that varies at least by one order of magnitude around  $G \sim 1$  as a function of magnetic field.[9]

As we show in section 1.2 both the data and theoretical expectations for models (1,2) differ markedly from the behavior of the homogeneously disordered films.

A spectacular property of the superconductor-insulator transition in granular materials is that a strong magnetic field applied to the system in the insulating regime results in a dramatic increase of the conductance. Qualitatively, the reason for this behavior in granular systems is that in the absence of the field the single electron excitations are absent due to superconducting gap while pairs are localized due to Coulomb energy and random induced charges. Large field suppresses superconducting gap, which allows transport by individual electrons that is characterized by a much larger tunneling amplitude and lower (by a factor of four) effective charging energy. This effect was reported by [20] where strong magnetic field was applied to Al grains immersed into Ge insulating matrix and giant negative magneto-resistance was observed. Similar behavior was reported for homogeneous films of InO deep in the insulating regime[21]. This similarity indicates that the main reason for this effect, which is that the pairing of the electrons survives deep in the insulating state, also holds for homogeneous films of InO. The quantitative theory of negative magnetoresistance in granular superconductors was developed in [22] for the case of relatively large inter-grain conductances  $G_{ij} \approx G \gg 1$ , in which case the negative magnetoresistance effect is small as  $1/G$ . Recent review of theoretical results on normal and superconductive granular systems can be found in [23].

#### 1.1.2. Coulomb suppression of $T_c$ in uniformly disordered thin films.

The scenario described above assumes that superconductivity remains intact inside each grain. An alternative mechanism for the suppression of superconductivity by Coulomb repulsion was developed by Finkelstein [24, 8], building upon earlier perturbative calculations [25]. Finkelstein effect becomes important for very thin strongly but homogeneously disordered films, as well as quasi-1D wires made out of such films [26]. Contrary to the Coulomb blockade scenario, the system is supposed to be "uniformly disordered", with no superstructures such as grains coupled together by weak junctions. Somewhat similar idea was proposed [27, 28] for three-dimensional materials near the localization threshold. The essence of Finkelstein effect is that Coulomb repulsion between electrons gets enhanced due to slow diffusion of electrons in highly disordered film, which results in the *negative* contribution to the effective Cooper attraction amplitude at small energy transfer  $\varepsilon$ :

$$\lambda(\varepsilon) = \lambda_0 - \frac{1}{12\pi g} \ln \frac{1}{\varepsilon\tau_*} \quad (3)$$

where  $g = h/(2e)^2 R_\square$  is dimensionless film conductance,  $\lambda_0$  is the "bare" Cooper attraction constant defined at the scale of Debye frequency  $\omega_D$ , and  $\tau_* = \max \tau, \tau(b/l)^2$ , where  $\tau$  and  $l = v_F \tau$  are the mean scattering time and mean free path, and  $b$  is the film thickness. The suppression of attraction constant Eq.(3) leads immediately (we assume here  $\omega_D \sim 1/\tau_*$ ) to the result obtained early on in the leading order of the perturbation theory [25]

$$\frac{\delta T_c}{T_c} = \frac{\delta \lambda}{\lambda^2} = -\frac{1}{12\pi g} \ln^3 \frac{1}{T_{c0}\tau_*} \quad (4)$$



The leading terms in the perturbation theory for  $T_c$  can be summed by means of the renormalization group method developed in [24]. In the leading order over  $1/g \ll 1$  one gets

$$\frac{T_c \tau_*)}{\hbar} = \left[ \frac{\sqrt{8\pi g} - \ln(\hbar/T_{c0}\tau_*)}{\sqrt{8\pi g} + \ln(\hbar/T_{c0}\tau_*)} \right]^{\sqrt{2\pi g}}, \quad (5)$$

According to Eq. (5),  $T_c$  vanishes at the critical conductance  $g_{cF} = \ln^2(\hbar/T_{c0}\tau_*)/(8\pi)$ , (which needs to be large enough for the theory to be self-consistent). At lower (but still large compared to unity) conductances, the material never becomes superconducting; it stays metallic at least down to very low temperatures  $T_{loc} \sim (\hbar/\tau_*) \exp(-4\pi g)$  where weak localization crosses over into the strong localization [29].

This mechanism of superconductivity suppression, described by Eq.(5), might be called "fermionic", as opposed to the "bosonic" mechanism discussed in previous subsection [10]. Within this mechanism, superconductivity is destroyed at relatively large conductances  $g_{cF} \geq 1$ , thus a *direct* superconductor-insulator transition does not seem to be a natural option.

The theory of the superconducting-insulator transition outlined above neglects the mesoscopic fluctuations of the interaction constant,  $g(\mathbf{r})$ . This assumption was questioned on phenomenological grounds by Kowal and Ovadyahu [30]. The role of these fluctuations become larger when superconductivity is strongly suppressed because as follows from (3), in this regime even small mesoscopic fluctuations of  $g(\mathbf{r})$  lead to a large spatial fluctuations of the effective coupling constant  $\lambda(\varepsilon, \mathbf{r})$ . In its turn, the fluctuations of the effective coupling lead to the local spatial fluctuations of the transition temperature  $T_c(\mathbf{r})$ , which becomes very strong,  $\delta T_c/\bar{T}_c \geq 1$ , for nearly-critical conductance  $g \approx g_{cF}$ , as shown in Ref. [31]. Note that mesoscopic fluctuations of  $T_c$  remain small in the universal case of short range disorder if Coulomb suppression of superconductivity is not taken into account, even in the vicinity of the upper critical field  $H_{c2}(0)$  at very low temperatures. [32, 33]

These results demonstrate the inherent inhomogeneity of superconducting state near the critical point at which it is destroyed by disorder. Thus, it seems likely that the regime close to the superconductor-insulator transition is described by the effective model of superconducting islands (appeared due to spatial fluctuations of local attraction constant) coupled by weak SNS junctions. The theoretically consistent description of this physics is still lacking, the difficulty can be traced to the absence of tunnel barriers separating fluctuation-induced superconducting islands from the surrounding media. In the absence of these barriers charging effects become non-local which makes the determination of the effective Coulomb energy a nontrivial problem, furthermore the presence of a large normal part implies dissipative (non-local in time) dynamics of the superconducting phase. A toy model of this type was solved in [34]; this model describes artificial superconductive islands in a good contact with disordered thin film.

In conclusion, in the fermionic mechanism the Coulomb interaction is enhanced by disorder leading to the suppression of superconductivity. The state formed when the superconductivity is suppressed is likely to be a poor metal characterized by a large resistivity and finite density of states at the Fermi level.



### 1.1.3. Localization versus Superconductivity.

The third alternative mechanism for the superconductor-insulator transition is due to the localization of single electrons. In this scenario the effects of Coulomb interaction are neglected, whereas local (in space) Cooper attraction is treated within standard BCS approximation. Here we focus on the case of bulk disordered materials or sufficiently thick films in which localization remains a three dimensional effect. Abrikosov and Gor'kov [35] and Anderson [36] have shown that potential disorder does not affect thermodynamic properties of usual s-wave superconductors. More precisely, this statement (based upon the presence of time-reversal symmetry and called "Anderson theorem") means that the parameter  $T_c\tau/\hbar$  does not appear in BCS theory as long as magnetic field and/or supercurrent are absent. However, localization of single-electron eigenstates at very strong disorder leads to appearance of an additional energy scale  $\delta_L = 1/\nu_0 L^3$ , where  $L$  is the single-electron localization length and  $\nu_0$  is the density of states (per single spin projection). The meaning of  $\delta_L$  is just average level spacing inside typical volume where wavefunction is localized. One expects that at large  $\delta_L$  the superconducting pairing between electrons is suppressed. Competition between superconductivity and Anderson localization was studied originally in mid-80's [2, 4, 3]. Their major conclusion was that Anderson theorem is valid and superconductivity survives provided that the condition

$$T_c \gg \delta_L \quad (6)$$

is satisfied. The reasoning leading to Eq.(6) is that for Cooper instability to develop, characteristic energy spacing between hybridized Cooper pairs (which are supposed to be localized in the same region of size  $L$ ) should be smaller than typical energy scale  $T_c$  corresponding to the Cooper instability. On the contrary, no superconducting long-range pairing seems possible when level spacing  $\delta_L$  strongly exceeds  $T_c$ , in spite of the presence of inter-electron attraction (we assume that Cooper attraction survives when the single electron states are localized as long as  $\delta_L$  is much smaller than Debye energy  $\omega_D$ ).

We will show below that the analysis presented in [2, 4, 3] is not complete in two important respects. First, the absence of long-range superconductive order does not necessarily mean that Cooper pairing is totally negligible; we will show that in the range  $T_c \ll \delta_L \ll \omega_D$  Cooper correlations leads to formation of the hard-gap insulator instead of usual variable-range one. This gap is of the same origin as the "parity gap" studied by Matveev and Larkin [37] in the context of ultra-small grains of good superconductive metal. Second, the notion of *eigenfunction fractality* (that was not known when the theory [2, 4, 3] was developed) has to be taken into account and leads to important physical consequences. In the present paper we are going to fill both these gaps; it will be shown that fractality of electron eigenfunctions changes qualitative features of superconductive state, and even modifies the condition  $\delta_L \approx T_c$  for the critical region where superconductivity is finally destroyed.

More recently the issue of competition between localization and superconductivity was reconsidered in the important paper by Ghosal, Trivedi and Randeria [5]. They considered two-dimensional lattice model of superconductivity with moderately strong local attraction (negative-U Hubbard model) and on-site disorder and studied it numerically by two methods: by solving the self-consistent Bogolyubov-de Gennes equations, and by solving BCS pairing equations in the basis of exact single-electron eigenstates. They demonstrated that with increase of local disorder superconducting state is transformed

into the insulating one. The latter possesses sharp gap in the density of states but does not show coherence peaks. The energy gap was found to be non-monotonic as function of the disorder strength. It was also shown that superconductivity is very inhomogeneous in the crossover region, with disorder-generated "islands" of large pairing amplitude. We will see below that qualitative features of the results obtained in Ref. [5] are very robust and survive in a continuum weak-coupling BCS model that we consider in the present paper (see section 2). The drawback of the treatment developed in Ref. [5] is that it does not allow the quantitative analysis of the physical properties as function of main parameters of the problem (coupling strength  $\lambda \ll 1$  and proximity of the Fermi-energy to the localization edge,  $|E_F - E_c| \ll E_F$ ), due to limitations imposed by purely numerical methods. A major drawback of most conventional numerical methods is their inability to study the regime characterized by dramatically different energy scales, in particular  $T_c \ll E_F$ . Development of the method to study this regime is the goal of the present paper.

The importance of the analytical treatment of the weak coupling regime  $T_c \ll E_F$  is demonstrated in particular, by the numerical work [38] which has studied the 3D disordered Hubbard model with strong local attraction (4 times larger than bandwidth). In this regime the electrons are strongly bound to each other even in translationally invariant systems. One expects that the mobility of the formed pairs is less than the mobility of the original electrons; this enhances the effect of the disorder. This expectation is conformed by the data [38]. We show that in the physically relevant regime of *weak* attraction, the situation is opposite: the superconductivity survives deep in the regime of localized states.

### 1.2. Experimental results on S-I transitions.

Phenomenologically one should distinguish at least three types of materials that display superconductivity suppression with the increase of the disorder: granular systems [20, 39], nominally homogeneous films that exhibit superconductor-metal-insulator transition and homogeneous films that show direct superconductor-insulator transition. [40] We shall discuss only the latter class in this paper, the materials that exhibit it are thick (more than 20 nm)  $\text{InO}_x$  films, thinner (around 4nm) TiN films and very thin (few atomic layers) Be films. Recent work reports similar behavior also in disordered epitaxial films of NbN with varying disorder [41]. The goal of this section is twofold: to discuss the data that allow to exclude Coulomb mechanisms (both fermionic and bosonic) of the superconductor-insulator transition in these films and to briefly summarize the data on these films that need theoretical explanation. We begin with the first.

The most direct experimental evidence that allows to exclude the 'fermionic' mechanism of superconductivity suppression discussed in section 1.1.2 in homogeneously disordered films that exhibit direct superconductor-insulator transition comes from the recent tunneling data. In these experiments one observed that the suppression of the superconductivity either by disorder or temperature is *not* accompanied by the suppression of the gap, which remains intact or even increases reaching  $2\Delta_1/T_c \in 6 - 9$ . [42] Instead, as the insulator is approached, one observes the disappearance of the local coherence peaks which, in addition, vary strongly from one point to another ( see also Ref. [43]) . This behavior (and especially the temperature dependence of tunnelling conductance) is in a striking contrast to what is expected for the fermionic mechanism. Less direct evidence is provided by the data [44, 45] showing that superconductivity exists up to a very strong

disorder corresponding to  $g \approx 1$ , which is at least a factor of two smaller than the one expected in the fermionic mechanism (5).

As explained in section 1.1.2 the basis of the fermionic mechanism is the idea that Coulomb repulsion is enhanced by disorder which results in the effective suppression of the attractive interaction that leads to superconductivity. The actual equations are derived in the assumption that bare Coulomb repulsion is very strong but is reduced by screening to the universal limit in which the effective Coulomb repulsion constant is equal to unity. The dimensionless parameter characterizing the strength of the Coulomb interaction and its screening is  $2\sigma/(T_c\kappa)$ , where  $\sigma = (e^2k_F/6\pi^2)(k_Fl)$  is the residual conductivity and  $\kappa$  is the dielectric constant due to electrons far from the Fermi energy ( $|E - E_F| > \omega_D$ ). Coulomb interaction is effectively strong provided that  $2\sigma/(T_c\kappa) \sim (\xi_0/a_{\text{scr}})^2/\kappa \gg 1$ , where  $a_{\text{scr}}$  is the Thomas-Fermi screening length,  $\xi_0$  is the coherence length in a dirty superconductor. If instead  $2\sigma/(T_c\kappa) \ll 1$  the coefficient in front of the logarithm in (3,5) becomes small so that enhancement of Coulomb repulsion become important only at exponentially low energy scales. In a very dirty metal (such  $\text{InO}_x$  film) with a short mean free path  $k_Fl \sim 0.3$  and low carrier density  $e^2k_F \sim 5000K$  (see Ref.[46]) the ratio  $\sigma/T_c \sim 10$ . Thus, the effects of Coulomb interaction in these films become unimportant if dielectric constant  $\kappa \gg 10$ . The direct measurements of the dielectric constant deep in the insulator regime give  $\kappa \geq 30$  [47], one expects that it can be only larger in the vicinity of superconductor-insulator transition, so  $2\sigma/(T_c\kappa) \ll 1$  in these films which makes the fermionic mechanism irrelevant.

The microscopic origin of this large dielectric constant is likely to be due to the low density of the carriers,  $n_e \sim 10^{21}\text{cm}^{-3}$  in these conductors, and the peculiar structure of their density of states in which the Fermi level is located in a large dip.[48]. In this situation the density of the electrons distant from the Fermi level,  $|E - E_F| > \omega_D$ , is high, which results in a large screening of the Coulomb interaction.

Now we turn to the possibility of the Coulomb driven transition similar to the one of Josephson arrays (section 1.1.1). This physics is due to the long range nature of the Coulomb interaction; the estimates of the associated energy scales given below show that Coulomb interaction is sufficiently well screened even in poor conductors so that the corresponding energy is too small compared with all other energy scales; this rules out this possibility. These arguments are quite general and apply to other effects that originate from the long range part of the Coulomb interaction.

We begin with energy scales that are known to be relevant experimentally for this problem. Namely, the superconducting gap on the ordered side and activation energy on the insulating side. These energies are large: the superconducting gap is around  $\Delta \sim 5K$  while the activation gap is even larger  $T_0 \sim 10 - 15K$  (see below). We now estimate the Coulomb interaction at the scale of the superconducting coherence length,  $\xi_0$ . Because  $T_c/E_F \lesssim 10^{-3}$  in these materials, this length, even for a very poor conductor, cannot be too short:  $\xi_0 \gtrsim 10\text{nm}$ . Large value of the dielectric constant in the parent insulating compounds,  $\kappa \geq 30$ , implies that in the absence of the mobile electrons with  $|E - E_F| < \omega_D$ , the effective charging energy at scales  $\xi_0$  would be  $E_{c0} = e^2/\kappa\xi_0 \lesssim 50 K$ . Screening by conduction electrons with energies  $T_c < |E - E_F| < \omega_D$  decreases it further. To estimate this effect we note that at scales less than  $\xi_0$  the properties of the electrons are similar to those at the mobility threshold. At the threshold, the dielectric constant grows with scale,  $L$ , according to the scaling law  $(L/l)^x$  with  $x \gtrsim 1$ . This results in the additional factor  $(l/\xi_0)^x$  in the effective Coulomb energy at scales  $\xi_0$  which reduces it to

$E_c \lesssim 1K$ . Thus, the effective Coulomb energy is much smaller than all relevant energy scales and cannot be the driving force of the transition. Note that this estimate becomes incorrect in the presence of thin insulating barriers between the grains, thus allowing for Coulomb driven transition in inhomogeneous materials. The absence of structural inhomogeneities that might lead to such barriers in films of  $\text{InO}_x$  was shown in [30]; later studies [49] also reported the absence of inhomogeneities in TiN films.

Another argument against Coulomb driven transition is provided by a completely different phenomenology of the transition in the films and in Josephson arrays: in the former one observes direct transition to the insulating state characterized by a large gap and activation behavior of resistivity, the transition can be driven either by the increase of disorder or by magnetic field. In contrast, in Josephson arrays the transition driven by the field is characterized by a large intermediate regime of temperature independent resistivity [9, 50]. Furthermore, there is no reason to expect the disappearance of coherence peaks in some places and not in others as one approaches the transition (reported in [42]) in the array of superconducting grains.

Finally, Coulomb mechanism cannot explain the large value of the activation energy in the insulating state in the vicinity of the transitions. One expects that when charging energy becomes large enough to suppress transport by Cooper pairs, single electrons should dominate transport which implies activation energy equal to superconducting gap. Instead one often observes large activation energies:  $T_0 \approx 15K$  in  $\text{InO}_x$  films (see Fig.1 of [21]) and even larger in Be ones [51].

We now summarize (see also the review [40]) the phenomenology of the direct superconductor-insulator transition in homogeneous films as exhibited by three different systems: thick amorphous  $\text{InO}_x$  films [46, 30, 21, 44, 52, 53], thin TiN films [54, 45, 55] and extra-thin (below 1 nm) Beryllium films [56, 51, 57]; somewhat similar phenomena were observed recently in the patterned Bi film with honeycomb array of holes [58].

1. On insulating side of SIT, low-temperature resistivity curves show simple activated behavior,  $R(T) \propto \exp(T_0/T)$ , which crosses over into Mott [30],  $R(T) \propto \exp(T_M/T)^{1/4}$ , or Efros-Shklovsky [45, 51],  $R(T) \propto \exp(T_{ES}/T)^{1/2}$  variable-range hopping *at higher* temperatures. This behavior is highly unusual: in hopping insulators where the activation is frequently observed at high temperatures it crosses over to some fractional (variable-range) behavior upon the temperature decrease.
2. At high magnetic fields the films on both sides of the SIT show large negative magnetoresistance [21, 44, 52, 53, 57, 55, 45]. It is important that such behavior was observed even in films characterized by a very high activation energy.
3. At low fields all insulating films close to SIT show positive magneto-resistance at low fields [21, 55, 45, 57, 59].
4. Ultra-low-temperature measurements on nearly-critical samples of a- $\text{InO}_x$  [52] and TiN [45] revealed a very sharp jump (by several orders of magnitude in current) in nonlinear  $I(V)$  curves.
5. The resistance of Be [57] and TiN films [55] approach the quantum resistance  $h/e^2$  at very strong magnetic fields and low temperatures. Very recently the importance of Zeeman pair-breaking for the properties in this regime was demonstrated in Ref. [60].
6. The properties of the quantum critical point that separates superconductor and insulator are not fully established. The samples corresponding to the critical disorder

which separates superconducting and insulating behavior display insulating behavior of the  $R(T)$ [61, 45, 51]; this suggests that the disorder driven superconductor-insulator transition is not described by a self-dual theory proposed in [16] or that the critical regime where this behavior sets in is very narrow. Weakly superconducting samples can be driven into insulating state by the application of magnetic field. Scaling (or a lack of thereof) near this quantum critical point is subject of controversy in both the value of the critical resistance and the scaling exponents. Some works[55, 61, 42] report critical value of the resistance larger than  $R_Q = 6.5k\Omega$  and exponents that do not agree with the theoretical predictions[17]. In contrast, recent paper[62] reports both the critical value of the resistance and exponent in a perfect agreement with the theoretical predictions based on dirty boson scenario[17].

These results can be summarized by the low temperature phase diagram in  $(H, G)$  plane sketched in Figure 1.

It is tempting to explain these observations by the scenario in which the disorder destroys the global superconducting coherence while preserving the local superconducting gap,  $\Delta$ , even in the insulating phase. Indeed, in the absence of pair coherence the conductivity is due to the thermally excited fermionic quasiparticles. The density of these excitations would be additionally suppressed by local superconductive gap  $\Delta$  that is formed at low temperatures:  $n_1(T) \sim \exp(-\Delta/T)$ . This would explain the crossover to activation behavior at low  $T$ . High magnetic field suppresses local  $\Delta(H)$  thus leading to very large negative magnetoresistance. Low-field positive magneto-resistance could be then associated with frustration induced by magnetic field which eliminates the last vestiges of superconducting coherence thereby shifting the array further into insulating side (whereas not yet affecting local superconducting gap).

This scenario would be naturally realized in the granular material where superconductivity remains intact in each grain whereas global coherence appears only due to Josephson coupling which competes with charging energy (see section 1.1.1) [63]. However, this assumption of hidden granularity of the SIT films is not plausible for many reasons explained above.

The correct theory should be also able to explain the large value of the activation energy on the insulating side of the transition. Assumption that it is due to the local superconducting gap in weakly coupled grains is not sufficient because this energy is higher than the gap in a less disordered film of the same series that shows superconductivity. Indeed, maximal observed values of  $T_0$  were about  $15K$  in work[21] and  $11K$  in work[30] which are significantly larger than maximal superconducting gap  $\Delta \approx 5K$  shown in Fig.1 of Ref. [46] (note that samples studied in [21] were from the same source as in [46, 30]). Furthermore, this assumption would lead to the conclusion that the transition is due to competition between Coulomb and Josephson energies which are both much smaller than  $T_0$ ; because  $E_J = G\Delta/2$  this would imply that  $G \ll 1$  in a direct contradiction with the data.

Large value of the activation energy, together with inefficiency of electron-phonon coupling at low  $T$  provides a natural explanation for a large jump in  $I(V)$  observed in the insulating state [64]. The detailed predictions of the theory [64] were recently verified experimentally in [65]. The important ingredient of this theory is a hard gap for single electron excitations, similar to the one directly observed in [42] and inferred

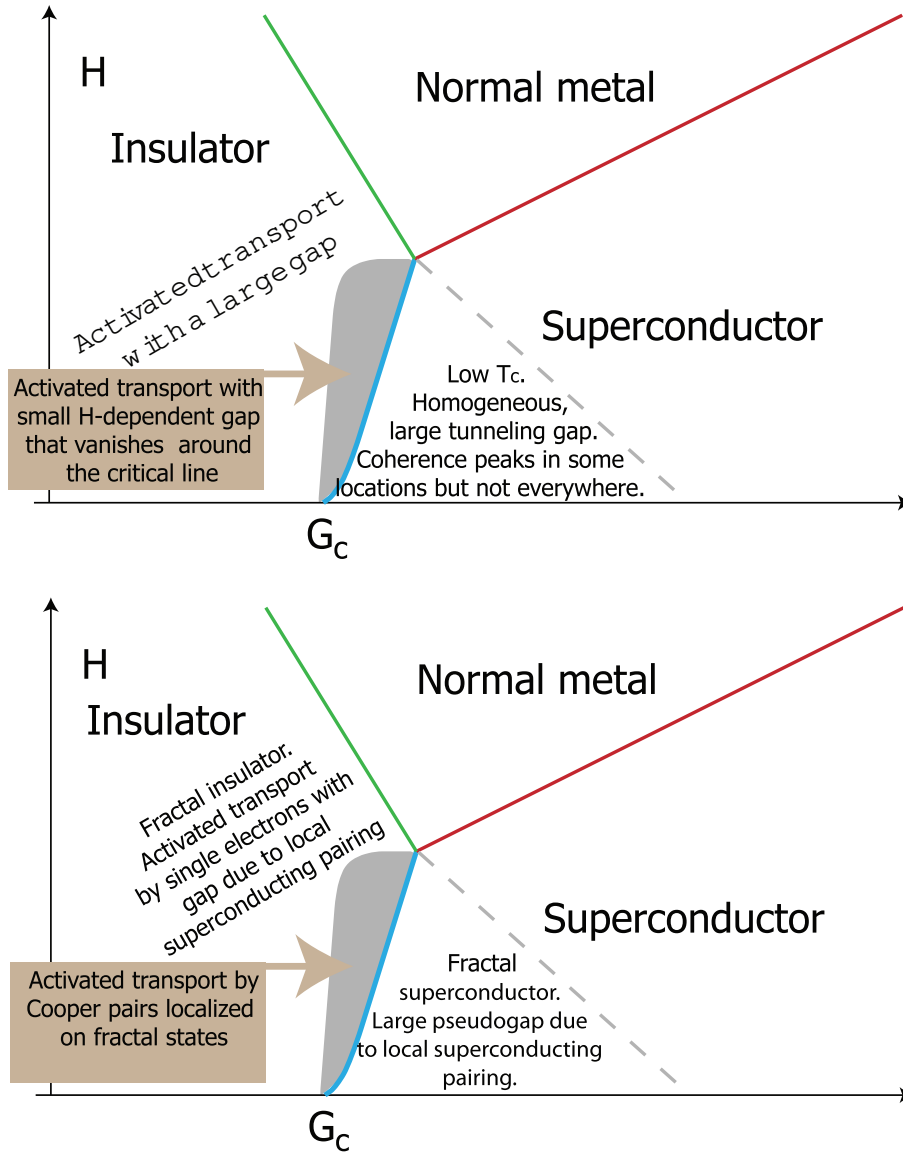


Figure 1: (Color online) Sketch of the experimental phase diagram of homogeneously disordered films (upper panel) at  $T \rightarrow 0$  and its interpretation in the theory of superconductivity developed in the electron system close to mobility edge (lower panel).

from the resistivity data. Thus, the phenomena of  $I(V)$  jumps does not impose additional constraints on microscopic theory. Moreover, very similar jumps were observed previously in the system which seems to have nothing to do with superconductivity [66].

Real challenge to the theory is presented by the magnetoresistance data from Ref.[21]: straightforward interpretation of the negative magnetoresistance data as being due to superconducting gap suppression in individual grains leads to unphysically large values of critical field needed to destroy the superconductivity in such grains. For instance, the field of 8 T was observed to produced only moderate (  $R(H = 8\text{T})/R(0) \approx 0.5$  ) negative magneto-resistance in a sample characterized by  $T_0 \approx 15\text{ K}$  (as determined in the temperature range 1.3–5 K). Interpreting this effect as being due to the suppression of the pairing gap, we find  $T_0 - T_0(H = 8\text{T}) \approx 0.7\text{ K}$ , which is about 5% of  $T_0$ . Interpolating this dependence we find that the field necessary to destroy completely the superconductivity in each grain is huge:  $H_{cg}^{\text{exp}} \sim 50 - 80\text{ T}$ .<sup>1</sup>

Such large values of the critical fields are impossible for realistic grain sizes. Indeed, critical orbital magnetic field for a small (radius  $R < \xi$ , where  $\xi = \sqrt{\hbar D/\Delta}$  is the coherence length) superconducting grain is [67, 22]

$$H_{cg}^{\text{est}} \approx \frac{1000\text{ T}}{R\xi}$$

where  $R$  and  $\xi$  are measured in nanometers. Using a typical diffusion constant for a poor metal  $D \approx 1\text{ cm}^2/\text{s}$  and allowing for a very high gap value  $\Delta = 10\text{ K}$ , we find  $\xi = 8.5\text{ nm}$ . Together with the lowest bound for the grain radius  $R = 6\text{ nm}$  in which the distance between the levels does not exceed the superconducting gap

$$\delta = (4\nu_0 R^3)^{-1} < \Delta$$

it leads to  $H_{cg}^{\text{est}} \lesssim 20\text{ Tesla}$  which is still much smaller than  $H_{cg}^{\text{exp}}$  above. These estimates did not take into account the spin effect of magnetic field that would further decrease the value of  $H_{cg}^{\text{est}}$ .

We conclude that the observed activation gap cannot be explained as BCS gap in small grains composing the material: it is too wide and too stable with respect to magnetic field.

A number of works argued that mesoscopic fluctuations might lead to the appearance of inhomogeneous superconductivity (self-induced granularity) in the vicinity of the transition even in the absence of structural granularity [30, 40, 45]. The direct computation shows that these speculations are correct for the fermionic mechanism of the superconductivity suppression in two dimensions [31]. We expect that the self-induced granularity that appears due to this mechanism does not lead to thin insulating barriers. It is therefore characterized by a small value of the Coulomb interaction between the 'grains'. Thus, it can be ruled out as a mechanism of direct superconductor-insulator transition in homogeneous films by the energy scale arguments given above.

An important unresolved issue is the nature of carriers responsible for the transport in the insulating state: are they Cooper pairs or single electrons? One expects that the presence of the superconducting gap in the insulating state implies that the transport is

---

<sup>1</sup>Data of Ref.[53] show that 32 Tesla field is not sufficient to fully suppress negative magnetoresistance.



dominated by Cooper pairs in the vicinity of the transition and this was indeed observed in ultrathin Bi films[68]. However, one expects that the transport is dominated by single electrons further in the insulating state where activation behavior was observed. Unfortunately there are no data to confirm this.

To summarize: experimental data on SIT in amorphous materials call for a new mechanism of a gap formation, which is somehow related to the superconductivity, but is different from the usual BCS gap formation. In the vicinity of SIT this mechanism should lead to a "pseudo-gap" features in  $R(T)$  behavior and tunneling data.

### 1.3. Main features of the fractal pseudospin scenario.

The fractal pseudospin mechanism (briefly presented in [69]) should be viewed as alternative to both 'boson' and 'fermion' scenarios. Here we argue that it is fully compatible with the data. The key elements of this approach are in fact quite old: (i) Anderson's reformulation [70] of the BCS theory in terms of "pseudo-spins", (ii) Matveev - Larkin theory [37] of parity gap in ultra-small superconducting grains and (iii) fractal properties of single-electron eigenfunctions with energies near the Anderson mobility edge [71, 72, 73].

Qualitatively, in this scenario the electrons near the mobility edge form strongly coupled but localized Cooper pairs (notion first introduced in [21, 61], see also [5]) due to the attraction of two electrons occupying the same localized orbital state. These pairs are characterized by a large binding energy which is responsible for the single electron gap  $T_0$  observed in transport measurement in the insulating state. At temperatures below  $T_0$  the system can be described as a collection of Anderson's  $S = \frac{1}{2}$  pseudo-spins, whose  $S_j^z$  components measure the Cooper pair occupation number and  $S_j^\pm$  components correspond to pair creation/annihilation operators. Superconductivity in this system is due to the tunneling of Cooper pairs from one state to another. It is essential that it competes not with the Coulomb repulsion but with the random energy of the pair on each orbital state. In spin language it is described as a formation of non-zero averages  $\langle S^\pm \rangle$  due to "off-diagonal"  $S_i^- S_j^+ + S_i^+ S_j^-$  coupling in the effective Hamiltonian which competes with random field in  $z$ -direction term  $h_i S_i^z$ . Large values of the binding energy and off-diagonal interactions are due to the properties of localized nearly-critical wavefunctions; the main features of these wavefunctions are their strong correlations both in real space and in energy space, and their sparsity in real space (see section 2.2). The resulting phase diagram is shown in Figure 1.

The fractal pseudospin scenario has many common features with the bosonic mechanism, but it is distinct from it in a few important respects:

- pseudo-gap energy scale  $T_0$  is independent from the collective energy gap  $\Delta$
- fractal nature of individual eigenstates implies a large "coordination number"  $Z \gg 1$  of interacting pseudospins away from the superconductor-insulator transition. Close to the transition  $Z$  drops, resulting in very inhomogeneous superconductive state and an abrupt decrease of  $T_c$ .
- distribution of superconducting order parameter in real space is extremely inhomogeneous, thus usual notion of space-averaged order parameter  $\bar{\Delta}$  is useless even qualitatively, and the "Anderson theorem" is not applicable.

In the main part of the paper we present theoretical arguments in support of this new scenario. We restrict our discussion to the three-dimensional problem which is appropriate for the electron wave function behavior in most films. It is possible that the physics in the near vicinity of the transition is dominated by large scales where the two dimensional nature of the films become important, the details of the crossover to this critical regime is beyond the developed theory. We will assume below that localization effects are not very strong, allowing for the presence of phonon-induced attraction between electrons. Clearly, the necessary condition for that is  $\delta_L \ll \omega_D$ .

The theory that we develop starts with the single electron states of the non-interacting problem, so it is not applicable to describe the physics in high magnetic fields where these states change significantly. Thus, interesting physics of the metallic state with resistance approaching  $h/e^2$  is beyond the applicability limits of our theory.

## 2. Model

### 2.1. BCS Hamiltonian for electrons in localized eigenstates.

We consider simplest model of space-local BCS-type electron-electron attraction,  $V_{int} = g\delta(\mathbf{r})$ . It is assumed, as usual, that this attraction is present for electrons with energies  $E$  in the relatively narrow stripe  $E \in E_F \pm \omega_D$  around Fermi energy. However, we will see below that in contrast with the usual BCS theory, the parameter  $\omega_D$  will not enter our final results. The Hamiltonian represented in the basis of exact single-electron eigenstates  $\psi_j(\mathbf{r})$  becomes

$$H = \sum_{j\sigma} \xi_j c_{j\sigma}^\dagger c_{j\sigma} - \frac{\lambda}{\nu_0} \sum_{i,j,k,l} M_{ijkl} c_{i\uparrow}^\dagger c_{j\downarrow}^\dagger c_{k\downarrow} c_{l\uparrow}, \quad (7)$$

where

$$M_{ijkl} = \int d\mathbf{r} \psi_i^*(\mathbf{r}) \psi_j^*(\mathbf{r}) \psi_k(\mathbf{r}) \psi_l(\mathbf{r}), \quad (8)$$

$\xi_j = E_j - E_F$  is the single-particle energy of the eigenstate  $j$  counted from Fermi level,  $c_{j\sigma}$  is the corresponding electron annihilation operator for the spin projection  $\sigma$ ,  $\nu_0$  is the density of states (per single spin projection) and  $\lambda = g\nu_0 \ll 1$  is dimensionless Cooper coupling constant.

Note that writing Hamiltonian in the form (7) we omitted the Hatree-type terms which do not contribute directly to the Cooper instability. Such terms are known to be negligible when single-electron states are extended (see discussion in Ref. [2]); the issue of their importance for critical and, especially, localized states is more delicate. Below in section 6.1 we present results for the superconducting transition temperature obtained with and without account of the Hatree-type terms. The comparison, shown in Fig. 25, demonstrates that these terms, while changing the quantitative results somewhat, do not affect our main qualitative conclusions. Therefore, in order to keep the arguments as simple as possible, we neglect Hatree terms in the main part of the following text. <sup>2</sup>

---

<sup>2</sup>However, those terms are important for a quantitative description of superconductivity in the region of localized single-particle states, as shown in Ref. [5] where 2D problem in the limit of strong disorder and strong attraction was studied numerically. In particular, they might lead to additional inhomogeneous broadening of the coherence peaks observed in tunneling experiments, see section 6.2.3

Unless specified, we will not consider magnetic field effects, thus eigenfunctions  $\psi_j(\mathbf{r})$  can be chosen real. In the following we will use frequently a simplified Hamiltonian (7) where only pair-wise terms  $i = j$  and  $k = l$  are taken into account:

$$H_2 = \sum_{j\sigma} \xi_j c_{j\sigma}^\dagger c_{j\sigma} - \frac{\lambda}{\nu_0} \sum_{jk} M_{jk} c_{j\uparrow}^\dagger c_{j\downarrow}^\dagger c_{k\downarrow} c_{k\uparrow}, \quad (9)$$

where

$$M_{jk} = \int d\mathbf{r} \psi_j^2(\mathbf{r}) \psi_k^2(\mathbf{r}). \quad (10)$$

Eq.(9) is the minimal Hamiltonian that includes hopping of pairs necessary to establish a global superconducting order. It plays the same role for our theory as the BCS Hamiltonian with  $i = \mathbf{p}$ ,  $j = -\mathbf{p}$ ,  $k = \mathbf{p}'$ ,  $l = -\mathbf{p}'$  for usual theory of superconductivity. We will discuss the accuracy of this approximation below in Sec. 4.2

### 2.1.1. Ultra-small metallic grain.

Here we rederive the known results for the model (9) applied to ultra-small metal grains; this derivation will provide the starting point for our solution of the model Hamiltonian (7) or (9) for the electrons with Fermi level near mobility edge.

Pairing correlations in metallic grains of very small volume  $V$ , with level spacing  $\delta = (\nu_0 V)^{-1}$  comparable to the bulk superconductive gap  $\Delta$  were considered in many papers, see review [74]. The issue which is most important for this work is the parity gap introduced in [37] to characterize pairing effects in ultra-small grains with  $\delta \ll \Delta$ . The work [37] assumed the simplified Hamiltonian (9) with identical matrix elements  $M_{jk} = 1/V$ .

More complete treatment of a weak electron-electron interaction in small metallic grains is given by [75] where it was argued that to the leading order in the small parameter  $\tau_0 \delta$ , where  $\tau_0$  is the flight (or diffusion) time for electron motion inside grain, all off-diagonal terms  $M_{ijkl}$  can be neglected. In the relevant terms the indices of  $M_{ijkl}$  should be pairwise equal. Because for small grains the wavefunctions  $\psi_j(\mathbf{r})$  are essentially random Gaussian variables subject only to orthogonality and normalization conditions, the matrix elements (10) appearing in the Hamiltonian (9) are given by

$$M_{j \neq k} = \frac{1}{V} \quad M_{jj} \equiv M_j = \frac{3}{V}, \quad (11)$$

so that the full Hamiltonian can be expressed in terms of the total number of electrons  $\hat{n}$ , the total spin  $\hat{\mathbf{S}}$  and the operator  $\hat{T} = \sum_k c_{k\downarrow} c_{k\uparrow}$  related to Cooper pairing correlations:

$$H_{uni} = \lambda \delta \left[ 2\hat{\mathbf{S}}^2 - \frac{1}{2}\hat{n}^2 \right] - \lambda \delta T^\dagger T \quad (12)$$

It is essential for the validity of (12) that all matrix elements  $M_{jk}$  with  $i \neq j$  are equal to  $1/V$ , while diagonal terms are three times larger, only in this case it is possible to represent Eq.(12) in terms of the total density, spin and pairing operators.

Attractive interaction implies that  $S = 0$  in the ground state. Because  $n$  is conserved for isolated grain the properties of this model in  $n = 0$ ,  $S = 0$  sector are equivalent to the properties of the simplified Matveev-Larkin model (9) which takes into account only

the last term in (12). The first term in (12) is important for the correct evaluation of the coefficient of the interaction term with  $j = k$  in Eq.(9) because only 1/3 of it should be assigned to the interaction in the Cooper channel, since other 2/3 contribute to the "n" and "S" terms of the Hamiltonian.

In the limit  $\delta \gg \Delta$  one can use the perturbation theory with respect to pairing Hamiltonian (12). In the lowest order in  $\lambda$ , neglecting all terms except diagonal ones, one finds that the energy of two identical grains with even number of electrons,  $n = 2k$ , and zero spin is by  $\Delta E = 3\lambda\delta$  less than the energy of the same two grains with  $2k + 1$  and  $2k - 1$  electrons and spin 1/2. <sup>3</sup> It means [37] that the average ground-state energy of a grain with even number of electrons is lower by "parity gap"  $\Delta_P = \frac{3}{2}\lambda\delta$  than the energy of the same grain with odd number of electrons. Note that Cooper pairing contributes 1/3 of this energy difference. This result is valid only in the limit of a very small coupling constant  $\lambda$ , when all the terms with  $j \neq k$  in Eq.(9) can be neglected. In a more general case these terms must be taken into account which leads [37] to the renormalization of the coefficient of the  $T^\dagger T$  term in the Hamiltonian (12) which becomes

$$\lambda_R = \lambda / (1 - \lambda \ln(\omega_D / \delta)). \quad (13)$$

After this renormalization the coefficient of the Cooper pairing becomes dominant. Introducing bulk energy gap  $\Delta = \omega_D e^{-1/\lambda}$ , one finds [37] parity gap which is valid for all  $\Delta \ll \delta$ :

$$\Delta_P = \frac{\delta}{2 \ln \frac{\delta}{\Delta}} + \lambda \quad (14)$$

where the second term is due to the first term in the Hamiltonian (12) and is small compared to the main term. The result (14) shows that parity gap grows with the decrease in the grain size. Note that parity gap (14) would not appear if one does not take into account the double-diagonal terms in (9), which are totally irrelevant in the usual BCS theory of bulk superconductivity. Below we will find somewhat similar behavior in the case of bulk Anderson insulators.

### 2.1.2. Vicinity of the mobility edge.

In the bulk Anderson insulator with the Fermi energy near the mobility edge, the typical energy scale replacing  $\delta$  is

$$\delta_L = 1 / (\nu_0 L_{loc}^3), \quad (15)$$

where  $L_{loc}$  is the localization length. It was argued in [2] that localization is irrelevant for superconductivity if  $T_c \gg \delta_L$ . In the opposite limit  $T_c \ll \delta_L$  pairing correlations between electrons localized on different orbitals are irrelevant. Localization length depends on the Fermi-energy (in the scaling region  $L_{loc} \gg \ell$ ) as

$$L_{loc} \approx \ell \left( \frac{E_0}{E_c - E_F} \right)^\nu, \quad (16)$$

---

<sup>3</sup>For different grains containing different number of particles one needs to take into account different chemical potentials in these grains but the final conclusion remains unchanged.

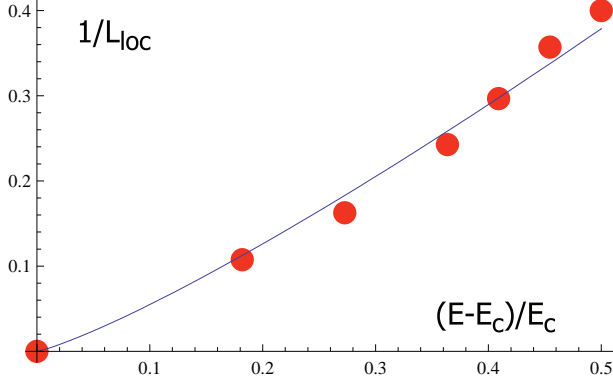


Figure 2: Inverse localization length as function of proximity to the mobility edge, obtained numerically for 3D Anderson model with Gaussian disorder of width  $W = 4$ . The values shown here were extracted from the numerical computation of the inverse participation ratio in this model and its conversion into the localization length by Eqs.(15,71). Full line is a fit to  $1/L_{loc} = 1.87 \cdot (E/E_c - 1)^{1.2}$ .

where  $E_c$  is the position of the mobility edge,  $\nu$  is the localization length exponent. Numerical data [76] show that in a very narrow vicinity of the mobility edge ( $(E_c - E_F)/E_c \lll 1$ ) of 3D Anderson model the localization length obeys the scaling dependence (16) with  $\nu \approx 1.57$ . As we shall see below, the range of energies relevant for the superconductor-insulator transition is relatively wide,  $(E_F - E_c)/E_c \lesssim 0.5$ ; in this broader range the localization length follows the same scaling behavior (16) but with a somewhat different exponent  $\nu \approx 1.2$ . We illustrate this by Fig. 2 that shows the localization length obtained for 3D Anderson model with Gaussian disorder (see section 2.2 and Eq.(23) below). The parameter  $\ell$  in Eq.(16) is the short-scale cutoff of the order of the elastic scattering length. The associated energy scale

$$E_0 = 1/(\nu_0 \ell^3) \quad (17)$$

depends on the microscopic details of the model of disorder and can be small compared to Fermi-energy  $E_F$  (see next subsection for the discussion of this issue).

We will assume that Fermi energy is not too close to the mobility edge so that

$$t \equiv \frac{E_c - E_F}{E_0} \gg \frac{T_c}{E_0} \quad (18)$$

The condition (18) means that localization properties of eigenstates  $\psi_j(\mathbf{r})$  do not vary appreciably within the energy stripe  $E_F \pm T_c$  mainly responsible for development of superconducting correlations. Violation of the condition (18) implies the absence of the particle-hole symmetry in the superconducting state; we expect anomalous Hall effect in the superconducting state and near transition in this regime. Using Eq.(16) we find

$$\delta_L = E_0 t^{3\nu} \quad (19)$$

Because  $3\nu \approx 4 \gg 1$ , the condition (18) is compatible with  $t \ll 1$  in a wide range of parameters which include both small and large ratios  $\delta_L/T_c$ . In the limiting case  $\delta_L \ll T_c$  the scale set by localization is much larger than the one set by superconductivity, so all

relevant statistical properties of matrix elements (10) can be computed at  $t = 0$ . We will refer to this case as the critical regime. We will see in section 4 that deep in the limit  $\delta_L/T_c \rightarrow 0$ , the transition temperature approaches its limiting value, which we denote as  $T_c^0$ . In contrast with the conclusions of Ref. [2], we will find that  $T_c^0$  may differ substantially from the usual BCS value  $T_c^{\text{BCS}} = \omega_D e^{-1/\lambda}$  for the metal with the same value of the Cooper attraction constant. Moreover, we find that the values of  $T_c^0$  are typically *larger* than  $T_c^{\text{BCS}}$  for weak couplings  $\lambda \ll 1$ . This unexpected result is related to the *fractality* of electron wavefunctions with energies close to the mobility edge.

## 2.2. Fractality and correlations of the wave functions near the mobility edge.

The exact single-particle eigenfunctions  $\psi_j(\mathbf{r})$  and eigenvalues  $E_j$  that enter the model Hamiltonian Eq.(7) should be found from the single-particle Hamiltonian with disorder. The conventional models of disorder are the continuous model of free electrons in a Gaussian random potential  $U(\mathbf{r})$ :

$$H_{1a} = \frac{\mathbf{p}^2}{2m} + U(\mathbf{r}), \quad (20)$$

or the tight-binding model with on-site energies  $\varepsilon_{\mathbf{n}}$  being random variables with the probability distribution  $\mathcal{P}(\{\varepsilon_{\mathbf{n}}\}) = \prod_{\mathbf{n}} p(\varepsilon_{\mathbf{n}})$ . The latter is known as the Anderson model, it is described by the Hamiltonian

$$H_{1b} = \sum_{\mathbf{n}} \varepsilon_{\mathbf{n}} a_{\mathbf{n}}^\dagger a_{\mathbf{n}} - \sum_{\mathbf{n}, \mathbf{m}=\mathbf{n}+\mathbf{a}} a_{\mathbf{n}}^\dagger a_{\mathbf{m}}. \quad (21)$$

The most common choice of the distribution function  $p(x)$  are the box distribution

$$p(\varepsilon) = \begin{cases} W^{-1}, & \text{if } x < |W/2| \\ 0, & \text{if } x > |W/2|. \end{cases} \quad (22)$$

or the Gaussian distribution

$$p(\varepsilon) = \frac{1}{\sqrt{2\pi} W} \exp \left[ -\frac{\varepsilon^2}{2W^2} \right]. \quad (23)$$

Increasing the disorder parameter  $W$  in the 3d Anderson model (21),(22) at a fixed Fermi energy  $E_F$  results in the Anderson localization transition at the critical disorder  $W = W_c$  (at  $E_F = 0$  the critical value of disorder is  $W_c = 16.5$  for the box distribution, Eq. 22). Alternatively, the localization transition occurs when  $E_F$  is increased at a fixed disorder  $W < W_c$  beyond the mobility edge  $E_c$ ; in the following we will mainly use the Gaussian model, Eq. (23). The same type of transition takes place in the continuous model Eq.(20). The changes in the statistics of wavefunctions resulting from this transition do not merely reduce to their localization. Well before all wavefunctions become localized they acquire a certain structure where a wavefunction occupies not all available space but a certain *fractal* inside the *correlation radius*  $L_{\text{corr}}$ . The global picture of an extended wavefunction resembles a "mosaic" made of such pieces of fractal with the characteristics size  $L_{\text{corr}}$ . This peculiar phase (called the "multifractal metal" in Ref.[77]) appears in the vicinity of the Anderson transition. It persists down to relatively weak disorder as long as the decreasing correlation length  $L_{\text{corr}}$  exceeds a microscopic length  $\ell$

which has a meaning of the minimal length (a pixel) of the fractal structure. In Anderson model with the box probability distribution the length  $\ell \approx a W_c^{1/3} \geq 2.5a$ , where  $a$  is the lattice constant; fractal effects disappear in this model at  $W < 3 \ll W_c$  only, see Ref. [77]. For the continuous model defined by Eq.(20) it is of the order of the elastic scattering mean free path.

As one approaches the mobility edge or the critical value of disorder, the correlation radius  $L_{\text{corr}}$  diverges so that the critical wavefunctions are pure fractal (or, strictly speaking *multifractal* [77]). On the localized side of the transition the wavefunctions inside the *localization radius*  $L_{\text{loc}}$  resemble the one inside an element of the mosaic structure of the multifractal metal. This "multifractal insulator" [77] exists in the vicinity of the Anderson transition and becomes an ordinary insulator at strong disorder when  $L_{\text{loc}} < \ell$ .

### 2.2.1. Wavefunction correlations at the mobility edge: algebra of multi-fractal states.

We start by describing the multi-fractal correlations of wavefunctions exactly at the mobility edge. To avoid confusion we note that for a finite 3d sample of the size  $L \times L \times L$  the mobility edge is smeared out. The critical multi-fractal states live in a spectral window around  $E_c$  of the width  $\delta E \propto L^{-1/\nu}$ , where  $\nu$  is the exponent of the localization (correlation) length  $L_{\text{loc}}(L_{\text{corr}}) \propto |E - E_c|^{-\nu}$ , such that the value of  $L_{\text{loc}}(L_{\text{corr}})$  inside this window is larger than  $L$ . The number of single-particle states in this window is proportional to  $L^{3(1-\frac{1}{3\nu})}$ . Because  $\nu$  is definitely larger than  $\frac{1}{3}$  (in fact, Harris criterion tells that  $\nu \geq 2/d = 2/3$ ) it tends to infinity as  $L \rightarrow \infty$ .

There is a vast numerical and analytical evidence [78] that the critical wavefunctions at the mobility edge obeys the multifractal statistics. This can be seen, for instance, in the behavior of the moments of the inverse participation ratio:

$$P_q = \nu_0^{-1} \sum_j \int d^d \mathbf{r} |\psi_j(\mathbf{r})|^{2q} \delta(E - E_j). \quad (24)$$

The moments (24) describe the effective volume occupied by the the wave function. At the mobility edge they scale with the size of the sample

$$\langle P_q \rangle \sim \ell^{-(d-d_q)(q-1)} L^{-d_q(q-1)} \propto L^{-d_q(q-1)}, \quad (25)$$

where  $d_q \leq 3$  is the corresponding fractal dimension. For the 3d Anderson model of the orthogonal symmetry class (real Hamiltonian) we obtain by numerical diagonalization the following results for the first two fractal dimensions: <sup>4</sup>

$$d_2 \approx 1.29 \pm 0.1, \quad d_4 \approx 0.72 \pm 0.1. \quad (26)$$

The fact that the fractal dimensions  $d_q$  depend on the order of the moment  $q$  implies the *multiractality* of the wave functions. The scaling arguments show that such behavior

---

<sup>4</sup>The fractal dimensions for bigger sample sizes have been studied recently by Rodriguez, Vasquez and Roemer[79]. They have found  $d_2 = 1.24 \pm 0.07$ ,  $d_4 = 0.63 \pm 0.07$ ,  $d_2^{\text{typ}} = 1.35 \pm 0.07$ ,  $d_4^{\text{typ}} = 1.02 \pm 0.2$ . They also point out on a large systematic error for  $d_4^{\text{typ}}$  related with the finite-size effect. In view of the fact that the critical  $q_c \approx 2.1...2.2$  is close to 2, the typical  $d_4^{\text{typ}}$  should be found from the condition Eq.(33). This gives an estimate  $d_4^{\text{typ}} = 0.84 \pm 0.04$ .



of  $\langle P_q \rangle$  implies the power-law correlations of wavefunction amplitudes at different space points:

$$C_q(0, \mathbf{r}) = \langle |\psi_j(\mathbf{r})|^{2q} |\psi_j(0)|^{2q} \rangle \sim L^{-2qd} (L/\ell)^{\beta_q} \left( \frac{L}{r} \right)^{d-\alpha_q}, \quad (27)$$

where  $\ell < r < L$ , and the exponents are equal to

$$\alpha_q = d_{2q}(2q-1) - 2d_q(q-1), \quad (28)$$

$$\beta_q = 2(q-1)(d-d_q) \quad (29)$$

Note that the sign of  $\alpha_q$  is positive provided that the moments  $P_q$  are only *moderately* fluctuating, so that the scaling behavior of  $\langle P_q^2 \rangle$  and  $\langle P_q \rangle^2$  is the same. This follows from the inequality

$$P_q^2 = \left( \sum_{\mathbf{r}} |\psi(\mathbf{r})|^{2q} \right)^2 > P_{2q} = \sum_{\mathbf{r}} |\psi(\mathbf{r})|^{4q}$$

and the definition of the fractal dimensions Eq.(25). However, from Eq.(26) it follows that

$$\alpha_2 = 3d_4 - 2d_2 \approx -0.43 \pm 0.5. \quad (30)$$

Although the error bars are rather large, it is likely that  $\alpha_2$  is *negative*.

This means that the second moment  $P_2$  is strongly, not moderately fluctuating, and the  $L$ -scaling of  $\langle P_2^2 \rangle$  is different from that of  $\langle P_2 \rangle^2$  in agreement with the early conjecture[80]. Indeed, our numerical simulations on the 3D Anderson model of the orthogonal symmetry class show that

$$\langle P_2^2 \rangle \propto L^{-2.16 \pm 0.1}, \quad \langle P_2 \rangle^2 \propto L^{-2.58 \pm 0.1}.$$

This is consistent with the observation [81] that the distribution function of the second moment  $\mathcal{P}_2(P_2) \propto P_2^{-p_2}$  has a power-law tail with  $p_2 \approx 2.6$  at relatively large values of  $P_2 \gg \langle P_2 \rangle \sim L^{-d_2}$  (which is cut at  $P_2 = 1$ ). As a result the average  $\langle P_2^2 \rangle$  is dominated by the far tail where the one-parameter scaling  $\mathcal{P}_2(P_2) = f_2(P_2/\langle P_2 \rangle)$  is no longer true. The distribution function  $\mathcal{P}_4(P_4)$  of the fourth moment  $P_4$  possesses even stronger tail with  $\mathcal{P}_4 \propto P_4^{-2.0}$  at  $P_4 \gg \langle P_4 \rangle$ . In this case the average  $\langle P_4 \rangle$  is considerably contributed by the rare events in the far tail of the distribution.

In the situation where the assumption of moderate fluctuations of  $P_q$  no longer holds and the rare events are important for averaging [78] the correct physical quantity is typical average  $\langle P_q \rangle_{\text{typ}} = \exp[\langle \ln P_q \rangle]$  instead of the usual one and the corresponding fractal dimensions should be defined by

$$d_q^{\text{typ}}(q-1) = -d \ln \langle P_q \rangle_{\text{typ}} / d \ln L. \quad (31)$$

Unlike the usual average, the typical average is determined by the body of the corresponding distribution function  $\mathcal{P}_q(P_q)$  provided that the tail exponent  $p_q$  is larger than 1. Computing the typical averages  $\langle P_q \rangle_{\text{typ}}$  and using Eq.(31) we obtained (see also a footnote <sup>4</sup> and Ref. [79] for comparison) for the orthogonal 3D Anderson model:

$$\begin{aligned} d_2^{\text{typ}} &\approx 1.40 \pm 0.1, & d_4^{\text{typ}} &\approx 1.08 \pm 0.1, \\ \alpha_2^{\text{typ}} &= 3d_4^{\text{typ}} - 2d_2^{\text{typ}} \approx +0.44 \pm 0.5. \end{aligned} \quad (32)$$

It is interesting to note [78] that if the tail exponent for a given  $q$ -th moment lies in the region  $1 < p_q < 2$  (i.e. the typical fractal dimension is determined by the body of the distribution for the corresponding moment  $P_q$  but the averaged moment is dominated by the rare events) the dependence of the typical fractal dimension on  $q$  is linear.<sup>5</sup>

$$d_q^{\text{typ}}(q-1) = q\alpha_+, \quad q > q_c, \quad (33)$$

where  $\alpha_+$  is a constant.

Substituting Eq.(33) into Eq.(28) we immediately obtain:

$$\alpha_q^{\text{typ}} = (2q-1)d_{2q}^{\text{typ}} - 2(q-1)d_q^{\text{typ}} = 0, \quad q > q_c. \quad (34)$$

The equality (34) is valid if the condition  $q > q_c$  is satisfied for both terms entering (28); in all other cases  $\alpha_q^{\text{typ}} > 0$ . Given also that for  $q > 1$   $d_{2q} < d_q < d$ , we obtain:

$$d > \alpha_q^{\text{typ}} > 0. \quad (35)$$

For 3D Anderson model of orthogonal symmetry class  $q_c \approx 2.2 \pm 0.1$  is very close to (but larger than) 2 (see Ref.[79]). This means that in a typical sample the  $r$ -dependence of the correlation function Eq.(27) is such that the integral over  $r$  is dominated by large distances. This will be important for the estimations of the matrix elements done below.

Long expressions Eqs.(28,29) for the exponents  $\alpha_q$  and  $\beta_q$  reflect few simple rules:

**Rule(i):** for  $r \sim L$  the two wavefunctions are statistically independent and the result can be found using Eq.(25):

$$\langle |\psi_j(0)|^{2q} \rangle^2 \sim [L^{-d} \langle P_q \rangle]^2 \sim L^{-2d_q(q-1)-2d}$$

**Rule (ii):** for  $r \sim \ell$  the result should be the same as for the coincident points  $r = 0$ , i.e.

$$\langle |\psi_j(\mathbf{0})|^{4q} \rangle = L^{-d} \langle P_{2q} \rangle \sim L^{-d_{2q}(2q-1)-d}.$$

These rules can be generalized to the case of correlation of *different* eigenfunctions

$$C_q(\omega, \mathbf{r}) = \langle |\psi_i(\mathbf{r})|^{2q} |\psi_j(0)|^{2q} \rangle$$

with the energy difference  $E_i - E_j = \omega$ . In this case the eigenfunctions become statistically independent for  $|\mathbf{r}| > L_\omega$ , where

$$L_\omega^d = \frac{1}{\nu_0 \omega}. \quad (36)$$

With this correction, applying the rules (i) and (ii) one can show that at  $\omega > \delta$  the only change in Eq.(27) is that the  $|\mathbf{r}|$ -dependent factor becomes  $(L_\omega/|\mathbf{r}|)^{d-\alpha_q}$  instead of  $(L/|\mathbf{r}|)^{d-\alpha_q}$ .

---

<sup>5</sup>This follows from the fact that the spectrum of fractal dimensions given by the Legendre transformation  $f(\alpha) = -\tau_q + q\alpha$ ,  $\alpha = \frac{d\tau_q}{dq}$ ,  $\tau_q = (q-1)d_q$  determines the scaling with the system size  $L$  of the number of sites  $M \propto L^{f(\alpha)}$  where  $|\psi(\mathbf{r}_i)|^2 \propto L^{-\alpha}$ . As a typical event cannot occur at a number of sites  $M < 1$  (which is only possible for a rare event),  $f^{\text{typ}}(\alpha)$  found from  $d_q^{\text{typ}}$  must be either positive (if  $\langle P_q \rangle = \langle P_q \rangle_{\text{typ}}$ ) or zero (if  $\langle P_q \rangle$  is dominated by the rare events and is different from  $\langle P_q \rangle_{\text{typ}}$ ). In the latter case the Legendre transformation implies  $[1 - qd/dq]\{(q-1)d_q^{\text{typ}}\} = 0$ , leading to the fact that  $(q-1)d_q^{\text{typ}}$  is proportional to  $q$ .

This allows us to estimate the *local* averages of *different wave functions*. In these averages the power law correlations will be seen in the energy space. Indeed, substituting  $|\mathbf{r}| \sim \ell$  in  $(L_\omega/|\mathbf{r}|)^{d-\alpha_q}$  one obtains:

$$\begin{aligned} C_q(\omega, 0) &= \nu_0^{-2} \sum_{i,j} \langle |\psi_i(\mathbf{0})|^{2q} |\psi_j(\mathbf{0})|^{2q} \delta(E - E_i) \delta(E' - E_j) \rangle \\ &\sim L^{-2qd} (L/\ell)^{\beta_q} \left( \frac{E_0}{\omega} \right)^{\gamma_q}, \quad \gamma_q = 1 - \frac{\alpha_q}{d}. \end{aligned} \quad (37)$$

where  $(\nu_0 L^d)^{-1} = \delta < \omega < E_0 = (\nu_0 \ell^d)^{-1}$ . For  $\omega < \delta$  the correlation function  $C_q(\omega)$  saturates.

Here, essentially the same rules work:

- (i) at large energy separations  $\omega \sim E_0$  the wavefunctions are statistically independent and
- (ii) at small energy separations  $\omega \sim \delta = (\nu_0 L^d)^{-1}$  the result should be of the same order as for the one single wavefunction ( $\omega = 0$ ).

This immediately gives rise to the relationship between  $\alpha_q$  and  $\gamma_q$  given in Eq.(37). In particular for  $q = 1$  one finds:

$$\gamma_1 \equiv \gamma = 1 - \frac{d_2}{d}. \quad (38)$$

The scaling relationship Eq.(38) has been first suggested by Chalker [71] and checked numerically in a number of works [77]. Fig.3 gives an evidence that the scaling relationship Eq.(37) between  $\gamma_q$  and  $\alpha_q$  holds true for  $q = 2$  as well. An important point is that finite-size corrections are quite large and should be taken into account for an accurate determination of the exponents  $\gamma_q$  (an example is presented in Figs.5,6 below).

So far we have discussed the correlation functions containing  $|\psi_i(\mathbf{r})|^2$  and thus independent of the random eigenfunction *phase*. The simplest *phase-dependent* correlation function is involved in the density-density correlation function:

$$\begin{aligned} K(\omega, \mathbf{r} - \mathbf{r}') &= \nu_0^{-2} \sum_{i,j} \langle \delta(E - E_i) \delta(E' - E_j) \\ &\times \psi_i(\mathbf{r}) \psi_i^*(\mathbf{r}') \psi_j^*(\mathbf{r}) \psi_j(\mathbf{r}') \rangle \end{aligned} \quad (39)$$

According to Ref.[71] the Fourier-transform of this correlation function is equal to:

$$K(\omega, \mathbf{q}) = \frac{1}{2\pi\nu_0} \frac{D(\omega, q) q^2}{(D(\omega, q) q^2)^2 + \omega^2}, \quad (40)$$

which is a generalization of the correlation function in the diffusion approximation for the case where the diffusion coefficient may depend on  $q$  and  $\omega$ . The main assumption [71] here is that at the critical point and for  $q \ll \ell^{-1}$ :

$$D(\omega, q) = q^{d-2} F(qL_\omega) = \begin{cases} L_\omega^{2-d}, & qL_\omega \ll 1 \\ q^{d_2} L_\omega^{2-d+d_2}, & qL_\omega \gg 1 \end{cases}. \quad (41)$$

One can easily see that this assumption is equivalent to the statement that at distances  $\ell < |\mathbf{r} - \mathbf{r}'| < L_\omega$  the correlation function  $K(\omega, \mathbf{r} - \mathbf{r}')$  has the same  $\mathbf{r} - \mathbf{r}'$ -dependence

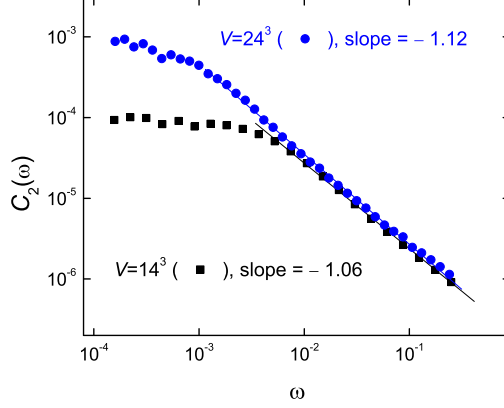


Figure 3: (Color online) Scaling relationship between  $\gamma_2$  and  $\alpha_2$  for the 3D Anderson model of the orthogonal symmetry class at two different system sizes  $L=14$  and  $L=24$ . The theoretical slope computed from Eqs.(37),(26) gives  $\gamma_2 \approx 1.14 \pm 0.03$ .

Eq.(27)(but with  $L \rightarrow L_\omega$  as explained above) as the correlation function of the local DoS  $C_1(\omega, \mathbf{r} - \mathbf{r}')$  that we discussed above. This requires non-trivial *phase correlations* in the eigenfunctions which allow to replace the *phase-dependent* average by its *phase-independent* counterpart:

$$\langle \psi_i(\mathbf{r}) \psi_i^*(\mathbf{r}') \psi_j^*(\mathbf{r}) \psi_j(\mathbf{r}') \rangle \Rightarrow \langle |\psi_i(\mathbf{r})|^2 |\psi_j(\mathbf{r}')|^2 \rangle \quad (42)$$

The replacement Eq.(42) illustrates the general rule

**Rule (iii):** To estimate the averages that cannot be expressed in terms of  $|\psi|^2$  (*phase-dependent averages*) one should find by permutation of space and/or energy variables the corresponding *phase-independent average* and apply rules (i) and (ii) in order to estimate the latter.

One should note, however, that this rule does not apply for  $|\mathbf{r}| > L_\omega$ . At such distances the phase correlations are no longer present, and the phase-dependent average vanishes exponentially while the  $\mathbf{r}$ -dependence of its phase-independent counterpart saturates.

### 2.2.2. Scaling estimates for matrix elements: mobility edge.

Now let us show how to use phenomenology of multifractal wavefunction statistics to estimate the matrix elements of local interaction  $M_{ijkl}$  given by Eq.(8). The simplest one  $M_i \equiv M_{iiii}$ , so called *super-diagonal* matrix element, is proportional to the inverse participation ratio  $P_2$ :

$$\langle M_i \rangle \approx 3\ell^{-(d-d_2)} L^{-d_2}. \quad (43)$$

Here and below we define microscopic length-scale  $\ell$  via its relation to the upper energy cutoff  $E_0 = 1/\nu_0\ell^3$ . The factor 3 in the above equation is of the same origin as in the statistics of eigenvectors of real Gaussian random matrices. Applicability of such a relation to the case of fractal wavefunctions was demonstrated in Ref. [82] for the case of

Anderson transition on a Cayley tree. Qualitative picture, emerging from their analysis, is that typical wavefunctions can be represented as products  $\psi_j(\mathbf{r}) = \chi_j(\mathbf{r})\Phi_\xi(\mathbf{r})$  where  $\chi_j(\mathbf{r})$  describes fast-oscillating functions specific for each eigenstate  $j$ , but insensitive to the vicinity of Anderson transition, whereas  $\Phi_\xi(\mathbf{r})$  has a meaning of smooth envelope function, which is however sensitive to the proximity of energy  $\xi$  to the mobility edge  $E_c$ . Combinatorial factor 3 in Eq.(43) is due to the fast-fluctuating “Gaussian” component  $\chi_j(\mathbf{r})$ .

The *diagonal* matrix element  $M_{ij} \equiv M_{ijij}$  with  $i \neq j$  can be easily found from Eq.(37);

$$\langle M_{ij} \rangle \equiv \mathcal{V}^{-1} M(\omega) \approx \mathcal{V}^{-1} \left( \frac{E_0}{\omega} \right)^\gamma, \quad (44)$$

where  $\mathcal{V} = L^d$  and  $\omega = \xi_i - \xi_j$ . The detailed numerical analysis of this matrix element has been done in Ref.[77]. Here we present in Fig.5 data for  $C_1(\omega) \equiv M(\omega)$  correlator for 3D Anderson model with Gaussian disorder ( $W = 4$ ) at the mobility edge, computed for three different system sizes. The plot of the density of states for the same model is presented in Fig. 4. The values of  $\gamma$  extracted for all three sizes are shown in the inset, together with extrapolation to  $L \rightarrow \infty$ , which leads to

$$\gamma \approx 0.57 \pm 0.02 \quad (45)$$

Below we will use this value of  $\gamma$  in our analysis. as well as the value of the pre-factor

$$E_0 = 2.08 \pm 0.25 \quad (46)$$

which is also extracted via large- $L$  extrapolation, as shown in Fig.6. In addition, we present in Fig.5 data for the same correlation function at  $E = 8.0$  in the localized part of the spectrum (to be discussed below in Sec. 2.2.5 and used in Sec. 6). Here we just note that the logarithmic slope of the  $M(\omega)$  function (rather deep inside localized band) is close to its value  $\gamma$  for the critical eigenstates.

A straightforward generalization of Eq.(44) is the matrix element

$$\int d^d \mathbf{r} \langle |\psi_{i_1}(\mathbf{r})|^2 \dots |\psi_{i_n}(\mathbf{r})|^2 \rangle \sim \mathcal{V}^{-(n-1)} \left( \frac{E_0}{\omega} \right)^{\gamma_n(n-1)}, \quad (47)$$

where  $\gamma_n$  is defined in Eq.(37), and all energy differences  $|\xi_{i_m} - \xi_{i_{m'}}|$  are assumed to be of the same order  $\omega$ .

The *off-diagonal* matrix element  $M_{ijkl}$  with all indices different and all energy differences of the same order  $\omega$  strongly fluctuates and therefore has zero average value. However, its average square modulus can be computed as following. We start by writing

$$\begin{aligned} \langle |M_{ijkl}|^2 \rangle &= \int d^d \mathbf{r} d^d \mathbf{r}' \\ &\langle \psi_i^*(\mathbf{r}) \psi_i(\mathbf{r}') \psi_j^*(\mathbf{r}) \psi_j(\mathbf{r}') \psi_k^*(\mathbf{r}) \psi_k(\mathbf{r}') \psi_l^*(\mathbf{r}') \psi_l(\mathbf{r}) \rangle \end{aligned} \quad (48)$$

Now we apply the rule (iii) of the previous subsection and define the phase-independent correlation function:

$$\langle |\psi_i(\mathbf{r})|^2 |\psi_j(\mathbf{r}')|^2 |\psi_k(\mathbf{r})|^2 |\psi_l(\mathbf{r}')|^2 \rangle \quad (49)$$

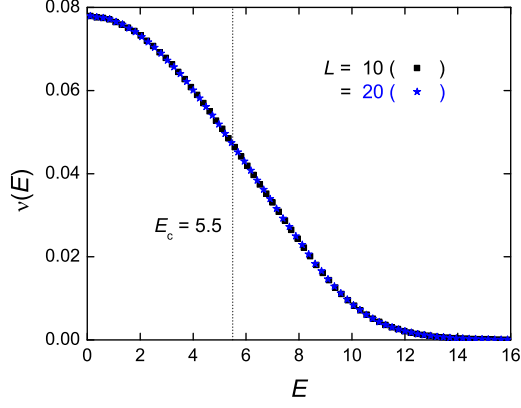


Figure 4: Density of states for the 3D Anderson model with Gaussian disorder with the width  $W = 4$  for the system size  $L = 10$  (black squares) and  $L = 20$  (blue stars).

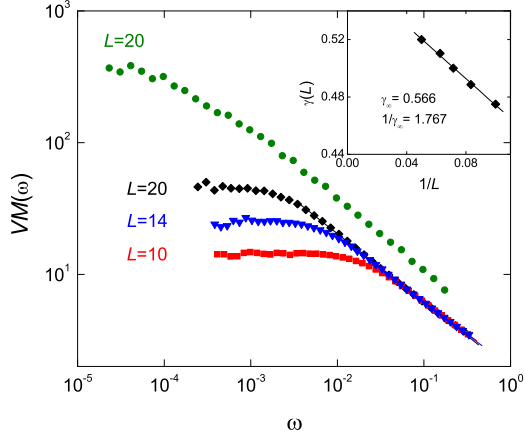


Figure 5: (Color online) Correlation function  $M(\omega)$  for 3DAM with Gaussian disorder and lattice sizes  $L = 10, 14, 20$  at the mobility edge  $E = 5.5$  (red squares, blue triangles and black diamonds) and at the energy  $E = 8$  inside localized band (green dots). Inset shows  $\gamma$  values for  $L = 10, 12, 14, 16, 20$ .

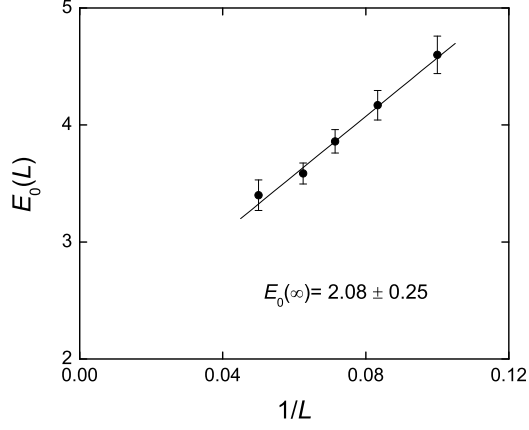


Figure 6: Pre-factor  $E_0$  for 3DAM with Gaussian disorder width  $W = 4$  at the mobility edge  $E_c = 5.5$ , for lattice sizes  $L = 10, 12, 14, 16, 20$

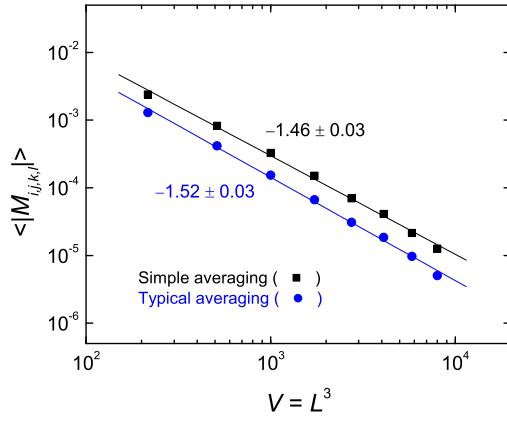


Figure 7: (Color online) Scaling with the system size of the off-diagonal matrix element. The theoretical exponent is  $-3/2$  according to Eq.(51).



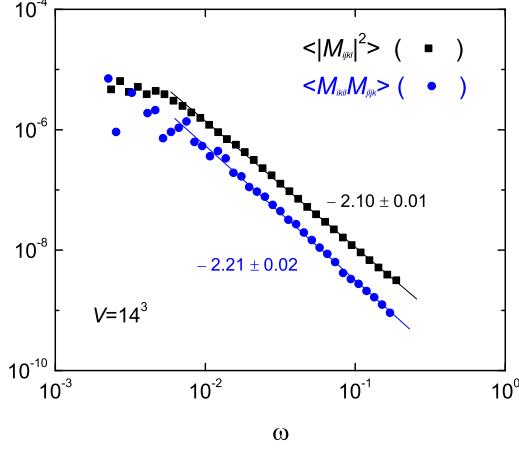


Figure 8: (Color online) Scaling with energy difference  $|E_i - E_j| \sim |E_i - E_k| \sim |E_i - E_l| \sim \dots \sim \omega$  of the off-diagonal  $\langle |M_{ijkl}|^2 \rangle$  (blue dots) and the product of semi-diagonal  $\langle M_{iikl} M_{jjkl} \rangle$  (black squares) matrix elements. The theoretical exponent found from Eqs.(51),(52) and (26) is equal to  $-2.13 \pm 0.1$ .

Using the rules (i), (ii), we estimate the phase-independent correlator as:

$$\frac{1}{\mathcal{V}^4} \left( \frac{L_\omega}{|\mathbf{r} - \mathbf{r}'|} \right)^{d-\alpha_2} \left( \frac{L_\omega}{\ell} \right)^{2(d-d_2)} \quad (50)$$

In order to obtain an estimation for  $\langle |M_{ijkl}|^2 \rangle$  one has to integrate Eq.(50) over  $\mathbf{r}$  and  $\mathbf{r} - \mathbf{r}'$ . The first integration is trivial and results in the factor  $\mathcal{V}$ . To estimate the result of the second integration we note that according to Eq.(35) in a typical sample the exponent  $d - \alpha_2^{\text{typ}}$  in the power law in Eq.(50) is smaller than  $d$ . This means that the integral over  $\mathbf{r} - \mathbf{r}'$  is dominated by large distances  $|\mathbf{r} - \mathbf{r}'| \sim L_\omega$ . Finally we obtain:

$$\langle |M_{ijkl}|^2 \rangle_{\text{typ}} \sim \frac{L_\omega^d}{\mathcal{V}^3} \left( \frac{E_0}{\omega} \right)^{2\gamma}. \quad (51)$$

The same rules applied to the correlation function  $\langle M_{ikil} M_{jljk} \rangle$  of *semi-diagonal* matrix elements give exactly the same answer:

$$\langle M_{ikil} M_{jljk} \rangle_{\text{typ}} \sim \frac{L_\omega^d}{\mathcal{V}^3} \left( \frac{E_0}{\omega} \right)^{2\gamma}. \quad (52)$$

However, the square modulus of the semi-diagonal matrix elements is much larger:

$$\langle |M_{ikil}|^2 \rangle_{\text{typ}} \sim L_\omega^d \ell^{-(d-d_2)} \mathcal{V}^{-2-d_2/d} (E_0/\omega)^\gamma. \quad (53)$$

The relevant phase-dependent correlation function and its phase-independent counterpart

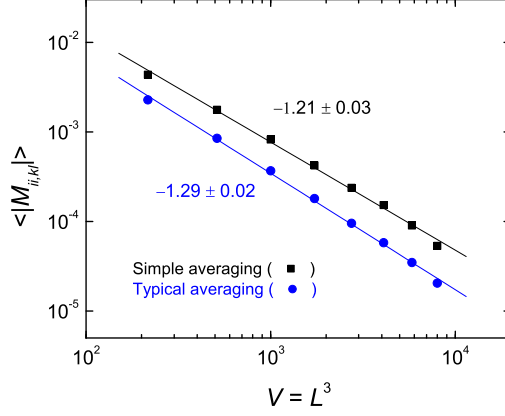


Figure 9: (Color online) System size scaling of semi-diagonal matrix element for the 3D AM. The theoretical exponent found from Eq.(53),(26) is equal to  $-1.21 \pm 0.02$  for the simple averaging and  $-1.24 \pm 0.02$  for the typical averaging.

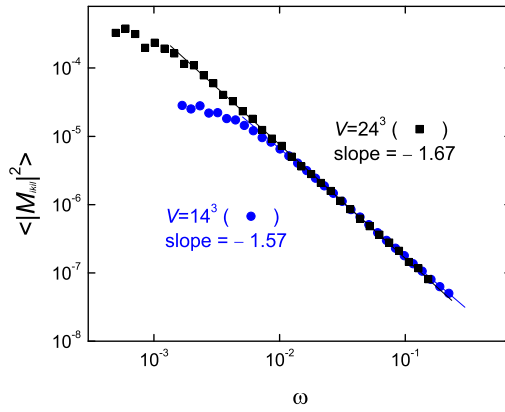


Figure 10: (Color online) Energy difference scaling of semi-diagonal matrix element for the 3D AM with two system sizes  $L = 14$  and  $L = 24$ . The theoretical exponent found from Eq.(53),(26) is equal to  $-1.57 \pm 0.03$ .

according to rule (iii) are:

$$\begin{aligned} & \langle |\psi_i(\mathbf{r})|^2 \psi_k(\mathbf{r}) \psi_l^*(\mathbf{r}) |\psi_i(\mathbf{r}')|^2 \psi_k^*(\mathbf{r}') \psi_l(\mathbf{r}') \rangle \Rightarrow \\ & \langle |\psi_i(\mathbf{r})|^2 |\psi_i(\mathbf{r}')|^2 |\psi_k(\mathbf{r})|^2 |\psi_l(\mathbf{r}')|^2 \rangle \end{aligned} \quad (54)$$

The latter for  $\ell \ll |\mathbf{r} - \mathbf{r}'| \ll L_\omega$  can be found in the following form:

$$\begin{aligned} & \langle |\psi_i(\mathbf{r})|^2 |\psi_i(\mathbf{r}')|^2 |\psi_k(\mathbf{r})|^2 |\psi_l(\mathbf{r}')|^2 \rangle \sim \\ & \sim \frac{1}{\mathcal{V}^4} \left( \frac{L_\omega}{|\mathbf{r} - \mathbf{r}'|} \right)^{\nu_1} \left( \frac{L_\omega}{\ell} \right)^{\nu_2} \left( \frac{L}{|\mathbf{r} - \mathbf{r}'|} \right)^{\nu_3}. \end{aligned} \quad (55)$$

At  $|\mathbf{r} - \mathbf{r}'| > L_\omega$  we assume that the  $\mathbf{r} - \mathbf{r}'$  dependence in the first factor in r.h.s. of Eq.(55) saturates.

Indeed, according to rule (i), at  $|\mathbf{r} - \mathbf{r}'| \sim L \gg L_\omega$  the following decoupling can be done:

$$\begin{aligned} & \mathcal{V}^4 \langle |\psi_i(\mathbf{r})|^2 |\psi_i(\mathbf{r}')|^2 |\psi_k(\mathbf{r})|^2 |\psi_l(\mathbf{r}')|^2 \rangle \approx \\ & \mathcal{V}^4 \langle |\psi_i(\mathbf{r})|^2 |\psi_k(\mathbf{r})|^2 \rangle \langle |\psi_i(\mathbf{r}')|^2 |\psi_l(\mathbf{r}')|^2 \rangle \sim \left( \frac{E_0}{\omega} \right)^{2\gamma}. \end{aligned} \quad (56)$$

This suggests that  $\nu_2 = 2(d - d_2)$ .

At  $|\mathbf{r} - \mathbf{r}'| \sim \ell$  according to rule (ii) all wavefunctions are effectively in one space point:

$$\begin{aligned} & \mathcal{V}^4 \langle |\psi_i(\mathbf{r})|^2 |\psi_i(\mathbf{r}')|^2 |\psi_k(\mathbf{r})|^2 |\psi_l(\mathbf{r}')|^2 \rangle \\ & \approx \mathcal{V}^4 \langle |\psi_i(\mathbf{r})|^4 |\psi_k(\mathbf{r})|^2 |\psi_l(\mathbf{r})|^2 \rangle \\ & \sim \left( \frac{L}{\ell} \right)^{d-d_2} \left( \frac{L_\omega}{\ell} \right)^{-3d_4+d_2+2d} \end{aligned} \quad (57)$$

Comparing Eqs.(57),(56) with Eq.(55) we find:

$$\nu_1 = 3(d_2 - d_4), \quad \nu_2 = 2(d - d_2), \quad \nu_3 = d - d_2. \quad (58)$$

The  $|\mathbf{r} - \mathbf{r}'|$  dependence in Eq.(55) is the power law  $|\mathbf{r} - \mathbf{r}'|^{-(\nu_1+\nu_3)}$  with the exponent  $(d - \alpha_2)$ . As in the case of the off-diagonal matrix elements considered above, for a typical realization of disorder this exponent is smaller than  $d$ . Therefore, the integral of the phase-dependent correlation function over  $(\mathbf{r} - \mathbf{r}')$  which determines the matrix element  $\langle |M_{ikil}|^2 \rangle_{\text{typ}}$  is dominated by large distances  $|\mathbf{r} - \mathbf{r}'| \sim L_\omega$  (for  $|\mathbf{r} - \mathbf{r}'| > L_\omega$  the phase-dependent correlation function decays exponentially). Thus plugging  $|\mathbf{r} - \mathbf{r}'| \sim L_\omega$  in Eq.(55) and multiplying the result by  $L_\omega^d$  and  $\mathcal{V}$  (for integration over the remaining coordinate  $\mathbf{r}$ ) we arrive at the announced result Eq.(53).

We conclude our analysis by noting that if instead of typical averaging the full ensemble averaging is performed, the exponent  $\alpha_2 = 3d_4 - 2d_2$  may be (and in the 3D Anderson model of orthogonal symmetry class is) negative, due to the contribution of rare untypical realizations. In this case the principle contributions to all correlations functions come from small distances  $|\mathbf{r} - \mathbf{r}'| \sim \ell$ . This changes the estimates in Eqs.(51),(52),(53): all those equations will acquire an extra factor

$$(\omega/E_0)^{\alpha_2/d} \quad (59)$$

which explicitly depends on the fractal dimensionality  $d_4$  and not only on  $d_2$ . Note, however, that in the particular case of the 3D orthogonal symmetry class, the exponent  $|\alpha_2/d| \sim 0.1$  is extremely small, so that an extra factor Eq.(59) is of order one for most of the practical purposes.

The predictions made on the basis of rules (i)-(iii) of the algebra of multifractal states are checked by numerical diagonalization of the 3d Anderson model of the orthogonal symmetry class and summarized in figures Fig.7-Fig.10. One can see a very satisfactory agreement for exponents of various power laws which were found numerically and derived theoretically using only one fractal dimension  $d_2$ .

Closing this subsection we conclude that the rules (i) – (iii) and the definition of multifractal dimensions Eq.(25) constitute the full set of rules necessary to estimate any correlation function of critical wavefunctions. This set of algebraic operations will be the main *analytical* tool to deal with the strongly disordered case considered in this paper.

### 2.2.3. Scaling estimates for matrix elements: multifractal insulator.

Estimates for the matrix elements on the localized side of the Anderson transition can be obtained from the corresponding formulae of the preceding subsection provided that the localization radius is larger than the characteristic length  $\ell$  (multifractal insulator). The only modification to be done in all the local averages  $\langle \dots \rangle$  is to replace  $L$  by  $L_{\text{loc}}$  and to add a factor  $(L_{\text{loc}}/L)^{nd}$  (where  $n$  is the number of different eigenfunctions in the average) that accounts for the probability for a point  $\mathbf{r}$  to be inside the localization radius of each of the wavefunctions. To apply these simple rules for the matrix elements of different wavefunctions with the energy separations  $\omega$ , one has also to make sure that all the corresponding length scales  $L_\omega = (\nu_0 \omega)^{-1/d}$  are smaller than the localization radius  $L_{\text{loc}}$ . This sets up an important condition which determines the frequency domain of the multifractal correlations (*multifractal frequency domain*):

$$E_0 > \omega > \delta_L = (\nu_0 L_{\text{loc}}^d)^{-1}. \quad (60)$$

In particular, under this condition we have:

$$\langle M_i \rangle = 3\ell^{-(d-d_2)} L_{\text{loc}}^{-d_2}, \quad (61)$$

which is much larger than the corresponding critical value Eq.(43). The combinatorial factor 3 in Eq.(61) arises because of the statistics of phase of wave function as explained above, see note after Eq.(43).

However, the estimate for the *average* diagonal matrix element  $M_{ij}$  does not change and is still described by Eq.(44). The reason is the additional (compared to  $M_i$ ) factor  $(L_{\text{loc}}/L)^d$  due to a small probability for *two* wavefunctions being localized close in space which exactly compensates for the replacement of  $\mathcal{V} \rightarrow L_{\text{loc}}^d$  in Eq.(44). One can easily check that the estimates for the average square of the off-diagonal matrix element Eq.(51), and the average of different semi-diagonal matrix element (52) also remain unchanged under the condition Eq.(60).

The average square of the semi-diagonal matrix element gets enhanced with respect to the critical case Eq.(53):

$$\langle |M_{ikil}|^2 \rangle_{\text{typ}} \sim \frac{1}{\mathcal{V}^2} \ell^{-(d-d_2)} L_{\text{loc}}^{-d_2} L_\omega^d (E_0/\omega)^\gamma. \quad (62)$$

This enhancement factor of  $(L/L_{\text{loc}})^{d_2}$  results in a regular scaling of  $\langle |M_{ikil}|^2 \rangle \propto \mathcal{V}^{-2}$  with the total volume.

Note, however, that in all cases the typical value of a matrix element  $|M^{typ}|$  of *well overlapping states* is much greater than the typical *average* value  $\langle |M| \rangle_{\text{typ}}$ , and it can be obtained from the corresponding expression for  $\langle M \rangle_{\text{typ}}$  (or  $\langle M^2 \rangle_{\text{typ}}$ ) by replacing the total volume  $\mathcal{V}$  by the localized volume  $L_{\text{loc}}^d$ . In particular, the typical value of the diagonal matrix element for well overlapping states is:

$$M_{ij}^{typ} \sim L_{\text{loc}}^{-d} \left( \frac{E_0}{\omega} \right)^\gamma. \quad (63)$$

This difference between the average value of a matrix element and the typical value for well overlapping states is due to the fact that the most of matrix elements in insulator are very small due to poor overlap of the corresponding states.

One can easily check that at  $\omega = \delta_L$  the typical absolute value of matrix elements of well overlapping states  $i, j, k, l$  does not depend on the number of different states and has a order of magnitude of the inverse participation ratio:  $|M^{typ}| \sim \ell^{-d} (\ell/L_{\text{loc}})^{d_2}$ . For  $\omega > \delta_L$  the matrix elements  $M^{typ}$  of well overlapping states get suppressed, and the suppression is stronger when the number of different states in the matrix element increases.

#### 2.2.4. Scaling estimates for matrix elements: multifractal metal.

On the metal side of the Anderson transition, the wave function is globally not a fractal (or multifractal), as the moments  $P_q$  are proportional to  $L^{-d(q-1)}$ . However, the correlations of different eigenfunctions (with the energy difference  $\omega$ ) show the same power-law  $\omega$ -behavior as the critical eigenfunctions [77] provided that  $\ell \ll L_\omega \ll L_{\text{corr}}$ . The physical meaning of the correlation length  $L_{\text{corr}}$  is a typical size of a fractal element of which the entire eigenfunction support is built. Thus, locally a wavefunction in a multifractal metal is identical to the one in a multifractal insulator inside the localization radius. However, the global normalization  $\sum_{\mathbf{r}} |\psi(\mathbf{r})|^2 = 1$  requires the reduction of  $|\psi|^2$  by a factor of  $L_{\text{corr}}^d/\mathcal{V}$  compared to the case of insulator. Thus, we can formulate the rule (valid provided that  $\ell \ll L_\omega \ll L_{\text{corr}}$ ) for the estimation of the matrix elements in the multifractal metal if their counterparts in the multifractal insulator are known. One has (i) to multiply the result for insulator by a factor  $(L_{\text{corr}}^d/\mathcal{V})^q$ , where  $q$  is the total number of  $|\psi|^2$  in the matrix element in order to take into account the normalization and (ii) to eliminate the overlap probability factor  $(L_{\text{corr}}^d/\mathcal{V})^n$ , where  $n$  is the number of different wavefunctions, which is no longer needed for the extended metal states. Thus the overall factor to add is  $(L_{\text{corr}}^d/\mathcal{V})^{q-n}$ . This immediately leads to

$$\langle M_i \rangle \sim \frac{1}{\mathcal{V}} (L_{\text{corr}}/\ell)^{d-d_2}, \quad (64)$$

$$\langle |M_{ikil}|^2 \rangle_{\text{typ}} \sim \frac{1}{\mathcal{V}^3} (L_{\text{corr}}/\ell)^{(d-d_2)} L_\omega^d (E_0/\omega)^\gamma. \quad (65)$$

The averages  $\langle M_{ij} \rangle$ ,  $\langle |M_{ijkl}|^2 \rangle$ , and  $\langle M_{ikil} M_{jljk} \rangle$  do not change and have the same order of magnitude on the both side of the transition provided that the condition Eq.(60) (with  $L_{\text{corr}}$  replacing  $L_{\text{loc}}$ ) is respected.

### 2.2.5. Matrix elements of the off-critical states beyond the multifractal frequency domain.

As we have seen in the previous subsections, in the multifractal metal and insulator characterized by the large correlation/localization length  $L_{\text{loc}}, L_{\text{corr}} \gg \ell$ , the wavefunction correlations are very similar to those of the critical multifractal states at the Anderson transition point. However, this correspondence is only valid if the energy separation  $\omega$  between the states lies in the multifractal frequency domain,  $\delta_L < \omega < E_0$ , bounded by effective level spacing,  $\delta_L$ , and high frequency cutoff,  $E_0$ . If one or several energy separations are beyond the multifractal frequency domain, the frequency-dependent factors in the estimates change. If all energy separations are larger than  $E_0$  the frequency-dependent factors decrease very fast, so  $E_0$  provides the high-frequency cut-off for all wave function correlations.

More delicate is the case where all energy separations are smaller than  $\delta_L$ . The behavior of the matrix elements in this region is different in the multifractal metal and in the insulator. In the multifractal metal, the  $\omega$ -dependent factors simply saturate [77]. In contrast, in the multifractal insulator they acquire additional powers of  $\ln(\delta_L/\omega)$ .

The logarithmic enhancement factor appearing in the insulator reflects the Mott's physics of the resonance mixing of states; this effect is also responsible for the logarithmic factors in the expression for the low-frequency conductivity:  $\sigma \sim \omega^2 \ln^{d+1}(\delta_L/\omega)$ . The key element of this phenomenon is that localized states with close energies cannot be considered independent even when the distance between centers of localization is large compared to  $L_{\text{loc}}$ . To understand the origin of the correlations, we repeat the Dyson arguments for the level statistics. Consider two typical localized states with small energy separation  $\delta E < \delta_L$  at distance  $R > L_{\text{loc}}$  from each other and vary the disorder potential. The states cease to become orthogonal to each other, their typical overlap decreases as  $t \sim \delta_L \exp(-R/L_{\text{loc}})$  with distance. The energy splitting of the two states becomes  $\omega = ((\delta E)^2 + t^2)^{1/2}$ . If  $R \lesssim L_{\text{loc}} \ln(\delta_L/\omega)$  the typical overlap between two states at distance  $R$  is larger than  $\omega$  which implies that small energy splittings are dominated by rare events when  $t \sim \delta E \sim \omega$ . This implies that in a typical situation the states at distance  $R$  hybridize forming superpositions  $\psi_{\pm}(\mathbf{r}) = \cos \alpha_{\pm} \psi_1(\mathbf{r}) + \sin \alpha_{\pm} \psi_2(\mathbf{r})$  of the parent states  $\psi_{1,2}(\mathbf{r})$  with  $\alpha_{\pm} \sim 1$ . This resonance hybridization makes even remote in space parent states mix with each other, provided that the distance between their centers of localization is less than the optimal one  $R \lesssim R_0 \sim L_{\text{loc}} \ln(\delta_L/\omega) \gg L_{\text{loc}}$ .

The definition of  $R_0$  convenient for numerical study is given in terms of the dipole-moment matrix element:

$$R_0^2(\omega) = d \frac{\sum_{i \neq j} x_{ij}^2 M_{ij} \delta(\omega - \xi_i + \xi_j)}{\sum_{i \neq j} M_{ij} \delta(\omega - \xi_i + \xi_j)} \quad (66)$$

where

$$x_{ij} = 2 \int d^d \mathbf{r} \psi_i^*(\mathbf{r}) x \psi_j(\mathbf{r}). \quad (67)$$

The definition (66,67) is useful in the range of relatively well-localized states, at  $\omega \ll \delta_L$ . One can easily check that for the extreme strong localization  $|\psi_{1,2}(\mathbf{r})|^2 = \delta(\mathbf{r} - \mathbf{r}_{1,2})$  the matrix element  $x_{ij} = x_1 - x_2$  corresponding to  $\psi_{i,j} = \psi_{\pm}$  is equal to the  $x$ -component of the distance between centers of localization of the parent states. The results of numerical computation of (66), (67) for the 3D Anderson model are presented in Fig.2.2.5 for  $E_F =$

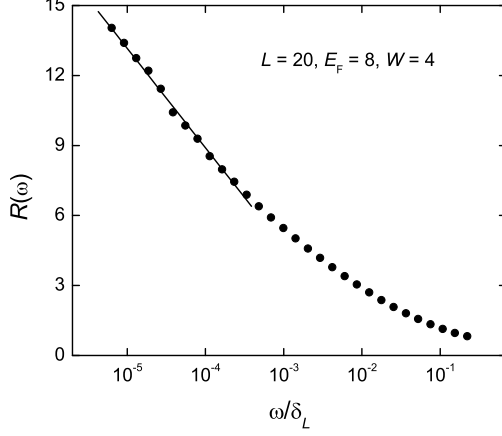


Figure 11: Logarithmic dependence of  $R_0$  on  $\omega$  for the 3D Anderson model with  $W = 4$  and  $E_F = 8.0$  well in the localized region. At this value of the energy the localization radius  $L_{\text{loc}} = (\nu_0 \delta_L)^{-1/3} \approx 3$  (this estimate follows from the data for  $\nu_0$  shown in Fig. 4 and for  $\delta_L$  shown in Fig. 27). The linear in  $\ln \omega$  fit at small  $\omega$  corresponds to  $R(\omega) = A \ln \delta_L / \omega + B$  with  $A = 1.9 \pm 0.05$ ,  $B = -8.1 \pm 0.4$ . It is valid in the region where  $R(\omega)$  is larger than  $2L_{\text{loc}}$ .

8.0. As expected,  $R_0(\omega)$  is linear in  $\ln(\omega)$  at very low values of  $\omega/\delta_L$ . However, there is a broad transient regime with essentially non-linear in  $\ln \omega$  behavior for moderately small  $\omega$ . It is important to note that the values of  $R(\omega)$  in this regime are smaller or comparable than  $2L_{\text{loc}}$  (estimated from the inverse participation ratio, with the use of data for the DoS value and typical level spacing  $\delta_L$ ) which is the minimum distance between centers of localization where the Mott's physics of resonance mixing strictly applies.

It was shown in Ref.[77] that the matrix element  $M_{ij}$  is proportional to  $R_0^{d-1}(\omega)$ . This result can be also justified by the perturbation theory arguments similar to those used in the derivation  $R_0 \sim L_{\text{loc}} \ln(\delta_L/\omega)$ . Consider the parent states that are strongly localized at sites  $m, n$  and have a distance  $R = |\mathbf{R}_m - \mathbf{R}_n|$  between centers of their localization. We now vary the realization of disorder and treat the matrix element of the corresponding change of the disorder potential  $H_{mn}$  as a perturbation. The amplitude of the eigenfunction  $|\psi_m(\mathbf{R}_n)|^2$  at a (remote from its center of localization  $\mathbf{R}_m$ ) site  $\mathbf{R}_n$  becomes of the order of

$$|\psi_m(\mathbf{R}_n)|^2 \sim \frac{|H_{nm}|^2}{(E_n - E_m)^2} \sim \left(\frac{\delta_L}{\omega}\right)^2 e^{-R/L_{\text{loc}}}.$$

The matrix element is given by

$$M_{ij} \propto \sum_{\text{parent states}} \sum_r |\psi_m(\mathbf{r})|^2 |\psi_n(\mathbf{r})|^2 \approx 2 |\psi_m(\mathbf{R}_n)|^2 \propto \left(\frac{\delta_L}{\omega}\right)^2 \int_{R_0}^{\infty} dR R^{d-1} e^{-R/L_{\text{loc}}}.$$

Here instead of summing over the parent states we integrate over the distance between

the centers of localization  $R$  taking into account the statistical repulsion of centers of localization at  $R < R_0 \sim L_{\text{loc}} \ln(\delta_L/\omega)$ . The final expression in terms of the integral over  $R$  is similar to the corresponding expression for the Mott's frequency-dependent conductivity but differs from it by an extra  $R^2$  because of the square of the dipole moment matrix element and an extra  $\omega^2$  in front of the integral. The estimate of the integral in the limit  $R_0 \gg L_{\text{loc}}$  finally gives  $M_{ij} \propto R_0^{d-1}$  and  $\sigma(\omega) \propto \omega^2 R_0^{d+1}$ .

Summarizing the results of this analysis we conclude that the Eq.(44) for  $M_{ij}$  in the multifractal insulator becomes

$$\langle M_{ij} \rangle = \mathcal{V}^{-1} \left( \frac{E_0}{\delta_L} \right)^{\gamma^{\text{eff}}} \begin{cases} \ln^2 \left( \frac{\delta_L}{\omega} \right), & \omega \ll \delta_L \\ \left( \frac{\delta_L}{\omega} \right)^{\gamma^{\text{eff}}}, & \omega \gg \delta_L \end{cases} \quad (68)$$

A simple analytic expression that smoothly interpolates between these two asymptotes in Eq.(68) can be written for the function  $M(\omega) = \mathcal{V} \langle M_{ij} \rangle$  with  $\omega = \xi_i - \xi_j$ :

$$M(\omega) = \frac{\left( \frac{E_0}{\delta_L} \right)^{\gamma^{\text{eff}}} \ln^2 \left( \frac{\delta_L}{\omega} + c \right)}{\left( \frac{\omega}{\delta_L} \right)^{\gamma^{\text{eff}}} \ln^2 \left( \frac{\delta_L}{\omega} + c \right) + 1}, \quad (69)$$

where the constant  $c > 1$ . One should also take into account small variations of the effective fractal dimension  $d_2^{\text{eff}}$  as  $E_F$  moves away from the mobility edge or the disorder parameter  $W$  moves away from the critical value [77]. This results in the dependence of the effective exponent:

$$\gamma^{\text{eff}} = 1 - d_2/d + a(\delta_L/E_0), \quad a > 0. \quad (70)$$

The energy scale  $\delta_L$  can be expressed through the inverse participation ratio  $\langle M_i \rangle$  in the form which is convenient for numerical simulations:

$$\delta_L = E_0 \left( \frac{\langle M_i \rangle}{3\nu_0 E_0} \right)^{\frac{3}{d_2}} \quad (71)$$

Finally, the upper fractality scale  $E_0$  can be found from the condition  $\mathcal{V} \langle M_{ij} \rangle \approx 1$  at  $\omega = E_0$ .

The enhancement, Eqs.(68,69), of the overlap of two localized wavefunctions results from the fact that the eigenfunctions which are anomalously close to each other in the energy space (closer than  $\delta_L$  for the localized wavefunctions) are automatically well overlapping, as they are just the symmetric and anti-symmetric combinations of the one and the same pair of localized wavefunctions with the optimal distance between their centers of localization being  $R_\omega \sim L_{\text{loc}} \ln(\delta_L/\omega)$ . The most important consequence of this phenomenon is that in 3D case the correlation function  $M(\omega)$  continues to grow at low frequencies as  $\log^2 \frac{\delta_L}{\omega}$ , which makes it possible to establish the superconductive order in some part of the domain  $T_c \ll \delta_L$ , as will be discussed below in section 6.

### 3. Insulating state.

In this section we discuss the physical properties of the insulating state in the vicinity of superconductor-insulator transition and show that it is characterized by the large



single particle gap which is responsible for the activation temperature dependence of conductivity,  $\sigma(T) \propto \exp(-T_I/T)$ , observed in many works[46, 30, 21] at low temperatures on the insulating side of the transition. We start by assuming that Fermi energy  $E_F$  is deep inside the region of localized states, so that the interaction of electrons from different localized orbitals is weak and leads merely to a small perturbation. Then the Hamiltonian (9) can be further simplified to

$$H_3 = \sum_{j\sigma} \xi_j c_{j\sigma}^\dagger c_{j\sigma} - g \sum_j M_j c_{j\uparrow}^\dagger c_{j\downarrow}^\dagger c_{j\downarrow} c_{j\uparrow}, \quad (72)$$

where the scaling estimate for the typical value of matrix elements  $M_j = \int dr \psi_j^4(r)$  is given by Eq.(61) above. We will refer to the last term in (72) as to the *local pairing coupling*; formally it looks like the “negative-U” local attraction considered in [5].

The operator product in the last term in Eq.(72) is identical to the occupation number product  $n_{j\uparrow} n_{j\downarrow}$  which is equal to 1 if both available electrons states are populated, and to 0 otherwise. Thus the only role of the interaction term in (72) is to shift down energies of all double-occupied orbitals. Note that one does not encounter such a term in usual theory of disordered superconductors, since  $M_i$  vanishes in the thermodynamic limit for delocalized electronic states (compare Eqs.(61),(64)).

Let us order all eigenstates  $\psi_j$  according to the increase of eigenvalues  $\xi_j$ . Then the last filled eigenstate  $\psi_m$  of the Fermi-sea (at  $T = 0$ ) for *even* total number of electrons is defined by inequality

$$2\xi_m - gM_m < 0 < 2\xi_{m+1} - gM_{m+1} \quad (73)$$

(we count all single-particle energies from the Fermi-energy). In a macroscopic system, the energy interval in (73) vanishes as the inverse volume,  $1/\mathcal{V}$ . Within the “even subspace” of the whole Hilbert space (i.e. each orbital is either empty or double-occupied), the local pairing can be fully accounted for by the redefinition  $\xi_j \rightarrow \tilde{\xi}_j = \xi_j - \frac{g}{2}M_j$ . However, single-occupied orbitals are not involved in this interaction.

The increase of thermodynamic potential  $\Omega$  due to addition of *odd* electron to the ground-state is

$$\begin{aligned} \delta\Omega_{oe} &= \xi_{m+1} = \xi_{m+1} - \tilde{\xi}_{m+1} + \tilde{\xi}_{m+1} = \\ &= \frac{g}{2}M_{m+1} + O(\mathcal{V}^{-1}) \end{aligned} \quad (74)$$

Using the Eq.(61) we estimate typical value of  $\delta\Omega_{oe}$ :

$$\delta\Omega_{oe}^{typ} = \frac{3}{2}g\ell^{-3}(L_{loc}/\ell)^{-d_2}. \quad (75)$$

where  $L_{loc}$  is the localization length for the states with  $E = E_F$ .

Consider now two single-electron excitations on top of a fully paired Fermi-sea defined by Eq.(73), which are produced by transferring of one electron from the  $m$ -th state to the  $m+1$ -th one. The energy of the two single-particle excitations (which results from the depairing) is

$$2\Delta_P^{(m)} = \xi_{m+1} - \xi_m + gM_m = \frac{g}{2}(M_m + M_{m+1}) + O(\mathcal{V}^{-1}) \quad (76)$$

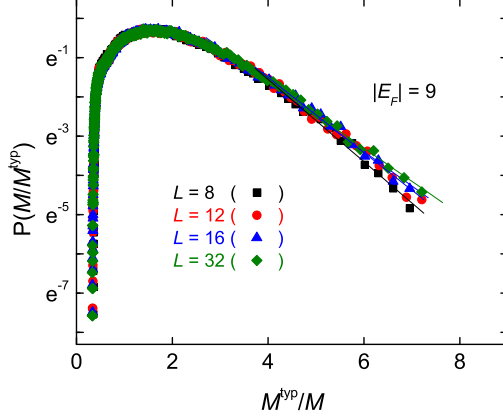


Figure 12: (Color online) Distribution of the inverse participation ratios  $P_2$  for the 3d Anderson model at the Fermi energy  $E_F = 9.0$  on the insulating side of SIT (the mobility edge  $E_c = 5.5$ ) for different system sizes.

thus the typical value of the pairing energy  $\Delta_P$  is also given by Eq.(75):

$$\Delta_P = \frac{3}{2}g\ell^{-3}(L_{loc}/\ell)^{-d_2} = \frac{3\lambda}{2}E_0 \left( \frac{E_c - E_F}{E_0} \right)^{\nu d_2} \quad (77)$$

In the right-hand side of (77) we reintroduced the dimensionless coupling  $\lambda = g\nu_0$  and the parameter  $E_0 = 1/(\nu_0\ell^3)$  which determines the high-energy cutoff for fractal correlations and we also employed Eq.(16). The average single-particle density of states  $\nu(\varepsilon)$  is determined by the probability distribution  $\mathcal{P}(M)$  of inverse participation ratios  $M_j$ . Namely, the probability to find an excitation with the energy  $\varepsilon$  coincides (in the limit  $\mathcal{V} \rightarrow \infty$ ) with the probability to find a value of inverse participation ratio  $M \leq \frac{2\varepsilon}{g}$ . Therefore

$$\nu(\varepsilon) = \nu_0 \int_0^{2\varepsilon/g} \mathcal{P}(M) dM \quad (78)$$

We have generated the distribution function  $\mathcal{P}(M)$  numerically, using the three dimensional Anderson model with the Gaussian distribution of local energies, Eq.(23) with  $W = 4$ . The mobility edge in such a model is located at  $|E| = 5.5$ .

Numerical data for the distribution function  $\mathcal{P}(M)$  are shown in Fig.12 for several sizes  $L$  and the Fermi energy  $E = 9.0$  in the localized part of the spectrum. These data demonstrate a sharp drop of  $\mathcal{P}(M)$  at the values of  $M$  much smaller than the typical value  $M^{\text{typ}}$ , as well as a considerable size-dependence of the slope. Fig.12 shows that the low  $M$  tail can be well approximated by the exponential dependence

$$\mathcal{P}(M) \propto e^{-c(M^{\text{typ}}/M)} \quad \text{for } M \ll M^{\text{typ}} \quad (79)$$

where the coefficient  $c$  depends on the energy  $E_F$ . We used the finite-size scaling together with an extrapolation to large  $L$  limit in order to get the values of  $c$  appropriate for a

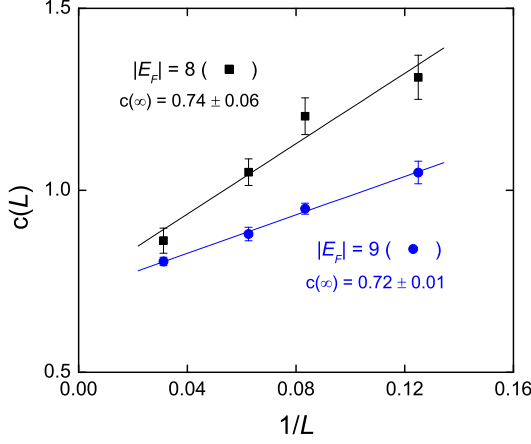


Figure 13: (Color online) The exponent  $c$  of the small-IPR tail of the distribution function  $P(M/M^{\text{typ}})$  at the energies  $E_F = 8.0$ , and  $9.0$  for different sizes  $L$ , together with extrapolated value  $c_\infty$  for each energy.

macroscopic system. The results obtained for energies  $E_F = 8.0$  and  $9.0$  are shown in Fig.13. The data shown in Fig.13 demonstrate that the extrapolated (at  $L \rightarrow \infty$ ) value of the coefficient  $c$  saturates in the interval

$$c \approx 0.73 \pm 0.05 \quad (80)$$

for the Fermi energies deep enough in the localized band. This is in agreement with the one-parameter character of the distribution  $\mathcal{P}(M) \equiv \mathcal{P}(M/M^{\text{typ}})$  in the  $L \rightarrow \infty$  limit.

In Fig. 14 we also present the linear scale data for the distribution function  $P(y)$  of local gaps  $\Delta_P$ , (at the Fermi-energy  $E_F = 8.0$ ), normalized to the typical value  $\Delta_P^{\text{typ}}$ . Note that the data both for large and for small  $y$  can be fitted quite accurately by an analytical expression shown on the plot which contains exponential factors and  $1/y^2$  dependence relevant for the intermediate  $1 < y < 6$ . This modification leads to a somewhat larger coefficient  $c$  in the exponential dependence  $e^{-c/y}$ .

We use the numerical data for  $\mathcal{P}(M)$  to obtain, according to Eq.(78), the average density of single-electron states. The results are shown (for the two Fermi-level positions  $E_F = 8.0$  and  $E_F = 9.0$ ) in Fig.15. Both plots for DoS  $\nu(\varepsilon)$  nearly coincide while expressed as functions of the reduced variables  $\varepsilon/\Delta_P$  in the most interesting region  $x \leq 1.5$ . At the lowest energies DoS decays exponentially,  $\nu_{<}( \varepsilon ) \approx \nu_0 e^{-c\Delta_P/\varepsilon}$ . The similar results for the low energy DoS were obtained in [5] (see Fig.16b of Ref. [5]).

Practically, the shape shown in Fig.15 implies the existence of a nearly hard gap

$$\Delta_1 = c_1 \Delta_P = \frac{3c_1}{2} \lambda E_0 \left( \frac{E_c - E_F}{E_0} \right)^{\nu d_2} \quad c_1 \approx 0.2 - 0.3 \quad (81)$$

The average density of states could be measured directly by the tunneling conductance via a large-area tunnel junction. The problem with such measurement in an insulator

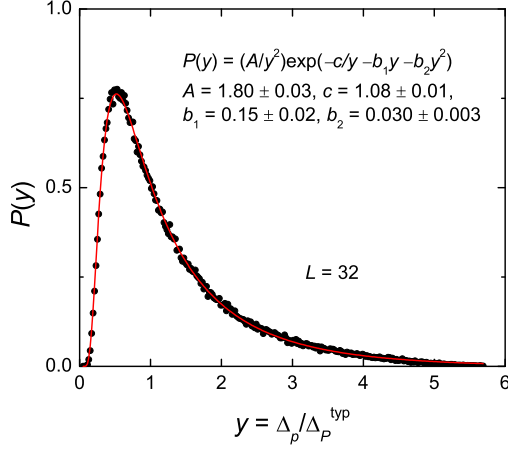


Figure 14: (Color online) Distribution function for the normalized local gaps  $y = \Delta_P / \Delta_P^{\text{typ}}$ , at the Fermi energy  $E_F = 8.0$  on the insulating side of SIT (the mobility edge  $E_c = 5.5$ ).

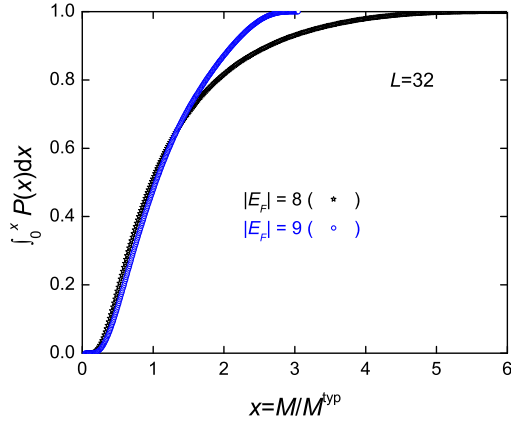


Figure 15: (Color online) Gap in the one-particle density of states due to local pairing of electrons on the localized states at the energies  $E_F = 8.0$  (black stars) and  $E_F = 9.0$  (blue circles). Scaling with  $x = M_i / M_{\text{typ}}$  for relatively small  $x$  is demonstrated.

is that electrons should be evacuated somewhere after tunneling, otherwise the strong Coulomb blockade would make the measurement impossible. A possible method to avoid the Coulomb blockade might be to study tunneling conductance through a relatively thin film with both its surfaces weakly coupled to metal contacts.

The local tunneling conductance measured by STM is expected to show a threshold behavior with  $\Delta_P^{(m)}$  corresponding to the state  $m$  localized near the observation point in real space and with  $\tilde{\xi}_m$  close to the Fermi energy. The local gap  $\Delta_P^{(m)}$  fluctuates from point to point and is distributed according to Fig.15. We are not aware of such measurements in the insulating state, the data on the superconducting side of SIT are given in Ref. [42], for temperatures both above and below  $T_c$ . We present detailed results for the tunneling conductance as a function of temperature in section 6.2.

Above the transition temperature the data [42] show large suppression of the density of states without any coherence peak that appear at the gap edges below  $T_c$ . The absence of coherence peaks at the gap threshold shows the qualitative difference between the local pairing gap due to simple binding of two localized electrons and the BCS gap appearing due to the *many-body correlations* within the energy range  $\sim \Delta_{\text{BCS}}$  around the Fermi-level that one expects in the small grain of superconductor. In the case of fractal localized states *all* filled (double-occupied) levels are shifted down in energy, thus the total number of states near the Fermi-energy (in a stripe of several  $\Delta_P$  width) is *not* conserved and there is no reason for appearance of a peak above the gap. In that sense, the local pairing (due to attraction!) plays the role similar to that of the Coulomb repulsion in suppressing the tunneling conductance.

The above results were obtained neglecting all matrix elements of interaction except from *super-diagonal* ones,  $M_j$ . We now discuss the validity of this approximation. Indeed, in the problem of ultra-small grains treated by Matveev and Larkin [37], the *diagonal* matrix elements  $M_{ij}$  were taken into account while calculating the parity gap (14), via the renormalization (13) of the local pairing energy. This renormalization was necessary (even for  $\lambda \ll 1$ ) due to the ultraviolet (UV) divergency in the Cooper loop diagrams. Pairing on the fractal eigenstates is of different nature: the frequency-dependence (44) of matrix elements  $M_{ij}$  eliminates the UV divergence, thus the virtual  $i \rightarrow j$  transitions can be neglected and the high-energy cutoff  $\omega_D$  is not necessary as long as  $\delta_L \gg T_c^0$ . Here  $T_c^0$  is the superconducting transition temperature for  $E_F$  at the mobility edge  $E_c$  given (within modified mean-field approximation developed below in section 4) by Eq.(164). Using of Eqs.(71,81,164) one can eliminate the model parameters  $E_0$  and  $\lambda$  and express the local gap  $\Delta_1$  via the observable quantities  $T_c^0$  and  $\delta_L$ :

$$\Delta_1 = \frac{3c_1}{2C^\gamma} \frac{\delta_L}{(\delta_L/T_c^0)^\gamma} \approx 0.2 \frac{\delta_L}{(\delta_L/T_c^0)^\gamma} \quad (82)$$

where for the 3D Anderson transition  $\gamma = 0.57$  and  $C \equiv C(0.57) \approx 3.1$ . The relation (82) shows that in the insulating region  $\delta_L \gg T_c^0$  due to the nonzero fractal exponent  $\gamma$  the local gap value  $\Delta_1$  grows with  $\delta_L$  much weaker than  $\delta_L$  itself. In the limit  $\gamma \rightarrow 0$  Eq.(82) transforms into the analog of the Matveev-Larkin relation (14), after a sub-leading term in the denominator of (82) is taken into account via a substitution  $\gamma (\delta_L/T_c^0)^\gamma \rightarrow (\delta_L/T_c^0)^\gamma - 1$ .

Now we turn to the discussion of the intrinsic low-temperature conductivity of the insulator with localized pairs. The binding of electrons into local pairs diminishes the

single-particle DoS and thus suppresses the variable-range hopping conductivity. A classical example of such an effect is the "Coulomb gap" due to Efros and Shklovsky: the soft gap  $\nu(E) \sim E^2$  in the average DoS leads to a transformation of the Mott law  $\sigma(T) \propto e^{-(T_M/T)^{1/4}}$  into the Efros-Shklovsky law  $\sigma(T) \propto e^{-(T_{ES}/T)^{1/2}}$ . In our case the low-energy states are exponentially rare, and their account leads to the logarithmic in temperature corrections to the activation energy determined by the hard gap (81):

$$\sigma(T) \propto \exp \left[ -\frac{T_0}{T \ln(T_0/T)} \right]. \quad (83)$$

where

$$T_0 = \frac{c}{3} \Delta_P \approx 0.25 \Delta_P \quad (84)$$

Note that the nearly activated behavior given by Eqs.(83) and (84) can hardly be distinguished from the purely activate one with the activation gap  $\Delta_1$  given by (81) or (82) in the limited temperature range available in most experiments.

We thus associate the spectral gap  $\Delta_1$  with the measured [46, 30] activation energy  $T_I$ . The external parameter  $(E_c - E_F)$  representing the disorder strength in Eq. (81) can be replaced with an experimentally more accessible parameter  $(1 - \sigma/\sigma_c) \propto (E_c - E_F)/E_0$ . Here  $\sigma$  is the high temperature conductivity and  $\sigma_c$  is the value of the conductivity where the parity gap  $\Delta_P$  first develops. We obtain

$$T_I = A(1 - \sigma/\sigma_c)^{\nu d_2}, \quad A \approx 0.5\lambda E_0 \quad (85)$$

where  $A$  is conductivity-independent. This equation predicts a moderate increase of  $T_I$  with disorder strength in agreement with the experimental data [46], see Fig. 16. The

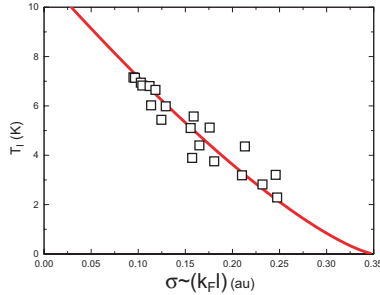


Figure 16: Experimental values of the gap from Ref.[46],  $T_I$  (boxes) and a fit to the equation (85) with  $\nu_{av} = 1$ ,  $d_2 = 1.3$ .

only fitting parameter used in Fig. 16 was the value of the constant  $A = 0.5\lambda E_0 \approx 10K$ . Assuming the applicability of the BCS theory for (less disordered) superconductive  $\text{InO}_x$  samples [46], and using [83] the estimates  $\omega_D \approx 500K$  for Debye frequency, we find  $\lambda \approx 0.2$  and  $E_0 \approx 100K$ .

Applicability of the scaling formulas to the above analysis is not obvious. Indeed, the value of  $1 - \sigma/\sigma_c \approx 2/3$  for the most insulating sample on the plot of Fig.16. We have demonstrated, however, that the correlation function  $M(\omega)$  (see Fig 5) which is closely related to the inverse participation ratio, is approximately described by the critical

scaling even deeply inside the insulating phase. Then assuming that Eq.(16) also holds approximately in a relatively wide interval of  $1 - \sigma/\sigma_c$  (although, perhaps, with some "average" exponent  $\nu_{av}$  instead of  $\nu$ ) we obtain an extrapolation of Eq.(85) for an entire interval of  $\sigma/\sigma_c$  relevant for the experiment. Note that the classical experiments on Si:P system have shown that unless the special care was taken to shrink the interval of  $1 - \sigma/\sigma_c$  to be much smaller than 1, the observed scaling of localization radius was characterized by the exponent  $\nu_{av} < 1.5$ , see Fig. 2. That is why it is not surprising that reasonable fit to the experimental data shown in Fig. 16 corresponds to the choice  $\nu_{av} = 1$ .

There are a few reasons why the estimated value of  $E_0 \approx 100K$  turned out to be low in comparison with the Fermi energy  $E_F \sim 0.3eV$  for amorphous  $InO_x$  samples with the electron density in the range of  $10^{21}cm^{-3}$ . This value implies that ratio  $E_0/E_F \sim 0.03$  is one order of magnitude lower than our estimate (46) obtained for the 3D Anderson model with Gaussian disorder (which, however, should not be expected to be quantitatively correct for a- $InO_x$ ). First, this estimate of  $E_0$  uses BCS formula to related the value of the critical temperature in the less disordered samples  $T_c \approx 3K$  [46] to the value of the coupling constant in all materials of these series. The BCS formula is however qualitatively wrong for the samples close to mobility edge, which are in the regime discussed in the section 4. In this regime the critical temperature is given by (164) which leads to a much lower value of the interaction constant  $\lambda \approx 0.02$ . The estimate for the upper energy cutoff  $E_0$  becomes  $1000K$  which is in agreement with (46). This estimate neglects the effect of thermal fluctuations discussed in section 4.2.5, the effect of these fluctuations is to reduce  $T_c$  so the actual value of the interaction constant corresponding to the sample close to the mobility edge with  $T_c \approx 3K$  might be slightly larger  $\lambda \approx 0.03 - 0.05$  corresponding to  $E_0 \approx 400 - 600K$ . These values of  $E_0/E_F \sim 0.1 - 0.3$  are roughly what one expects from the analysis of the three dimensional Anderson model. Finally, we note that appearance of low energy scales in the insulating samples of  $InO_x$  was conjectured in the early paper [84] for completely different reasons. All these arguments demonstrate that the values of  $\lambda$  and  $E_0$  that we obtain from the fit of the experimental data are roughly what one should expect in these samples.

The reasonable fit to the data was made possible by a small value of the exponent in Eq.(85) which is substantially less than  $\nu d \approx 3$  due to eigenfunction fractality. Thus, the data [46] provide the indirect evidence for the eigenfunctions fractality in the insulating samples of  $InO_x$ .

#### 4. Cooper instability near the mobility edge: the formalism.

In this section we develop approximation schemes to treat the Cooper instability and superconducting order formation in the regime when the Anderson theorem [35, 36] is not valid due to very strong disorder. Namely, in section 4.1 we give two versions of the modified mean-field approximations, MFA, for determination of the superconductive transition temperature  $T_c$ ; in section 4.2 we derive an analog of the Ginzburg-Landau functional which is necessary to estimate the role of fluctuations beyond the modified MFA, and in section 4.4 we give an alternative method of  $T_c$  determination: the virial expansion. The nature of approximations involved in the modified MFA and the virial expansion methods are very different, thus reasonable agreement between the results obtained by these methods indicates the validity of both of them. We show that in a wide region near the mobility edge the dependence of the superconducting critical temperature

on the interaction constant can be found *analytically* with the accuracy up to a pre-factor of the order of one despite of the presence of strong thermal and mesoscopic fluctuations. In a more disordered sample the critical temperature can be determined using the semi-analytical approach of virial expansion applied to the *pseudo-spin Hamiltonian*. The results of this section allow to suggest the pseudo-spin Hamiltonian that provides a unified description of superconductivity in homogeneously disordered (*non-granular*) systems including the BCS regime and the region close to the superconductor-insulator transition.

#### 4.1. Modified mean-field approximation.

The goal of this subsection is to develop two versions of a modified mean-field approximations that can be used to determine the critical temperature of a fractal superconductor. We start from the standard Abrikosov-Gor'kov-Anderson [35, 36] mean-field equation for  $T_c$  of a disordered superconductor:

$$\Delta(\mathbf{r}) = \int d^d \mathbf{r}' K(\mathbf{r}, \mathbf{r}') \Delta(\mathbf{r}'). \quad (86)$$

The kernel  $K(\mathbf{r}, \mathbf{r}')$  is defined by

$$K(\mathbf{r}, \mathbf{r}') = \frac{g}{2} \sum_{ij} \eta_{ij} \psi_i(\mathbf{r}) \psi_j(\mathbf{r}) \psi_j(\mathbf{r}') \psi_i(\mathbf{r}'), \quad (87)$$

where  $\psi_j(\mathbf{r})$  are exact single-electron wavefunctions and

$$\eta_{ij} = \frac{\tanh(\xi_i/2T) + \tanh(\xi_j/2T)}{\xi_i + \xi_j}, \quad \eta_i \equiv \eta_{ii}. \quad (88)$$

Within the standard mean-field approximation, one neglects the spatial variations of  $\Delta(\mathbf{r})$ . Then integrating over  $\mathbf{r}$  in Eq.(86) and using the orthogonality and normalization of different single-particle wavefunctions one can eliminate all  $\psi_i(\mathbf{r})$  out of Eq.(86). Note that it is only possible if the wave functions are real,  $\psi_i^*(\mathbf{r}) = \psi_i(\mathbf{r})$ , i.e. the time-reversal symmetry is preserved. This leads immediately to the well-known equation for  $T_c$  in terms of DoS function  $\nu(\xi)$ :

$$1 = \frac{g}{2} \sum_i \eta_i \equiv \frac{\lambda}{2\nu_0} \int d\xi \nu(\xi) \eta(\xi) \quad (89)$$

where  $\eta_i \equiv \eta_{ii} = \xi_i^{-1} \tanh(\xi_i/2T)$ .

However, the approximation of a constant  $\Delta$  cannot be used under strong disorder conditions near the mobility edge. Physically it is due to strong mesoscopic fluctuations of the local DoS function  $\nu(\xi, \mathbf{r})$ , see [4]. Below we propose a modification of the MFA scheme which makes it possible to account for the major part of mesoscopic DoS fluctuations.

To construct the modified MFA, we note that the appearance of the solution to the Eq.(86) is equivalent to the divergence of the series  $\text{Tr}(1 - K)^{-1} = \sum_{n=0}^{\infty} \text{Tr} K^n$ . By d'Alambert criterion the latter is equivalent to the condition

$$\lim_{n \rightarrow \infty} \frac{\text{Tr} K^{n+1}}{\text{Tr} K^n} = 1. \quad (90)$$



Explicitly, the trace  $\text{Tr}K^n$  can be written as

$$\begin{aligned} \text{Tr}K^n &= (g/2)^n \sum_{i_1 j_1 \dots i_n j_n} \eta_{i_1 j_1} \dots \eta_{i_n j_n} \\ &\times M_{j_n i_n i_1 j_1} M_{j_1 i_1 i_2 j_2} \dots M_{j_{n-1} i_{n-1} i_n j_n}, \end{aligned} \quad (91)$$

where  $M_{ijkl}$  is defined in Eq.(8).

Now we make a crucial approximation: we neglect all the *off-diagonal matrix elements* in Eq.(8) with more than two different indices. The *diagonal* matrix elements  $M_{ij} = M_{iijj} = M_{ijij} = M_{ijji}$  with only two different indices will be retained. By so doing, we neglect thermal fluctuations of the superconductive order parameter; we also neglect a part of mesoscopic fluctuations, whereas the most important type of the them (i.e. fluctuations of the local density of states) will be taken into account. Thus our approach has a meaning of a modified mean-field approximation. The neglected off-diagonal terms determine the strength of fluctuations on top of the modified MFA solution. We derive the corresponding Ginzburg-Landau functional and estimate the role of such fluctuations in subsection 4.2 below.

There are two ways to impose the “diagonal constraints” the for matrix elements  $M_{ijkl}$ : (i) to set  $i_l = j_l$  thus imposing  $n$  constrains in Eq.(92), or (ii) to set  $j_l = j_{l'}$  or  $j_l = i_{l'}$  with  $l \neq l'$ . In this case one imposes  $2n - 2$  constrains, so that only 2 summations will remain. As any summation gives a macroscopically large number of terms, one can neglect all terms corresponding to (ii) in the thermodynamic limit  $N \rightarrow \infty$ . Thus, upon neglect of off-diagonal matrix elements one finds eventually

$$\text{Tr}K^n \approx (g/2)^n \sum_{i_1 \dots i_n} \eta_{i_1} \eta_{i_2} \dots \eta_{i_n} M_{i_n i_1} M_{i_1 i_2} \dots M_{i_{n-1} i_n}, \quad (92)$$

where  $M_{ik}$  are defined in Eq.(10). It is easy to show now that the condition given by Eq.(90), with  $\text{Tr}K^n$  defined by Eq.(92), is equivalent to the solvability condition for the equation

$$\Delta_i = \frac{g}{2} \sum_k \Delta_k \eta_k M_{ki}, \quad (93)$$

which is the basis of the modified MFA we will be using below.

The set of new order parameters  $\Delta_i$ , entering Eq.(93), represent the superconducting “ordering field” acting onto a pair of electrons occupying the  $i$ -th orbital  $\psi_i(\mathbf{r})$ . The idea of the approximation is that, instead of using a constant (in real space) order parameter  $\Delta(\mathbf{r}) = \Delta$ , we assume a *smooth* dependence of  $\Delta_i$  on the single-electron energies  $\xi_i$ . Under such an assumption, together with the replacement of  $M_{ik}$  matrix elements by their averages (according to Eq.(44)), the Eq.(93) can be transformed into the integral equation

$$\Delta(\xi) = \frac{\lambda}{2} \int d\zeta \eta(\zeta) M(\xi - \zeta) \Delta(\zeta) \quad (94)$$

Eq.(94) is a natural generalization of the BCS mean field equation which follows from it at  $M(\omega) = 1$ . However, allowing for the energy dependence of  $M(\omega)$  may lead to drastic consequences. Indeed, a simple scaling analysis of this equation with “critical”  $M(\omega) = (E_0/\omega)^\gamma$  given by Eq.(44) leads to the power-law dependence of the critical temperature on the attraction interaction constant  $\lambda$ :

$$T_c \propto E_0 \lambda^{1/\gamma}, \quad (95)$$

where  $\gamma$  is defined in Eqs.(38,45).

We encounter an unexpectedly strong increase of  $T_c$  in the small  $\lambda$  limit with respect to the usual result,  $T_c \propto \exp(-1/\lambda)$  for a conventional BCS superconductor (with the same  $\lambda$ ). The price to pay for this increase is a very strong inhomogeneity in the real space of the local pairing amplitude:

$$\tilde{\Delta}(\mathbf{r}) = \frac{g}{2} \sum_k \Delta_k \eta_k \psi_k^2(\mathbf{r}). \quad (96)$$

The corresponding analysis will be presented in subsection 5.3.

To demonstrate the validity of the solution (96), one needs to plug it into Eq.(86) and to use "diagonal approximation"

$$\int d^d \mathbf{r} \psi_i^2 \psi_j(\mathbf{r}) \psi_i(\mathbf{r}) = M_{ij} \delta_{ij}$$

together with Eq.(93).

The transformation from Eq.(93) to Eq.(94) is not exact: we replaced the fluctuating matrix elements  $M_{ik}$  by their averages according to Eq.(44). Thus Eq.(94) contains an additional (with respect to Eq.(93)) mean-field-type approximation. One can eliminate this additional approximation. For this purpose, let us define the new matrix  $\hat{Q}$  and vectors  $\phi_i$ :

$$Q_{ik} = \frac{g}{2} \sqrt{\eta_i \eta_k} M_{ik} \quad \phi_i = \Delta_i \sqrt{\eta_i} \quad (97)$$

Then the solvability condition for Eq.(93) transforms into the condition that the largest eigenvalue  $k_{\max}$  of the symmetric matrix  $\hat{Q}$  becomes equal to unity. This condition is equivalent to the instability onset with respect to formation of a superconducting order parameter  $\Delta_i$ , as will be seen below in subsection 4.2.1.

In the thermodynamic limit the condition  $k_{\max} = 1$  implies global superconductivity only if the corresponding eigenvector of the matrix  $\hat{Q}$  is *extended*. Otherwise,  $k_{\max} = 1$  means formation of local "islands" of new phase with uncorrelated local order parameters in these islands, it does not immediately result in any global order parameter (for the discussion of relevant examples see [85, 86]). Eigenfunctions of the  $\hat{Q}$  matrix may be localized, if the effective "coordination number" (the bandwidth)  $Z$  of this matrix stays finite in thermodynamic limit. General estimate for the coordination number is  $Z \sim \nu_0 T_c L_{loc}^d$  because the relevant energy window populated by "active" single-particle states (taking part in formation of the many-body superconductive state) is of the order of  $T_c$ , and each eigenstate  $|i\rangle$  is coupled by the the matrix elements  $M_{ij}$  to all neighbors  $|j\rangle$  in the localization volume  $L_{loc}^d$ . This argument shows that as long as the single electron eigenstates are delocalized,  $E_F < E_c$  and *within diagonal approximation*, the effective coordination number  $Z = \infty$  and no localization of the  $\hat{Q}$  eigenstates is possible. However, this conclusion becomes invalid when the off-diagonal matrix elements  $M_{ijkl}$  are taken into account: the lowest eigenstates of the full kernel  $K(r, r')$  get localized. The most important physical consequence of this localization is that, as the temperature is decreased, the superconductivity first appears in small, well separated regions, similarly to the situation realized in superconductors with inhomogeneous  $T_c$  [87]. In the regime of delocalized single electron states a further decrease of temperature results in a more homogeneous superconductivity. As the Fermi energy is increased past the mobility edge,

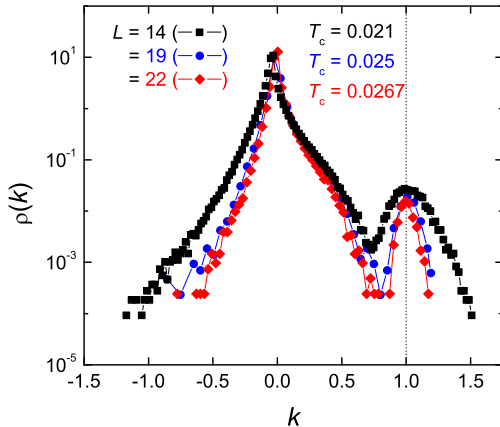


Figure 17: (Color online) Density of states  $\rho(k)$  of the matrix  $\hat{Q}$ , with peak near  $k = 1$ , for  $L = 14$  (black squares),  $L = 19$  (blue dots) and  $L = 22$  (red diamonds).

single electron states get localized and the issue of the  $\hat{Q}$ -eigenfunction localization and resulting inhomogeneity become relevant even within the "diagonal approximation", we discuss this regime in section 6.

Here we present, as an example, the numerically obtained spectrum of the  $\hat{Q}$  matrix for a finite system at the mobility edge. Fig. 17 shows the averaged (over 2000 realizations) density of states for the  $\hat{Q}$  matrix generated for the 3D Anderson model with Gaussian on-site disorder of the strength  $W = 4$ , at the energy  $E = 5.5$  corresponding to the mobility edge. Three system sizes,  $L = 14, 19, 22$  were analyzed. In a finite system the peaks of the finite width are seen in the density of states  $\rho(k)$  near  $k = 1$ . One sees that with the system size increase, the peaks become more narrow, so it is natural to assume that they evolve into a  $\delta$ -function peak in the  $L \rightarrow \infty$  limit. The corresponding temperature (chosen so that to pin the DoS peak position to  $k = 1$ ) is thus associated with  $T_c$ .

In subsection 5.2 we compare results for the critical temperature  $T_c$  obtained by the three methods: modified analytical MFA equation (94), numerical generation of the spectrum of the temperature-dependent matrix  $\hat{Q}$ , with the temperature  $T = T_c$  adjusted so to locate the peak in  $\rho(k)$  at  $k = 1$ , and virial expansion method, to be described in subsection 4.4..

Our modified MFA method is similar in spirit to the usual BCS mean-field approximation: it neglects both thermal and mesoscopic fluctuations of the pairing field  $\Delta(\mathbf{r})$  with respect to its "background configuration". The essence of the modification we used is that our background configuration is *not uniform in real space*. Instead it is given by the function  $\tilde{\Delta}(\mathbf{r})$  defined in Eq.(96). In order to estimate the strength of fluctuations we neglected, we will develop, in the next subsection 4.2, a Ginzburg-Landau description for the order parameter field configurations  $\Delta(\mathbf{r})$  which are *close to the background field*  $\tilde{\Delta}(\mathbf{r})$ .

#### 4.2. Ginzburg - Landau functional.

Here we derive the free energy functional  $F[\Psi(\mathbf{r})]$  defined in terms of a *smooth* envelope function

$$\Psi(\mathbf{r}) = \Delta(\mathbf{r})/\tilde{\Delta}(\mathbf{r}) \quad (98)$$

and valid near the transition temperature  $T_c$  for  $\Psi(\mathbf{r})$  field which smoothly varies in space.

We start by writing the action in terms of the Grassmann fields  $\varphi_n$

$$\begin{aligned} S = & \sum_n \varphi_n^* (-i\omega_n + H_1) \varphi_n + \sum_n \varphi_{-n}^* (i\omega_n + H_1) \varphi_{-n} \\ & - g \sum_{n_1, n_2, n_3} \varphi_{n_1+n_3}^* \varphi_{n_1-n_3}^* \varphi_{-n_1+n_2} \varphi_{-n_1-n_2}. \end{aligned} \quad (99)$$

where  $H_1$  is the single-particle part of the Hamiltonian, given e.g. by Eq.(20) or Eq.(21);  $g$  is the interaction constant and  $n$  and  $n_{1,2,3}$  are the Matsubara frequency summation indices. We decouple the interaction term via the Hubbard-Stratonovich transformation involving the auxiliary field  $\Delta(\mathbf{r}; \Omega_n)$ . Below we focus on the static  $n = 0$  component of this field. In doing so we neglect quantum fluctuations of the order parameter but take into account the thermal and mesoscopic fluctuations.

We expand the Grassmann fields over the eigenstates  $\psi_i(\mathbf{r})$  of the single-electron problem

$$\varphi_n(\mathbf{r}) = \sum_j \chi_j^{(n)} \psi_j(\mathbf{r}) \quad (100)$$

and represent the thermodynamic potential  $S[\Delta, \Phi]$  as

$$S = \frac{1}{g} \sum_r |\Delta(\mathbf{r})|^2 + \sum_n \sum_{i,j} \bar{\Phi}_i^{(n)} \begin{pmatrix} (-i\omega_n + \xi_i) \delta_{ij} & \Delta_{ij} \\ -\Delta_{ij}^* & (-i\omega_n - \xi_i) \delta_{ij} \end{pmatrix} \Phi_j^{(n)}, \quad (101)$$

where

$$\Phi_i^{(n)} = \begin{pmatrix} \chi_i^{(n)} \\ \chi_i^{(-n)*} \end{pmatrix}, \quad \bar{\Phi}_i^{(n)} = (\chi_i^{(n)*} \quad \chi_i^{(-n)}).$$

and

$$\Delta_{ij} = \sum_{\mathbf{r}} \Delta(\mathbf{r}) \psi_i(\mathbf{r}) \psi_j(\mathbf{r}) \equiv \sum_k D_k R_{kij}. \quad (102)$$

Here we defined

$$R_{kij} = \int d\mathbf{r} \psi_k(\mathbf{r}) \psi_i(\mathbf{r}) \psi_j(\mathbf{r}) \quad D_k = \int d\mathbf{r} \Delta(\mathbf{r}) \psi_k(\mathbf{r}) \quad (103)$$

Note that the way we decoupled the interaction term is specific to the superconductive correlations. A generic Hubbard-Stratonovich field should contain also a component  $V(\mathbf{r}; \Omega_n)$  coupled to the combination  $(\chi_i^{(n)})^* \chi_i^{(n)}$  which corresponds to interaction in the particle-hole channels. We neglect such interactions in this subsection and will study their effect in subsection 6.1 in connection with the  $S_i^z S_j^z$  terms in the *pseudo-spin* Hamiltonian.

The matrix variables  $\Delta_{ij}$ , which appeared naturally in the second term of the action *are not mutually independent*. Indeed, the number of independent components of the (discretized) field  $\Delta(\mathbf{r})$  scales with system volume as  $\propto \mathcal{V}$ , whereas the number of matrix elements  $\Delta_{ij}$  scales as  $\mathcal{V}^2$ . The matrix elements  $\Delta_{ij}$  are mutually constrained due to the ortho-normality conditions  $\int d\mathbf{r} \psi_i(\mathbf{r}) \psi_j(\mathbf{r}) = \delta_{ij}$ .

Now one can complete the Hubbard-Stratonovich transformation by performing the Gaussian integration over  $\Phi_j^{(n)}$  to obtain the  $\text{Tr} \ln$  of the corresponding matrix in Eq.(101). In addition, one can represent the first term in Eq.(101) in terms of the coefficients  $D_i$  of expansion of  $\Delta(\mathbf{r})$  over the full set of single particle wave functions  $\psi_i(\mathbf{r})$ . Expanding the  $\text{Tr} \ln$  over  $D_i$  up to fourth order, we obtain free energy functional in the form

$$F[D_i] = \frac{1}{g} \sum_{ij} D_i^* \mathcal{K}_{ij} D_j + \frac{1}{4} \sum_{ijkl} D_i D_j^* \mathcal{J}_{ijkl} D_k D_l^*, \quad (104)$$

where

$$\mathcal{K}_{ij} = \delta_{ij} - \frac{g}{2} \sum_{\mu\nu} R_{i\mu\nu} \eta_{\mu\nu} R_{j\mu\nu}. \quad (105)$$

In Eqs.(104),(105) we denote

$$\mathcal{J}_{ijkl} = \sum_{\nu_1, \nu_2, \nu_3, \nu_4} R_{i\nu_4\nu_1} R_{j\nu_1\nu_2}^* R_{k\nu_2\nu_3} R_{l\nu_3\nu_4}^* \zeta_{\nu_1\nu_2, \nu_3\nu_4} \quad (106)$$

where the function  $\zeta(\dots)$  is defined by

$$\zeta_{\nu_1\nu_2, \nu_3\nu_4} = \zeta_{\nu_2\nu_1, \nu_4\nu_3} = \zeta_{\nu_3\nu_4, \nu_1\nu_2} = \frac{1}{(\xi_{\nu_1} - \xi_{\nu_3})(\xi_{\nu_4} - \xi_{\nu_2})} [\eta_{\nu_1\nu_2} + \eta_{\nu_3\nu_4} - \eta_{\nu_3\nu_2} - \eta_{\nu_1\nu_4}]. \quad (107)$$

Below we will use Eqs.(104)-(107) to derive the effective Ginzburg-Landau functional  $F[\Psi(\mathbf{r})]$  in the form

$$F_{GL}[\Psi(\mathbf{r})] = \nu_0 T_c^2 \int d\mathbf{r} \left( a(\mathbf{r}) \Psi^2(\mathbf{r}) + \frac{b}{2} \Psi^4(\mathbf{r}) + C |\nabla \Psi(\mathbf{r})|^2 \right) \quad (108)$$

The factor  $\nu_0 T_c^2$  in (108) is introduced so that to keep  $\Psi$  and  $a(T)$  dimensionless. The physical properties of the superconductor described by functional (108) are controlled by four parameters:  $a = \langle a(\mathbf{r}) \rangle$ ,  $b$ ,  $C$ , and by the strength  $W$  of fluctuations  $\delta a(\mathbf{r}) = a(\mathbf{r}) - a$  defined as

$$\begin{aligned} W &= \int d\mathbf{r} \langle \delta a(\mathbf{r}) \delta a(\mathbf{r}') \rangle = \\ &= \mathcal{V}^{-1} \int d\mathbf{r}_1 d\mathbf{r}_2 d\mathbf{r}_3 d\mathbf{r}_4 \langle \delta K(\mathbf{r}_1, \mathbf{r}_2) \delta K(\mathbf{r}_3, \mathbf{r}_4) \rangle. \end{aligned} \quad (109)$$

where  $\delta K(\mathbf{r}, \mathbf{r}') = K(\mathbf{r}, \mathbf{r}') - \langle K(\mathbf{r}, \mathbf{r}') \rangle$ . We are able to describe the spatial fluctuation by one parameter,  $W$ , because  $\delta a(\mathbf{r})$  correlations are short-ranged compared to the typical scale of  $\Psi(\mathbf{r})$  variations.

#### 4.2.1. Transition temperature: coefficient $a(T)$ .

We begin by evaluating the coefficient  $a$  that vanishes at the transition point,  $a(T) = \tilde{a}(T - T_c)$ . For this calculation it is sufficient to use a constant  $\Psi(\mathbf{r}) = \Psi$ . Now let us transform the first term of Eq.(104), using Eqs.(105,96,102,103). We assume here that  $\Delta_j$  obey the matrix equation (93), i.e. the local order parameter coincides with  $\tilde{\Delta}(\mathbf{r})$  defined in Eq.(96). The result reads

$$\frac{F_2}{\Psi^2} = \frac{g}{4} \sum_{ij} \Delta_i \Delta_j \eta_i \eta_j M_{ij} - \frac{g^2}{8} \sum_{ijk} \Delta_i \Delta_j \eta_i \eta_j \eta_{kl} M_{iikl} M_{kljj} \quad (110)$$

where we used the "fusion rule" following from the completeness of the set of  $\psi_j(\mathbf{r})$ :

$$\sum_i R_{kli} R_{pqi} = M_{klpq}. \quad (111)$$

and an equivalent form of Eq.(93) written in terms of  $D_i$  and  $\Delta_{jk}$  variables:

$$D_i = \frac{g}{2} \sum_{kl} \eta_{kl} \Delta_{kl} R_{ikl}. \quad (112)$$

To determine the coefficient  $a$  we neglect the off-diagonal terms  $M_{iikl}$  with  $k \neq l$  in Eq.(110) and thus reduce it to

$$F_2^{(0)} = \frac{1}{2} \Psi^2 \sum_{ij} \left[ \left( \hat{Q} \right)_{ij} - \left( \hat{Q}^2 \right)_{ij} \right] \phi_i \phi_j \quad (113)$$

where  $\hat{Q}$  and  $\phi_i$  are defined in Eq.(97). In the continuum limit one writes  $\xi_i \rightarrow \xi$ ,  $M_{ij} \rightarrow \frac{1}{V} M(\xi - \zeta)$ ,  $\sum_i \rightarrow V \nu_0 \int d\xi$  and thus the bilinear form (113) transforms into

$$F_2^{(0)} = \frac{\nu_0 V}{2} \Psi^2 \int \int d\xi d\zeta L(\xi, \zeta) \phi(\xi) \phi(\zeta) \quad (114)$$

where

$$L(\xi, \zeta) = Q(\xi, \zeta) - \int d\xi_1 Q(\xi, \xi_1) Q(\xi_1, \zeta), \quad (115)$$

with the kernel

$$Q(\xi, \zeta) = \frac{\lambda}{2} \sqrt{\eta(\xi) \eta(\zeta)} M(\xi - \zeta) \quad (116)$$

The function  $\phi(\xi)$  is, by construction, an eigenfunction of the integral equation with the kernel  $Q(\xi, \zeta)$ ; its eigenvalue  $k(T)$  approaches 1 at  $T = T_c$ . At this stage we need to specify the normalization condition for the function  $\phi(\xi)$ :

$$\int d\xi \Delta^2(\xi) \eta(\xi) \equiv \int d\xi \phi^2(\xi) = \frac{2T_c^2}{\gamma} \quad (117)$$

The form of the normalization condition Eq.(117) was chosen to enable a smooth crossover to the conventional (non-fractal) BCS case  $\gamma \rightarrow 0$ , when  $\phi_{\gamma=0} = T \sqrt{\eta(\xi)}$ . To get the equations valid in the crossover regime we need to introduce the high-energy cutoff  $\Omega_D$  so

that all integrals over  $d\xi$  go over the range  $|\xi| < \Omega_D$ . Then a straightforward modification of the normalization condition

$$\int_{-\Omega_D}^{\Omega_D} d\xi \Delta^2(\xi) \eta(\xi) = \frac{2T_c^2 \ln \frac{\Omega_D}{T_c}}{\gamma \ln \frac{\Omega_D}{T_c} + 1} \quad (118)$$

(that reduces to (117) when  $\gamma \gg 1/\ln \frac{\Omega_D}{T_c} = \lambda$ ) allows one to recover the BCS limit at a fixed  $\Omega_D$  and  $\gamma \rightarrow 0$ . We are mainly interested in the case of intermediate to strong fractality,  $\gamma \sim 0.6$ , and weak interaction  $\lambda \ll 1$ , so we shall use the simplified condition (117) appropriate in this limit.

Making use of Eq.(117) we reduce the expression (114) to

$$F_2^{(0)} = \nu_0 \mathcal{V} T^2 \Psi^2 \gamma^{-1} [k(T) - k^2(T)] \quad (119)$$

Since  $1 - k(T) \ll 1$  at  $T \approx T_c$ , it is sufficient to evaluate the derivative  $dk/dT|_{k=1}$ . We find it by rewriting the kernel (116) in a dimensionless form:

$$\bar{Q}(x, y) = \frac{\lambda_T}{2|x - y|^\gamma} \sqrt{\frac{\tanh(x) \tanh(y)}{xy}},$$

where  $\lambda_T = \lambda(E_0/2T)^\gamma$ . Clearly,  $d \ln k(T)/d \ln(T) = -\gamma$ , and, finally, the coefficient  $a(T)$  is expressed only in terms of the ratio of  $T/T_c$ :

$$a(T) = \frac{T - T_c}{T_c} \quad (120)$$

Note that the order parameter  $\Psi$  introduced in Eq.(98) is dimensionless, whereas  $\Delta$  has a dimension of energy.

#### 4.2.2. Quartic term: coefficient $b$

Now we turn to the computation of the coefficient  $b$  in the expansion (108). Our starting points are Eqs.(104) and (106,107). As in the previous part we may use here  $\Psi(\mathbf{r}) = \text{const}$ , thus  $\Delta(\mathbf{r})$  is proportional to  $\tilde{\Delta}(\mathbf{r})$  defined in Eq.(96). Therefore using Eqs.(96), (103) we may substitute  $D_i = \frac{g}{2} \sum_a \Delta_a \eta_a R_{iaa}$  in the fourth order in  $D_i$  term of Eq.(104) reducing this term to the following form:

$$\begin{aligned} F_4 = & \frac{1}{4} \left( \frac{g}{2} \right)^4 \sum_{ijkl} \sum_{abcd} \sum_{\nu_1 \dots \nu_4} \Delta_a \Delta_b \Delta_c \Delta_d \eta_a \eta_b \eta_c \eta_d \\ & \times R_{i\nu_4 \nu_1} R_{j\nu_1 \nu_2} R_{k\nu_2 \nu_3} R_{l\nu_3 \nu_4} R_{iaa} R_{jbb} R_{kcc} R_{ldd} \zeta_{\nu_1 \nu_2, \nu_3 \nu_4} \end{aligned} \quad (121)$$

Now we do summations over  $i, j, k, l$  using the fusion rule (111), and then neglect the off-diagonal matrix elements, i.e. we set everywhere  $M_{\nu_1 \nu_2 aa} \rightarrow \delta_{\nu_1 \nu_2} M_{\nu_1 a}$ . Summations over  $a, b, c, d$  can be done now with the use of modified MFA equations (93). Finally, we proceed from the last remaining summation over  $\nu_1$  to integration, and find

$$F_4 = \frac{\nu_0 \mathcal{V}}{32T^2} \Psi^4 \int \frac{d\xi}{2T} \Phi \left( \frac{\xi}{2T} \right) \Delta^4(\xi) \quad (122)$$

where

$$\Phi(x) \equiv 16T^3 \lim_{\forall \xi_\alpha \rightarrow 2Tx} \zeta_{ij,kl} = \frac{1}{x^2} \left( \frac{\tanh(x)}{x} - \frac{1}{\cosh^2(x)} \right)$$

with the function  $\zeta_{ijkl}$  defined in Eq.(107). In the limit  $\gamma \rightarrow 0$  we have  $\Delta(\xi) = \text{const}$  and the integral in (122) reduces to

$$\frac{1}{32} \int dx \Phi(x) = \frac{7\zeta(3)}{16\pi^2} = \frac{1}{2} b_{\text{BCS}},$$

leading to the standard BCS result for the  $b$  coefficient in Eq.(108). In general case we find

$$b = \frac{1}{4} \int dx \Phi(x) x^2 \coth^2(x) \bar{\phi}^4(x) \quad (123)$$

where  $\bar{\phi}(x) = T^{-1/2} \phi(2Tx)$  and  $\phi(\xi)$  is the  $k = 1$  eigenfunction of the kernel (116) subject to the normalization condition (117).

#### 4.2.3. Gradient term: coefficient $C$ .

We now turn to calculation of the gradient term of the functional (108). Note that previously employed "diagonal approximation" for the matrix elements  $M_{ijkl}$  is not sufficient for that purpose. In order to find the coefficient  $C$  we need to take into account the off-diagonal matrix elements  $M_{ijkl}$  which contain pairs of different levels with nearby energies:  $|\xi_i - \xi_j| \sim |\xi_k - \xi_l| \sim \omega(q)$ , with  $\omega(q \rightarrow 0) \rightarrow 0$ . The reason for that is similar to the one which applies to the standard BCS Hamiltonian with the reduced interaction term  $g \sum_{\mathbf{p}, \mathbf{p}'} c_{\uparrow, \mathbf{p}}^\dagger c_{\downarrow, -\mathbf{p}} c_{\downarrow, \mathbf{p}'}^\dagger c_{\uparrow, -\mathbf{p}'}^\dagger$ . One has to allow for the non-zero momentum of a pair and thus go beyond the "diagonal approximation" in  $\mathbf{p}$  and  $\mathbf{p}'$  in order to be able to compute the *phase rigidity*  $C$  which is related with the supercurrent.

We first illustrate this statement using the standard theory of disordered superconductors as an example, see e.g. [88]. In that case, quadratic term of the free energy expansion (104) can be represented in the coordinate space:

$$F[\Delta(\mathbf{r})] = \int d\mathbf{r} d\mathbf{r}' \left[ \frac{1}{g} \delta(\mathbf{r} - \mathbf{r}') - K(\mathbf{r}, \mathbf{r}') \right] \Delta(\mathbf{r}) \Delta(\mathbf{r}') \quad (124)$$

where

$$K(\mathbf{r}, \mathbf{r}') = \nu_0 T \sum_{\omega_n} \sum_{ij} \frac{\psi_i(\mathbf{r}) \psi_j(\mathbf{r}) \psi_i^*(\mathbf{r}') \psi_j^*(\mathbf{r}')}{(\xi_i - i\omega_n)(\xi_j + i\omega_n)} \quad (125)$$

Here  $\omega_n = \pi T(2n + 1)$  and (125) is the equivalent form of Eqs.(87,88). As the standard procedure goes, one averages the kernel (125) over disorder in the semiclassical approximation and obtains the Fourier-transformed kernel

$$\bar{K}(q) = 2\pi\nu_0 T \sum_{\omega_n} \frac{1}{Dq^2 + 2|\omega_n|} \quad (126)$$

where  $D$  is the diffusion coefficient. Finally one obtains for the coefficient  $C$  in Eq.(108) the well known result

$$C^{(0)} = -\frac{1}{\nu_0} \left. \frac{dK(q)}{dq^2} \right|_{q \rightarrow 0} = \frac{\pi}{8} \frac{D}{T_c} \quad (127)$$



In order to generalize this derivation to the case of strong disorder it is convenient to introduce two particle spectral function

$$g(q, \Omega) = \frac{1}{\mathcal{V}\nu_0} \sum_{ij} \int d\mathbf{r} d\mathbf{r}' e^{i\mathbf{q}(\mathbf{r}-\mathbf{r}')} \delta(\xi_i - \xi_j - \Omega) \times \langle \psi_i(\mathbf{r}) \psi_j(\mathbf{r}) \psi_i^*(\mathbf{r}') \psi_j^*(\mathbf{r}') \rangle \delta(E_F - \xi_i). \quad (128)$$

The average kernel in Eq.(125) can be expressed through this two particle function:

$$\overline{K}(q) = \nu_0 T \sum_{\omega_n} \int \frac{d\xi d\xi' g(q, \xi - \xi'; E)}{(\xi - i\omega_n)(\xi' + i\omega_n)} \quad (129)$$

In the diffusive limit the spectral function is

$$g(q, \Omega) = \frac{1}{\pi} \frac{Dq^2}{\Omega^2 + (Dq^2)^2}. \quad (130)$$

and its substitution into Eq.(129) gives back Eq.(126).

This derivation of the standard result demonstrates that the small  $q$ -dependence of the averaged kernel  $\overline{K}(q)$  comes from matrix elements of the operator  $e^{iq(\mathbf{r}-\mathbf{r}')}$  between eigenstates  $\psi_i(\mathbf{r})$ ,  $\psi_j(\mathbf{r})$  with nearby energies  $|\xi_i - \xi_j| \sim Dq^2$ . Notice that diagonal approximation used in previous sections corresponds to  $i = j$  in Eq.(125). In this approximation one neglects the off-diagonal terms  $M_{ijkl}$  completely and gets  $g(q, \Omega) = \delta(\Omega) f(q)$ , where

$$f(q) = \int d\mathbf{r} d\mathbf{r}' \langle \psi_i^2(\mathbf{r}) \psi_i^2(\mathbf{r}') e^{i\mathbf{q}(\mathbf{r}-\mathbf{r}')} \rangle$$

For delocalized wavefunctions which occupy all the available volume one can write

$$\mathcal{V}^2 \langle \psi_i^2(\mathbf{r}) \psi_i^2(\mathbf{r}') \rangle \approx \mathcal{V}^2 \langle \psi_i^2(\mathbf{r}) \rangle \langle \psi_i^2(\mathbf{r}') \rangle = 1 + O(1/g),$$

where  $g \gg 1$  is the dimensionless conductance. Then  $f(q = 0) = 1 + O(1/g)$  and  $f(q \neq 0) = O(1/g)$ . The jump in  $f(q)$  at  $q = 0$  implies that in the diagonal approximation the coefficient  $C$  is infinite in a metal which is obviously wrong. However, the value of  $K$  at  $q = 0$  can be determined correctly in the diagonal approximation because at  $q = 0$  the spectral function  $g(q, \Omega) \rightarrow \delta(\Omega)$  both in the diagonal and in the diffusive approximation Eq.(130).

The correct derivation of the coefficient  $C$  in case of a strong disorder has to take into account a non-uniformity of the "background configuration" of the superconducting order parameter given by Eq.(96). We follow the same logics as in the derivation of the  $a$  and  $b$  coefficients in previous sections. Note that the  $q$ -dependence comes from the second term of the matrix (105) which leads to the second sum in Eq.(110). We focus on this term and repeat the steps of the derivation which led to Eq.(110) using now a weakly modulated  $\Psi(\mathbf{r}) = \Psi_q e^{i\mathbf{q}\mathbf{r}}$  with small  $q$ . The second term of (110) becomes (in the continuous form, after replacing  $\sum_j \rightarrow \mathcal{V}\nu_0 d\xi$ ):

$$\int d\mathbf{q} F_2^{(2)}(q) = - \int d\mathbf{q} |\Psi_q|^2 \frac{g^2}{8} \int d\xi d\omega d\omega_1 d\omega_2 \Delta(\xi_+ + \omega_1) \Delta(\xi_- + \omega_2) \times \eta(\xi_+, \xi_-) \eta(\xi_+ + \omega_1) \eta(\xi_- + \omega_2) M_4(q; \omega, \omega_1, \omega_2) \quad (131)$$

where  $\xi_{\pm} = \xi \pm \omega/2$ ; the function  $\Delta(\xi) = \phi(\xi)/\sqrt{\eta(\xi)}$  obeys Eq.(94) and is normalized according to Eq.(117), and the function  $M_4(q; \omega, \omega_1, \omega_2)$  is defined by

$$M_4(q; \omega, \omega_1, \omega_2) = \mathcal{V}^{-1} \left\langle \sum_{ijkl} \delta(\xi_{ij} - \omega) \delta(\xi_{ki} - \omega_1) \delta(\xi_{lj} - \omega_2) \delta(E - \xi_i) I_{ijkl}(q) \right\rangle,$$

where  $\xi_{ij} = \xi_i - \xi_j$

$$I_{ijkl}(q) = \int d\mathbf{r} d\mathbf{r}' e^{i\mathbf{q}(\mathbf{r}-\mathbf{r}')} \psi_i(\mathbf{r}) \psi_j(\mathbf{r}) \psi_i(\mathbf{r}') \psi_j(\mathbf{r}') \psi_k^2(\mathbf{r}) \psi_l^2(\mathbf{r}') \quad (132)$$

The function  $M_4(q; \omega, \omega_1, \omega_2)$  replaces function  $g(q, \omega)$  employed in the standard derivation of the  $|\nabla\Psi|^2$  term for diffusive superconductors. The additional terms  $\psi_k^2(\mathbf{r})$  and  $\psi_l^2(\mathbf{r}')$  (and the summation over the corresponding states  $k$  and  $l$ ) arise due to the *essentially*  $\mathbf{r}$ -dependent "background configuration" which  $\mathbf{r}$ -dependence is expressed through  $\psi^2(\mathbf{r})$  by Eq.(96).

The main source of fluctuations of  $M_4$  are the spatial fluctuation of the eigenfunctions whereas the spectral fluctuations are relatively weak. Neglecting spectral fluctuations, one can switch from summation over indices  $i, j, k, l$  to integration over the energy variables  $\xi_i, \xi_j, \xi_k, \xi_l$  with the constant DoS and consider the average  $I(q, \{\omega\}) = \langle I_{ijkl}(q) \rangle$  as a function of all energy differences  $\omega, \omega_1, \omega_2$ . Then the expression for the coefficient  $C$  in the Ginzburg-Landau functional Eq.(108) takes the form

$$C = \frac{1}{8T_c^2} \lambda^2 \nu_0 \int d\xi d\omega d\omega_1 d\omega_2 \Delta(\xi + \omega/2 + \omega_1) \Delta(\xi - \omega/2 + \omega_2) \times \eta(\xi + \omega/2, \xi - \omega/2) \eta(\xi + \omega/2 + \omega_1) \eta(\xi - \omega/2 + \omega_2) J(\{\omega\}), \quad (133)$$

where  $J(\{\omega\}) = -\mathcal{V}^3 \frac{dI(q, \{\omega\})}{dq^2} \Big|_{q=0}$ .

The next step is to estimate  $I(\{\omega\})$  using the rules formulated in section 2.2. We begin by considering the critical wavefunction statistics. Applying the rule (iii) we find the phase-independent counterpart to the combination of eigenfunctions in Eq.(132). It happens to coincide with the one for the square of the off-diagonal matrix element  $M_{ijkl}$  and is given by Eqs.(49),(50). Then expanding Eq.(132) up to  $q^2$  and integrating over  $(\mathbf{r} - \mathbf{r}')$  up to  $|\mathbf{r} - \mathbf{r}'| \sim L_\omega$  we obtain an expression similar to Eq.(51) but containing an extra factor  $L_\omega^2$  due to the expansion of  $e^{i\mathbf{q}(\mathbf{r}-\mathbf{r}')}$  up to  $q^2$ :

$$J(\{\omega\}) \sim \mathcal{V}^3 L_\omega^2 \langle |M_{ijkl}|^2 \rangle_{\text{typ}} \sim L_\omega^{d+2} \left( \frac{E_0}{\omega} \right)^{2\gamma}. \quad (134)$$

In Eq.(134) we assumed all energy differences to be of the same order  $\omega_1 \sim \omega_2 \sim \omega$ . The estimate Eq.(134) holds true on the insulator side of the Anderson transition as long as  $\omega \gg \delta_L$  (see the discussion in section 2.2.4 and Eq.(60)).

Now we have to estimate the result of integration over the energy variables in Eq.(133). Using the asymptotic behavior of  $\Delta(\omega) \propto \omega^{-\gamma}$  which follows from (94), (see section 4.1) and  $\eta(\omega) \propto \omega^{-1}$  and Eq.(134) power counting shows that for  $T_c > \delta_L$  the integral is dominated by  $\omega \sim \omega_1 \sim \omega_2 \sim T_c$  and can be estimated by

$$C \sim \left( \frac{1}{\nu_0 T_c} \right)^{\frac{2}{d}} \lambda^2 \left( \frac{E_0}{T_c} \right)^{2\gamma} \sim \left( \frac{1}{\nu_0 T_c} \right)^{\frac{2}{d}}, \quad (T_c \gg \delta_L). \quad (135)$$

Remarkably, the enhancement factor depending on the fractal exponent  $\gamma$  is canceled by the coupling constant  $\lambda$  due to Eq.(95), and the result is not sensitive to fractality and is essentially the same as in Refs.[4, 3]. This cancellation occurs due to the presence of the additional (with respect to the standard expression Eq. 128) factors  $\psi_k^2(\mathbf{r})$  and  $\psi_l^2(\mathbf{r})$  in the integral  $I_{ijkl}(q)$  defined in Eq.(132); without these factors, the final result for  $C$  would contain extra small factor  $\sim (T_c/E_0)^\gamma$ .

Note that the coefficient  $C$  is dominated by the off-diagonal matrix elements only in metal or in very weak insulator. As one moves towards a strong insulator where  $T_c < \delta_L$ , the main contribution to  $C$  becomes the one that originates from the diagonal approximation and can be roughly estimated as

$$C \sim L_{\text{loc}}^2, \quad (\delta_L > T_c) \quad (136)$$

in the diagonal approximation. The estimate (136) is based on the simplest picture that wavefunctions localized at distances larger than localization length  $L_{\text{loc}}$  do not overlap. In fact, as we discuss in section 6.1, this approximation is a bit too crude as it misses an important logarithmic factor which increases  $C$  values in the range  $T_c \ll \delta_L$ , see Eq.(179).

#### 4.2.4. Mesoscopic fluctuations: coefficient $W$ .

Disorder always leads to spatial fluctuations of parameters which enter the Ginzburg-Landau functional; the major effect is due to fluctuations of  $a(T, \mathbf{r})$ . Universal mesoscopic fluctuations (which provide a lower bound for the strength of this effect) were studied in Ref. [4] for usual disordered superconductors and more recently in [31] for 2D films with the strong Finkelstein effect. Here we follow the same general approach but implement it in the Fock space instead of the coordinate space.

We start from the Eq.(110) for the quadratic part of the free energy. Previously we neglected off-diagonal matrix elements  $M_{ijkk}$  entering the second term of (110); now our goal is to estimate the strength of mesoscopic fluctuations produced by these matrix elements. Thus we represent the second term as

$$F_{22} = -\frac{\Psi^2}{2} \sum_{ij} \left( (\hat{Q}^2)_{ij} + \Gamma_{ij} \right) \phi_i \phi_j \quad (137)$$

where  $\hat{Q}$  is defined in Eq.(97) and

$$\Gamma_{ij} = \frac{g^2}{4} \sum_{k \neq l} M_{ikkl} M_{kljj} \eta_{kl} (\eta_i \eta_j)^{\frac{1}{2}} \quad (138)$$

The matrix  $\Gamma_{ij}$  contains corrections from the (previously neglected) off-diagonal matrix elements. Its average  $\overline{\Gamma_{ij}}$  contributes to the shift of the critical temperature which can be estimated using scaling arguments developed in section 2.2.2. The result is that the relative shift due to the off-diagonal matrix elements is  $(\delta_{\text{off}} T_c)/T_c \sim 1$ .

Here we are interested in the strength of *mesoscopic fluctuations*  $W$  defined in Eq.(109) and thus calculate the free energy cumulant:

$$(\nu_0 T^2)^2 W = \frac{1}{\Psi^4 \mathcal{V}} \langle \langle F_{22} F_{22} \rangle \rangle = \frac{1}{4\mathcal{V}} \sum_{i_1 i_2 i_3 i_4} \phi_{i_1} \phi_{i_2} \phi_{i_3} \phi_{i_4} \langle \langle \Gamma_{i_1, i_2} \Gamma_{i_3, i_4} \rangle \rangle \quad (139)$$

Using Eq.(138) and switching to a continuum representation, we obtain the irreducible correlation function  $\langle\langle\Gamma\Gamma\rangle\rangle$ :

$$\begin{aligned} \langle\langle\Gamma_{i_1,i_2}\Gamma_{i_3,i_4}\rangle\rangle = & \left(\frac{g^2}{4}\right)^2 (\nu_0\mathcal{V})^4 \sqrt{\eta_{i_1}\eta_{i_2}\eta_{i_3}\eta_{i_4}} \int \dots \int d\xi_m d\xi_n d\xi_k d\xi_l \eta_{mn}\eta_{kl} \int \dots \int d^d\mathbf{r}_1 d^d\mathbf{r}_2 d^d\mathbf{r}_3 d^d\mathbf{r}_4 \\ & \langle\langle\psi_{i_1}^2(\mathbf{r}_1)\psi_{i_2}^2(\mathbf{r}_2)\psi_{i_3}^2(\mathbf{r}_3)\psi_{i_4}^2(\mathbf{r}_4)\psi_{m,n}^{(2)}(\mathbf{r}_1)\psi_{m,n}^{(2)}(\mathbf{r}_2)\psi_{k,l}^{(2)}(\mathbf{r}_3)\psi_{k,l}^{(2)}(\mathbf{r}_4)\rangle\rangle, \end{aligned}$$

where the double brackets  $\langle\langle\dots\rangle\rangle$  denote the cumulant average defined by (we use below indices  $i_1\dots$  instead of  $\psi_{i_1}^2\dots$  etc.):  $\langle\langle i_1 i_2 i_3 i_4 m n k l \rangle\rangle = \langle i_1 i_2 i_3 i_4 m n k l \rangle - \langle i_1 i_2 m n \rangle \langle i_3 i_4 k l \rangle$  and  $\psi_{m,n}^{(2)}(\mathbf{r}) \equiv \psi_m(\mathbf{r})\psi_n(\mathbf{r})$ .

We now estimate the coefficient  $W$  for the critical states near the Anderson transition point. First of all we note that the decoupled average  $\langle i_1 i_2 m n \rangle \langle i_3 i_4 k l \rangle$  depends only on the two of the three independent differences in coordinates  $R_{s,s'} = |\mathbf{r}_s - \mathbf{r}_{s'}|$  ( $s, s' = 1, \dots, 4$ ), while the cumulant average depends on all the three of them and vanishes when  $R_{s,s'} > L_\omega$  (as before we assume that all the energy differences are of the same order  $\omega$ ). In the region where all  $R_{s,s'} < L_\omega$  the decoupled average is smaller than the cumulant one. Assuming all the differences of coordinates are of the same order  $R_{s,s'} \sim R$  and applying the rules (i) – (iii) of section 2.2.1 we obtain at  $R < L_\omega$ :

$$\begin{aligned} & \left\langle \left\langle \psi_{i_1}^2(\mathbf{r}_1)\psi_{i_2}^2(\mathbf{r}_2)\psi_{i_3}^2(\mathbf{r}_3)\psi_{i_4}^2(\mathbf{r}_4)\psi_{m,n}^{(2)}(\mathbf{r}_1)\psi_{m,n}^{(2)}(\mathbf{r}_2)\psi_{k,l}^{(2)}(\mathbf{r}_3)\psi_{k,l}^{(2)}(\mathbf{r}_4) \right\rangle \right\rangle \sim \\ & \left\langle \psi_{i_1}^2(\mathbf{r}_1)\psi_{i_2}^2(\mathbf{r}_2)\psi_{i_3}^2(\mathbf{r}_3)\psi_{i_4}^2(\mathbf{r}_4)\psi_{m,n}^{(2)}(\mathbf{r}_1)\psi_{m,n}^{(2)}(\mathbf{r}_2)\psi_{k,l}^{(2)}(\mathbf{r}_3)\psi_{k,l}^{(2)}(\mathbf{r}_4) \right\rangle \sim \\ & \left\langle \psi_{i_1}^2(\mathbf{r}_1)\psi_{i_2}^2(\mathbf{r}_2)\psi_{i_3}^2(\mathbf{r}_3)\psi_{i_4}^2(\mathbf{r}_4)\psi_m^2(\mathbf{r}_1)\psi_n^2(\mathbf{r}_2)\psi_k^2(\mathbf{r}_3)\psi_l^2(\mathbf{r}_4) \right\rangle \sim \\ & \sim \mathcal{V}^{-8} \left( \frac{L_\omega}{R} \right)^{3d-2\alpha_2-\alpha_4} \left( \frac{L_\omega}{\ell} \right)^{4(d-d_2)}, \end{aligned}$$

where  $\alpha_2 = 3d_4 - 2d_2$ ,  $\alpha_4 = 7d_8 - 6d_4$ . Indeed, at  $R \sim L_\omega$  eigenfunctions in different space points are statistically independent and the corresponding averages can be decoupled. The result is  $\mathcal{V}^{-8}(L_\omega/\ell)^{4(d-d_2)}$  in agreement with Eq.(37). At  $R \sim \ell$  all eigenfunctions can be considered in one space point and the averaging then gives  $\mathcal{V}^{-8}(L_\omega/\ell)^{7(d-d_8)}$ . The last estimate coincides with Eq.(25) at small energy separations  $L_\omega \sim L$  where one can consider all eigenfunctions to be identical, and it corresponds to all eigenfunctions independently averaged at large energy separations when  $L_\omega \sim \ell$ . The decoupled average estimated in the same way using Eqs.(49),(50) is of the order of  $\mathcal{V}^{-8}(L_\omega/R)^{2d-2\alpha_2}(L_\omega/\ell)^{4(d-d_2)}$  and thus is smaller at  $R \ll L_\omega$  than the cumulant average by the factor  $(L_\omega/R)^{d-\alpha_4}$ .

Now we estimate the result of the four spatial integrations: over difference of coordinates  $R_{12} = |\mathbf{r}_1 - \mathbf{r}_2|$ ,  $R_{13} = |\mathbf{r}_1 - \mathbf{r}_3|$  and  $R_{23} = |\mathbf{r}_3 - \mathbf{r}_2|$  and one free integration which results in the factor  $\mathcal{V}$ . At this point it is important that the dependence of the cumulant average on  $R_{12}, R_{13}, R_{23}$  is symmetric and such that the power of  $R$  is typically smaller than  $3d$ , as  $\alpha_q^{\text{typ}} > 0$  (see Eq.(35)). This means that the main contribution to the integrals over  $R_{12}, R_{13}, R_{23}$  comes from the region  $R_{12} \sim R_{13} \sim R_{23} \sim L_\omega$ . This is a crucial circumstance that eliminates the dependence on higher fractal dimensions.

Thus we arrive at

$$\int d\{\mathbf{r}\} \left\langle \left\langle \psi_{i_1}^2(\mathbf{r}_1) \psi_{i_2}^2(\mathbf{r}_2) \psi_{i_3}^2(\mathbf{r}_3) \psi_{i_4}^2(\mathbf{r}_4) \psi_{m,n}^{(2)}(\mathbf{r}_1) \psi_{m,n}^{(2)}(\mathbf{r}_2) \psi_{k,l}^{(2)}(\mathbf{r}_3) \psi_{k,l}^{(2)}(\mathbf{r}_4) \right\rangle \right\rangle \\ \sim \mathcal{V}^{-7} L_\omega^{3d} \left( \frac{E_0}{\omega} \right)^{4\gamma}.$$

The remaining energy integration is estimated in the same way as in the previous subsection. As before, the dominant contribution comes from the energies within a strip of width  $T_c$  near the Fermi energy. The final result reads

$$\langle F_{22} F_{22} \rangle \sim \lambda^4 \nu_0 \mathcal{V} T_c^3 \left( \frac{E_0}{T_c} \right)^{4\gamma} \sim \nu_0 \mathcal{V} T_c^3. \quad (140)$$

Again, as in Eq.(135), the enhancement factor which depends on the fractal exponent  $\gamma$  cancels out exactly by the coupling constant  $\lambda$ , and the final result for the coefficient  $W$  is

$$W \sim \frac{1}{\nu_0 T_c}, \quad (\delta_L \ll T_c). \quad (141)$$

This result was obtained using the definition (109) which makes sense if the spatial scale  $L_a$  of  $a(\mathbf{r})$  fluctuations is small compared to the scale of  $\Psi(\mathbf{r})$  variation. We expect that the same estimate (141) is valid if both length-scales are of the same order.

In the limit of strong insulator, one can repeat the above analysis to arrive at

$$W \sim L_{\text{loc}}^3, \quad (\delta_L > T_c). \quad (142)$$

This result is obtained in the diagonal approximation.

#### 4.2.5. Ginzburg parameters for thermal and mesoscopic fluctuations

Now we use the results given by Eqs.(120,123,135,141) to estimate the relative width of the fluctuation region near the thermal transition into a fractal superconductor state. First we estimate the Ginzburg parameter  $\text{Gi}$  which determines the reduced temperature range  $|1 - T/T_c| < \text{Gi}$  where thermal fluctuations are strong in a 3D system [89]:

$$\text{Gi} \sim \frac{b^2}{C^3 (\nu_0 T_c)^2} \sim 1, \quad (\delta_L \ll T_c) \quad (143)$$

The relative width of “smearing” of the superconductive transition due to positional disorder is given by the parameter  $\text{Gi}_d$  defined as follows (see e.g. Ref.[87]):

$$\text{Gi}_d \sim \frac{W^2}{C^3} \sim 1, \quad (\delta_L \ll T_c) \quad (144)$$

The estimates (143) and (144) demonstrate that the modified mean-field approximation developed in this section can be used (with relative accuracy of the order of unity) in order to estimate  $T_c$  of a fractal superconductor. Based on this result we conclude that in the region of extended and weakly localized single-particle states with  $\delta_L \ll T_c$  the thermal fluctuations of the order parameter phase and the mesoscopic fluctuations

of the local  $T_c$  which were not taken into account in the modified MFA can at most reduce the global  $T_c$  by a factor of the order of one compared to the modified MFA result, Eq.(95) but can hardly lead to a modification of the functional dependence of  $T_c$  on the interaction constant  $\lambda$ . This is the most important conclusion of this subsection.

Another conclusion concerns the *role of the off-diagonal matrix elements* in the region of extended and weakly localized single-particle states. These matrix elements are completely neglected in modified MFA which nevertheless gives accurate results. They are, however, necessary for the correct account of the thermal fluctuations and the local  $T_c$  mesoscopic fluctuations. The off-diagonal matrix elements also determine the electromagnetic response and are necessary for calculation of the critical current, as both properties are related with the gradient term in the Ginzburg-Landau functional Eq.(108).

In the region  $\delta_L \gg T_c$  the use of the simplified estimate  $C \sim L_{\text{loc}}^2$  would lead to the conclusion that the parameters  $G_i$  and  $G_{i_d}$  are large:

$$G_i \sim G_{i_d} \sim \frac{1}{(\nu_0 T_c L_{\text{loc}}^3)^2} \sim \frac{1}{Z_{\text{eff}}^2}, \quad (\delta_L > T_c)$$

where  $Z_{\text{eff}} \sim T_c/\delta_L$  is the effective coordination number to be discussed later on in relation with the *pseudo-spin Hamiltonian*. In fact, more accurate estimate for  $Z_{\text{eff}}$  given by Eq.(179) in section 6.1 below shows that both  $G_i$  and  $G_{i_d}$  remain of the order of one in the broad range of large  $\delta_L/T_c$  ratios.

#### 4.3. Pseudo-spin Hamiltonian.

As we will see below, there is a sufficiently wide range of parameters on the insulating side of the Anderson transition where the superconducting transition temperature  $T_c$  is of the order of its value  $T_c^{(0)}$  right at the Anderson transition point while the pairing gap  $\Delta_P$  introduced in section 3 is much larger than  $T_c$ . This means that practically the entire region where  $T_c$  gradually decreases with increasing disorder falls into this *pseudo-gap regime*. The modified MFA does not work in this regime because Ginzburg parameters  $G_i$  and  $G_{i_d}$  are larger than 1. However, the problem can be significantly simplified by making use of the large value of the gap  $\Delta_P$  between states with even and odd number of particles occupying any orbital  $\psi_i(\mathbf{r})$ . Namely, as the creation of the *odd state* with one particle on an orbital takes a large energy  $2\Delta_P$  to break the pair, the transitions between the even (having two or no particles on any orbital) and odd states described by the *off-diagonal* matrix elements can be neglected. Technically, it is equivalent to neglecting all the off-diagonal matrix elements and considering the sectors of Hilbert space with even and odd states as completely decoupled. Restricting ourselves to the low-energy *even* sector one can rewrite [36] the Hamiltonian Eq.(7) in the form of a *pseudo-spin Hamiltonian* with the spin operators  $S_i^\pm$ ,  $S_i^z$  acting in the Fock space of orbitals  $|i\rangle \equiv \psi_i(\mathbf{r})$  and the *diagonal matrix elements*  $M_{ij}$  playing a role of the coupling matrix. The most general form of this Hamiltonian is:

$$\begin{aligned} H_{PS} &= \sum_j \xi_j (2S_j^z + 1) - \frac{g_\perp}{2} \sum_{ij} M_{ij} (S_i^+ S_j^- + S_i^- S_j^+) \\ &- g_\parallel \sum_{ij} M_{ij} S_i^z S_j^z. \end{aligned} \quad (145)$$

where the set of operators

$$S_j^+ = c_{j,\uparrow}^+ c_{j,\downarrow}^+ \quad S_j^- = (S_j^+)^{\dagger} \quad S^z = \frac{1}{2} \left( \sum_{\sigma} c_{j,\sigma}^+ c_{j,\sigma} - 1 \right) \quad (146)$$

is equivalent to the set of spin- $\frac{1}{2}$  operators  $\mathbf{S} = \frac{1}{2}\boldsymbol{\sigma}$ . Here  $\xi$  is random energy distributed with density  $\nu$  in some interval around 0.

The Hamiltonian Eq.(145) is the basis of theory of the *pseudogap superconductivity* we will develop in section 6. However, it is valid in *any* case where the off-diagonal matrix elements may be neglected for this or another reason. It was originally suggested by Anderson [36] for a BCS superconductor where the off-diagonal matrix elements are small in the parameter  $T_c/E_F$ . It is parametrically justified in the pseudo-gap region where the energy denominator associated with the even-odd transitions is large since  $\Delta_P \gg T_c$ . However, the estimate of the Ginzburg parameters  $\text{Gi} \sim \text{Gi}_d \sim 1$  (see discussion in section 6.1 and (179)) shows that it is also useful for a *semi-quantitative* (up to a factor of order one) determination of the transition temperature of the fractal superconductor near the Anderson localization transition. We will use this Hamiltonian in order to obtain the phase diagram as a function of  $(T, E_F)$  in the entire region spanning BCS and the pseudo-gap regime.

#### 4.4. Virial expansion method.

In this subsection we develop a new approach based on the virial expansion method applied to the pseudo-spin Hamiltonian Eq.(145) and use it to determine the superconductive transition temperature and thus the full phase diagram of the disordered superconductor. The approximations implied by this method are completely different from the ones of modified MFA. It will turn out to be very useful in order to find the precise limit of applicability of modified MFA and determine  $T_c$  in the region of localized single-particle states where the parameters  $\text{Gi}$  and  $\text{Gi}_d$  can be large.

Developing our scheme, we follow the approach of Larkin and Khmel'nitsky [90] who first used the virial expansion method to determine the temperature of magnetic phase transition in metallic alloys (see also [91]). The idea of this method is to express the free energy as a series, where each term contains an *exact* contribution from a fixed number of local variables (e.g. spins for the problem of magnetic impurities):

$$F = \sum_{n=1}^{\infty} \mathcal{F}^{(n)} = \sum_i F_i + \sum_{i>j} (F_{ij} - F_i - F_j) + \sum_{i>j>k} (F_{ijk} - F_{ij} - F_{jk} - F_{ik} + F_i + F_j + F_k) + \dots \quad (147)$$

Here  $F_i = -T \ln \text{Tr} e^{-H_i/T}$  is the free energy of a single  $i$ -th spin in a field,  $F_{ij} = -T \ln \text{Tr} e^{-(H_i + H_j + H_{ij})/T}$  is the exact free energy of two interacting spins, etc. The terms in the brackets in the second sum and higher order sums cancel each other for large space separations (e.g.  $|\mathbf{r}_i - \mathbf{r}_j|$  for the second order term) so that corresponding variables become essentially independent.

When the system is approaching a phase transition, all terms of the virial expansion become relevant and an actual calculation of critical singularities becomes impossible.

However, the virial expansion method can be used in order to find an approximate *location* of the transition point. Indeed, consider the virial expansion for some susceptibility

$$\chi(T) = \sum_{n=1}^{\infty} \chi_n(T) \quad (148)$$

which must diverge at  $T = T_c$ . The value of  $T_c$  can be determined from the condition that  $T_c$  corresponds to the *limit of convergence* of the series Eq.(148):

$$\lim_{n \rightarrow \infty} \frac{\chi_{n+1}(T_c)}{\chi_n(T_c)} = 1. \quad (149)$$

In practice, an exact *analytical* calculation of  $\chi_n$  with large  $n$  is very cumbersome, such calculations being usually limited by the first few terms,  $n = 1, 2, 3, \dots$ . In the following we will use instead of Eq.(149) the approximate truncated criterion

$$\chi_2(T_c) = \chi_3(T_c). \quad (150)$$

This step constitutes the key approximation of the virial method of calculation of  $T_c$ . It consists in an extrapolation (in general, uncontrolled) into the thermodynamic limit of properties found with exact treatment of few-spin systems.

We now apply this idea to the specific problem of the calculation of superconducting transition temperature corresponding to the Hamiltonian Eq.(145). The relevant susceptibility is defined with respect to the "ordering" field  $\Delta$  which enters the Hamiltonian via the source term

$$V_{\Delta} = - \sum_j (\Delta S_j^+ + \Delta^* S_j^-) \quad (151)$$

Transition into a superconducting state is signaled by the divergence of the Cooper susceptibility

$$\chi(T) = - \frac{\partial^2 F}{\partial \Delta \partial \Delta^*} = \sum_{n=1}^{\infty} \chi_n(T) \quad (152)$$

Below we will describe calculation of the lowest-order virial expansion terms  $\chi_n(T)$  with  $n = 1, 2, 3$  defined in accordance with Eq.(147) as:

$$\begin{aligned} \chi_1 &= \sum_i \chi_i^{(1)} \\ \chi_2 &= \sum_{n>m} (\chi_{nm}^{(2)} - \chi_n^{(1)} - \chi_m^{(1)}) \\ \chi_3 &= \sum_{n>m>l} (\chi_{nml}^{(3)} - \chi_{nl}^{(2)} - \chi_{ml}^{(2)} - \chi_{nm}^{(2)} + \chi_n^{(1)} + \chi_m^{(1)} + \chi_l^{(1)}) \end{aligned} \quad (153)$$

where  $\chi_i^{(1)}, \chi_{ij}^{(2)}, \chi_{ijl}^{(3)} \dots$  are the Cooper susceptibilities of the system of 1, 2, 3 ... spins. These susceptibilities can be expressed through the eigenvalues  $\lambda_{\alpha}(\Delta)$  of the  $N$ -spin Hamiltonian:

$$\chi^{(N)} = - \frac{1}{Z_0} \sum_{\alpha} e^{-\lambda_{\alpha}^{(0)}/T} \gamma_{\alpha}, \quad (154)$$



where  $Z_0 = \sum_{\alpha} e^{-\lambda_{\alpha}^{(0)}/T}$ , and  $\gamma_{\alpha}$  is the sensitivity of the  $\alpha$ -th eigenvalue of the  $N$ -spin Hamiltonian to the  $\Delta$  perturbation:

$$\lambda_{\alpha}(\Delta) = \lambda_{\alpha}^{(0)} + |\Delta|^2 \gamma_{\alpha} + o(|\Delta|^2). \quad (155)$$

In order to compute the  $N$ -spin susceptibility  $\chi_{nml\dots N}^{(N)}$  one has to represent the  $N$ -spin Hamiltonian as a  $2^N \times 2^N$  matrix. The single-spin susceptibility can be found easily:

$$\chi_1(T) = \sum_i \frac{1}{2\xi_i} \tanh \frac{\xi_i}{T} = \nu_0 \ln \left( \frac{4e^{\mathbf{C}} E_b}{\pi T} \right) \quad (156)$$

where  $E_b$  is the upper energy cutoff and  $\mathbf{C} = 0.577\dots$  is the Euler constant.

The two-spin Hamiltonian is given by the 4 by 4 matrix

$$\begin{aligned} H^{(2)} &= \begin{pmatrix} \xi_+ - \frac{1}{2}J_{12}^{\parallel} & \Delta & \Delta & 0 \\ \Delta^* & -\xi_- + \frac{1}{2}J_{12}^{\parallel} & -(J_{12}^{\perp})^* & \Delta \\ \Delta^* & -J_{12}^{\perp} & \xi_- + \frac{1}{2}J_{12}^{\parallel} & \Delta \\ 0 & \Delta^* & \Delta^* & -\xi_+ - \frac{1}{2}J_{12}^{\parallel} \end{pmatrix} \\ &\equiv H_0^{(2)} + V, \end{aligned} \quad (157)$$

where  $\xi_{\pm} = \xi_1 \pm \xi_2$ ,  $J_{ij}^{\parallel} = \frac{g_{\parallel}}{2} M_{ij}$ ,  $J_{ij}^{\perp} = \frac{g_{\perp}}{2} M_{ij}$ ; and the perturbation term  $V \propto \Delta$ . Using the Hamiltonian (157) we calculate  $\lambda_{\alpha}^{(0)}$  and  $\gamma_{\alpha}$  and then use Eq.(154) to obtain second virial term  $\chi_2(T)$ . We give here its simplest form corresponding to  $J_{12}^{\parallel} = 0$ , the full answer being given in the Appendix A:

$$\begin{aligned} \chi_2 &= \sum_{i>j} \left[ \frac{J_{ij}^{\perp}}{2E_+E_-} \tanh \left( \frac{E_+}{T} \right) \tanh \left( \frac{E_-}{T} \right) + \frac{1}{2E_+} \tanh \left( \frac{E_+}{T} \right) \right. \\ &\quad \left. + \frac{1}{2E_-} \tanh \left( \frac{E_-}{T} \right) - \frac{1}{2\xi_i} \tanh \left( \frac{\xi_i}{T} \right) - \frac{1}{2\xi_j} \tanh \left( \frac{\xi_j}{T} \right) \right] \end{aligned} \quad (158)$$

where

$$E_{\pm} = \frac{1}{2}(\xi_i + \xi_j) \pm \frac{1}{2}\sqrt{(\xi_i - \xi_j)^2 + |J_{ij}^{\perp}|^2}. \quad (159)$$

are the exact energies of the two-spin problem.

The three-spin susceptibility  $\chi_3$  requires the solution of the cubic equations which is too long to be written here. The corresponding derivation is given in Appendix A in a form suitable for numerical calculations.

For the standard BCS problem with  $M_{ij} = \frac{1}{V} \rightarrow 0$ , the renormalized energies  $E_{\pm}$  coincide with the bare ones  $\xi_i$  and  $\xi_j$ , and the first term in Eq.(158) is the leading one. In this case the summations over the two energy variables become independent and one gets  $\chi_2(T) = g^2 \nu_0 \ln^2 \left( \frac{4e^{\mathbf{C}} E_b}{\pi T} \right)$ . Applying the simplest truncated criterion  $\chi^{(1)}(T_c) = \chi^{(2)}(T_c)$ , one finds the correct result:  $T_c = (4e^{\mathbf{C}}/\pi) E_b e^{-1/\lambda}$ . In the same way one can show that *any* truncated criterion  $\chi_n(T_c) = \chi_{n+1}(T_c)$  gives the same correct result for  $T_c$  of the BCS problem.

This is no longer true for the case where  $M_{ij}$  has essential energy dependence, as it has in the fractal case where  $M_{ij}$  is given by Eq.(44). In this situation the double

sum in  $\chi_2$  and the corresponding multiple sums in the higher-order susceptibilities  $\chi_n$  do not factorize. Moreover, all  $\chi_n$  with  $n \geq 2$  are dominated by the low-energy region  $\xi \sim T$  and do not contain any logarithmic divergence, in contrast to  $\chi_1$ . This is why the simplest truncated criterion  $\chi_1(T) = \chi_2(T)$  does not make much sense: the corresponding solution depends on the upper energy cutoff  $E_b$ , while for any other truncated criterion  $\chi_n(T) = \chi_{n+1}(T)$  with  $n \geq 2$  the solution is independent of  $E_b$ . It is for this reason that we used Eq.(150) to find an approximate transition temperature. Note, however, that the temperature  $T_{1-2}$  found numerically for the 3D Anderson model with critical disorder from the simplest truncated criterion  $\chi_1(T_{1-2}) = \chi_2(T_{1-2})$  gives values of  $T_{1-2}$  which are close to  $T_{2-3}$  found from Eq.(150) for a meaningful values of the upper energy cutoff  $E_b$ .

So far we completely neglected the presence of the odd sector of the Hilbert space. This is justified in the region of the pseudo-gap superconductivity where the pairing gap  $\Delta_P \gg T_c$ . However, even when being decoupled from the even sector, the odd sector cannot be ignored completely in a general case of  $\Delta_P \sim T_c$ . The reason for that can be easily seen from Eq.(154) which is valid in a general case too. Decoupling of the two sectors manifests itself in vanishing of all "partial" susceptibilities  $\gamma_\alpha$  corresponding to the states  $\alpha$  of the odd sector. Thus only the eigenvalues  $\lambda_\alpha^{(0)}$  corresponding to the even sector appear in the sum in Eq.(154). This is not true for the partition function  $Z_0$ , where *all* states contribute. For  $\Delta_P \gg T$  one can neglect  $e^{-\lambda_{\text{odd}}/T}$  compared to  $e^{-\lambda_{\text{even}}/T}$  and arrive at the result given in Appendix Appendix A. However, in the BCS and the fractal region where  $\Delta_P < T_c$  the susceptibility will be substantially decreased by "statistical dilution" of the even states by the odd ones.

From the standard theory of the BCS superconductivity it is well known that in all expressions the temperature dependence appears as the factor  $\tanh\left(\frac{\xi}{2T}\right)$ . In contrast to it, the Eqs.(156, 158) contain factor  $\tanh\left(\frac{\xi}{T}\right)$ . This gives a simple rule to adjust the virial expansion scheme to the case of vanishing  $\Delta_P$ :

$$\tanh \frac{E_i}{T} \rightarrow \tanh \frac{E_i}{2T} \quad (160)$$

Thus the temperature  $T_{2-3}$  found from the formalism described in Appendix Appendix A should be simply divided by 2 to find the corresponding approximation for the transition temperature in the region of extended single-particle states. In Appendix Appendix B we present the derivation of the virial susceptibilities for the general case of an arbitrary pairing gap  $\Delta_P$  (still, neglecting off-diagonal matrix elements, which mix the "even" and "odd" subspaces of the Hilbert space). In particular, we show there that as long as the renormalization of energy levels (i.e. the difference between  $E_+$  and  $\xi_i$  in Eq.(159)) can be neglected, one can find (see Eq.(B.2)) the whole family of distribution functions  $F(\varepsilon, \Delta_P)$  that interpolate between the two limiting cases,  $\Delta_P \gg T_c$  and  $\Delta_P \ll T_c$ .

In the region of extended and weakly localized single-particle states the renormalization of energy levels is indeed negligible which justifies the approach made in the derivation of (B.2) in this regime. This renormalization is not small in the region of a strong pseudo-gap but in this regime one can project the pseudo-spin Hamiltonian Eq.(145) into a truncated Hilbert space that consists of the *even subspace* only. Thus,

both these limiting cases should be well described by a simple replacement rule:

$$\tanh\left(\frac{\varepsilon}{T}\right) \rightarrow F(\varepsilon, \Delta_P) = \frac{\sinh\left(\frac{\varepsilon}{T}\right)}{\cosh\left(\frac{\varepsilon}{T}\right) + e^{-\Delta_P/T}}, \quad (161)$$

where  $\Delta_P = \langle \Delta_P \rangle$ . Application of this replacement rule to all the formulae obtained in the pseudo-spin model is expected to take correctly into account the effect of "dilution" by the odd sector. With this modification the pseudo-spin Hamiltonian Eq.(145) becomes a unified tool to describe (semi-quantitatively or better) the entire region spanning weakly disordered BCS superconductor to the Anderson insulator.

## 5. Superconducting state very close to mobility edge.

In this section we derive the main physical properties of the three dimensional disordered superconductor with the Cooper attraction characterized by the single-electron states that are critical or very weakly localized. As explained above, a very important property of these wave functions is their fractality which is responsible for the unusual properties of these superconductors. In the regime considered here the number of paired electrons in localization volume is still large, which allows us to neglect the level spacing  $\delta_L$  compared to other relevant energy scales:

$$\delta_L = E_0 \left( \frac{E_c - E_F}{E_0} \right)^{3\nu} \ll T_c.$$

The most important quantity that characterizes a superconductor is its transition temperature and the single particle gap. To compute them we analyze the modified MFA developed in subsection 4.1 and determine the critical temperature  $T_c$  and the gap function  $\Delta(\xi)$ . Then in subsection 5.2 we compare  $T_c$  obtained by the modified MFA with the results of two other methods based on the "diagonal" approximation: the spectral analysis of the discrete modified MF equation with the *fluctuating* kernel  $\hat{Q}$ , and the virial expansion method. We show that the results for the transition temperature  $T_c$  obtained by different methods are in a good mutual agreement but exhibit a strongly enhancement of  $T_c$  compared to the expectations based on Anderson theorem. Finally, in subsections 5.1-5.5 we use Ginzburg-Landau functional derived in subsection 4.2 in order to estimate the fluctuation corrections to these results, to calculate the distribution function of the local order parameter near  $T_c$ , the local density of states at low temperatures and the superfluid density.

### 5.1. Pairing in the modified mean-field approximation.

The linearized modified mean-field equation for fractal superconductor was derived in subsection 4.1, see Eq.(94). It can be generalized for an arbitrary  $T < T_c$  where a non-zero gap function  $\Delta(\xi)$  develops:

$$\Delta(\xi) = \frac{\lambda}{2} \int d\zeta \frac{M(\xi - \zeta)\Delta(\zeta)}{\sqrt{\zeta^2 + \Delta^2(\zeta)}} \tanh \frac{\sqrt{\zeta^2 + \Delta^2(\zeta)}}{2T} \quad (162)$$

A straightforward calculation shows that near the transition temperature Eq.(162) leads to the same result as the Ginzburg-Landau functional with coefficients found in section

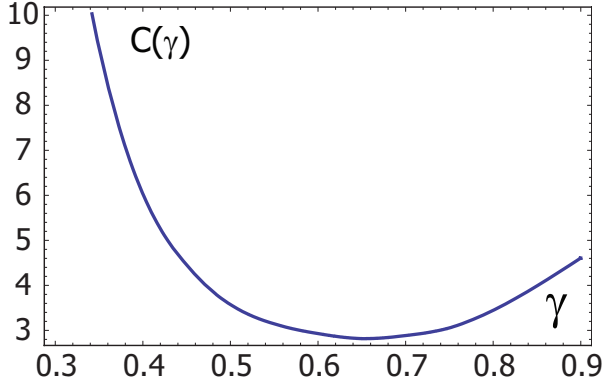


Figure 18: Numerical prefactor  $C(\gamma)$  appearing in the equation for the transition temperature (164) obtained by numerical solution of linearized integral equation (163).

4.2 above. The properties of the superconducting phase in the vicinity of the transition temperature can be found from the solution of the linearized integral equation, equivalent to (94):

$$\Delta(\xi) = \frac{\lambda}{2} \int d\zeta \frac{M(\xi - \zeta)\Delta(\zeta)}{\zeta} \tanh \frac{\zeta}{2T} \quad (163)$$

Eqs.(162,163) with the power-law kernel  $M(\omega)$  given by Eq.(44) can be solved numerically. Its solution depends on the fractal exponent  $\gamma$  which controls the power of the kernel. In particular, the critical temperature is found to be

$$T_c^0(\lambda, \gamma) = E_0 \lambda^{1/\gamma} C(\gamma) \quad (164)$$

where the function  $C(\gamma)$  is plotted in Fig.18. As was already mentioned above, the power-law dependence on the interaction constant  $\lambda$ , instead of the exponential dependence  $e^{-\frac{1}{\lambda}}$  in the standard BCS theory, implies a dramatic enhancement of  $T_c$  by disorder if interaction constant  $\lambda$  is small. This result could be important for observation of superconductivity in a system of cold fermions with weak attraction trapped in a disordered lattice. The solution for  $\Delta(\xi)$  at  $T = T_c$  is shown in Fig.19a for  $\gamma = 0.57$  corresponding to the 3D Anderson model. At large  $\xi \gg T_c$  this function decays as  $\Delta(\xi) \propto \xi^{-\gamma}$ , as demonstrated in Fig.19b.

The maximum value of the function  $\Delta(\xi)$  is attained at  $\xi = 0$  for all temperatures. In the  $T \rightarrow 0$  limit we find

$$\Delta_0(0) = E_0 \lambda^{1/\gamma} D(\gamma) \quad (165)$$

where the function  $D(\gamma)$  is plotted in Fig.20a. The ratio  $2D(\gamma)/C(\gamma)$ , which characterizes the ratio of low-temperature spectral gap to the transition temperature, is shown as function of  $\gamma$  in Fig.20b. Coincidentally, this ratio for the 3D Anderson model with the fractal exponent  $\gamma = 0.57$  turns out to be rather close to the BCS value 3.5. This implies that unfortunately it is difficult to distinguish the fractal 3D superconductors from conventional BCS ones by measuring  $2\Delta/T_c$  value.

Evident strange feature of  $D(\gamma)$  and  $2D(\gamma)/C(\gamma)$  behavior is that they do not seem to approach the BCS limit at small  $\gamma$ . The reason is the same as was discussed in section

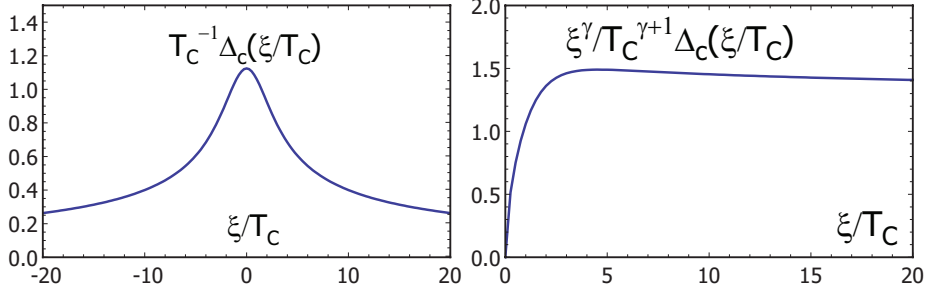


Figure 19: (a) Functional dependence of the gap function  $\Delta(\xi)$  for  $T = T_c$  at  $\gamma = 0.57$  that corresponds to the largest eigenvalue of the linearized integral gap equation (163). (b) Asymptotic behaviour of  $\Delta(\xi)$  at large  $\xi/T$ .

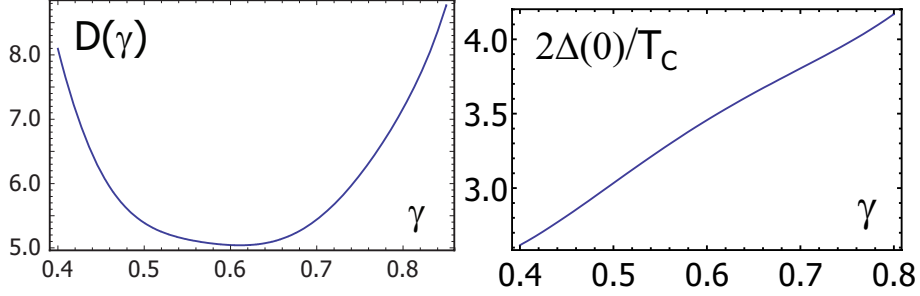


Figure 20: (a) Prefactor  $D(\gamma)$  in the equation (165) for the maximum value  $\Delta(0)$  of the  $T = 0$  obtained from the numerical solution of the non-linear gap equation (162). (b) Ratio  $2\Delta(0)/T_c$  that follows from (165) with  $D(\gamma)$  shown here and (164) with  $C(\gamma)$  shown in Fig.18

4.2.1 around Eq. (118): in order to get the correct crossover to the non-fractal limit  $\gamma \rightarrow 0$ , one needs to introduce the upper energy cutoff  $\Omega_D$ . Indeed, the BCS limit is reached at  $\gamma \ll \ln^{-1} \frac{\Omega_D}{T_c} \ll 1$  which is never satisfied if the upper energy cutoff is infinite as in the calculations here.

### 5.2. Comparison of $T_c$ values obtained in three different approximations.

General modified MFA equation (164), with the parameter  $C(\gamma) \approx 3.1$  evaluated for  $\gamma = 0.57$ , and the estimate (46) for  $E_0$ , gives

$$T_c^0 = (6.5 \pm 0.8)\lambda^{1.77} \quad (166)$$

As we explained above, there are two different types of corrections to this formula: the corrections caused by the off-diagonal matrix elements in the original Hamiltonian, and the corrections due to approximations made within the “diagonal approximation”, in particular, the continuum approximation that neglects the fluctuation of spectrum and the matrix elements which are taken to be a power-law function of the energy difference. An estimate of the contribution from off-diagonal matrix elements is given in section 4.2.5. In order to clarify the role of the static fluctuations of the spectrum, we determine the

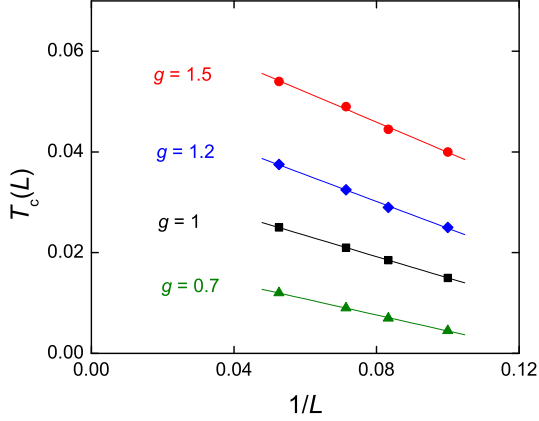


Figure 21: Transition temperatures determined via  $\rho(k)$  spectrum, for a number of coupling constants and system sizes between  $L = 10, 12, 14$  and  $19$ .

transition temperature for the same 3D Anderson model using two other methods. We first determine it from the condition  $\lambda_{\max} = 1$  (see section 4.1) where  $\lambda_{\max}$  is the largest eigenvalue of the matrix kernel  $\hat{Q}$  defined by Eq.(97) that contains matrix elements  $M_{ij}$  corresponding to the specific realization of disorder in finite size samples. This method adapts modified MFA to the case of strong spatial fluctuations. Second, we apply the virial expansion method as described in section 4.4. Because here we consider the regime  $\Delta_P \ll T_c$ , we use the replacement rule Eq.(160) to take account of the dilution of pseudospin states. In both methods we observe strong finite-size effects as shown in Fig.21,22.

The extrapolation to infinite system sizes gives the values of  $T_c$  as function of the dimensionless coupling constant  $\lambda$  shown in Fig.23. As one can see, all these methods give the results close to each other and to the result Eq.(166) of the modified MFA at  $\gamma = 0.57$ . The conclusion that we draw from this apparent coincidence is that all approximations involved in these methods are reasonable. Specifically, it seems that one can neglect the fluctuations of the single-particle DoS and the matrix elements  $M_{ij}$  at the mobility edge; one can also use the small- $n$  truncated criterion for  $T_c$  in the virial expansion method. The main correction to the results of the *analytical* modified MFA given by Eqs.(162) comes from the off-diagonal matrix elements. However, even this correction is able to reduce the transition temperature at most by a factor of the order of unity leaving all the results of modified MFA *semi-quantitatively correct*.

### 5.3. Pairing amplitude in the real space

The real-space pairing amplitude corresponding to the solution  $\Delta_i$  of Eq.(93) can be determined from Eq.(96) for  $T \approx T_c$ . To demonstrate that  $\hat{\Delta}(\mathbf{r})$  corresponds to strongly spatially inhomogeneous solution, we calculate the averaged square of the pairing

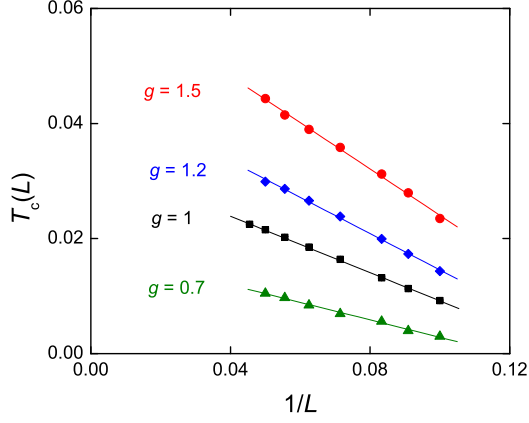


Figure 22: Transition temperatures determined via the virial expansion, for a number of coupling constants and system sizes between  $L = 10$  and  $L = 22$ .

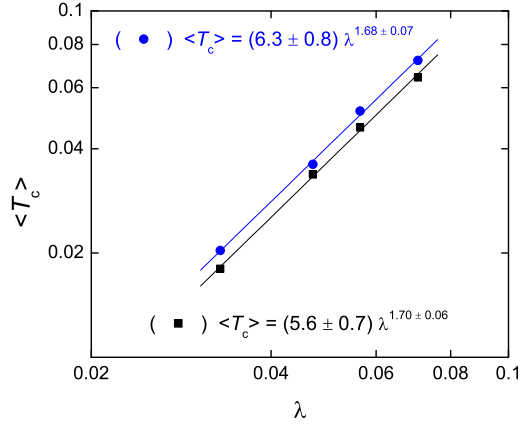


Figure 23: (Color online) The results for transition temperature as function of dimensionless coupling: the  $\hat{Q}$ -kernel analysis (blue dots) and the virial expansion (black squares), extrapolated to  $L = \infty$ ; The Fermi-energy is fixed at the mobility edge.

amplitude

$$\overline{(\tilde{\Delta}(\mathbf{r}))^2} \equiv \frac{1}{V} \int d^d \mathbf{r} \tilde{\Delta}^2(\mathbf{r}) = \lambda \int_0^\infty d\xi \eta(\xi) \Delta_c^2(\xi) \quad (167)$$

where we used the definition (10) and Eqs.(93,94) to derive the r.h.s. of the above equation. Then we calculate its simple average

$$\overline{\tilde{\Delta}(\mathbf{r})} \equiv \frac{1}{V} \int d^d \mathbf{r} \tilde{\Delta}(\mathbf{r}) = \lambda \int_0^\infty d\xi \eta(\xi) \Delta_c(\xi) \quad (168)$$

From Eqs.(168,167) we conclude that

$$f = \frac{\left(\overline{\tilde{\Delta}(\mathbf{r})}\right)^2}{\overline{(\tilde{\Delta}(\mathbf{r}))^2}} = \lambda \mathcal{Q}(\gamma) = \frac{\mathcal{Q}(\gamma)}{C^\gamma(\gamma)} \left(\frac{T_c}{E_0}\right)^\gamma \ll 1 \quad (169)$$

where the dimensionless function

$$\mathcal{Q}(\gamma) = \gamma \left( \int_0^\infty \frac{d\xi}{\xi} \tanh \frac{\xi}{2T_c} \frac{\Delta_c(\xi)}{T_c} \right)^2 ; \quad \mathcal{Q}(0.57) = 3.1 \quad (170)$$

The small ratio (169) gives the estimate of the space fraction where pairing correlations are well established. Indeed, consider a toy model where  $\Delta(\mathbf{r}) = \Delta_0$  in a fraction  $f$  of the whole space, and zero otherwise. Then we find  $\overline{\tilde{\Delta}(\mathbf{r})} = f\Delta_0$  and  $\overline{(\tilde{\Delta}(\mathbf{r}))^2} = f\Delta_0^2$ , leading to the ratio (169) equal to  $f$ . In a realistic case  $\Delta(\mathbf{r})$  take a continuum of values, so one can use this ratio as a proper *definition* of the fraction of space with well developed superconductive gap.

Note that the regions in space where the superconductive gap is appreciable constitute a *finite* fraction of the entire space, despite the fact that fractal support of any *single-particle* wavefunction occupies *vanishing* fraction of the entire space. Therefore the global spatial pattern of superconductivity is not a fractal but rather is reminiscent of that of the *multi-fractal metal* [77].

The above estimate was done for a region near  $T_c$ . At temperatures much below  $T_c$ , (96) should be replaced by the similar equation in which the argument  $\xi_k$  is replaced by  $\sqrt{\xi_k^2 + \Delta_k^2}$ . As one might expect, one ends up with the same estimates in which  $T_c$  gets replaced by  $\Delta_0(0)$ .

Higher moments of the distribution function  $P[\tilde{\Delta}(\mathbf{r})]$  can be estimated using the algebra of multi-fractal states discussed in section 2.2, see Eq.(47). Straightforward generalization of Eq.(169) gives

$$\frac{\left(\overline{\tilde{\Delta}(\mathbf{r})}\right)^n}{\overline{(\tilde{\Delta}(\mathbf{r}))^n}} \propto (T_c/E_0)^{(1-d_n/d)(n-1)} \quad (171)$$

Therefore the moments of  $\tilde{\Delta}(\mathbf{r})$  contain information about all fractal dimensions  $d_n$ . This is because the fractality of single-particle states manifests itself *locally* at a scale smaller than  $L_T \sim (\nu_0 T_c)^{-1/d}$ , above this length the order parameter and other properties of the superconductor become homogeneous, similar to what happens in a multi-fractal metal [77] which has a sparse fractal structure within the correlation length. Thus, this state should be properly named *fractal superconductor*.



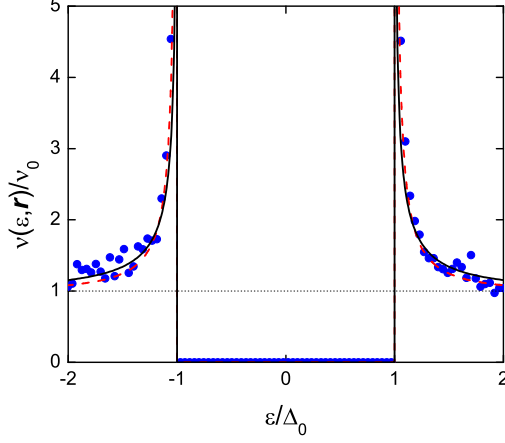


Figure 24: Local zero-temperature density of states at the mobility edge of the 3D Anderson model, averaged over 5x5 square (blue dots); average  $T = 0$  superconductive DoS at the mobility edge, according to Eq.(173), shown by dashed red line; the BCS density of states with the same gap value (full black line).

#### 5.4. Low-temperature density of states.

Local density of states (DoS) in the superconducting state is given by

$$\nu(\varepsilon, \mathbf{r}) = \frac{1}{2} \sum_j \left( 1 + \frac{\xi_j}{\varepsilon} \right) [\delta(\varepsilon - \varepsilon_j) + \delta(\varepsilon + \varepsilon_j)] \psi_j^2(\mathbf{r}) \quad (172)$$

where  $\varepsilon_j = \sqrt{\xi_j^2 + \Delta^2(\xi_j)}$  and  $\Delta(\xi)$  is the solution of the gap equation (162). We begin with the calculation of the average DoS:

$$\nu(\varepsilon) = \nu_0 \left| \frac{d\xi(\varepsilon)}{d\varepsilon} \right| \quad (173)$$

where the function  $\xi(\varepsilon)$  is defined as the (positive-valued) inverse function for  $\varepsilon(\xi) = \sqrt{\xi^2 + \Delta^2(\xi)}$ .

We plot in Fig.24 the local DoS (at  $T = 0$ ) obtained numerically using Eq.(172), as well as the average DoS obtained from Eq.(173) for  $\gamma = 0.57$ ; the usual BCS DoS is shown for comparison.

Note that the terms  $\xi_j/\varepsilon$  in the parenthesis in Eq.(172) were irrelevant while calculating the average DoS because contributions from  $\xi = \pm\xi(\varepsilon)$  cancel out. There is no such cancellation for the higher moments of  $\nu(\varepsilon, \mathbf{r})$ . In particular, these terms might lead to an asymmetry of local DoS:  $\nu(\varepsilon, \mathbf{r}) \neq \nu(-\varepsilon, \mathbf{r})$ . To quantify this asymmetry we define the antisymmetric part of the DoS:  $\nu_a(\varepsilon, \mathbf{r}) = \frac{1}{2}(\nu(\varepsilon, \mathbf{r}) - \nu(-\varepsilon, \mathbf{r}))$ . Using then Eqs.(172,173), we find the variance

$$\overline{\nu_a^2(\varepsilon, \mathbf{r})} = \frac{1}{2} \left( \nu(\varepsilon) \frac{\xi(\varepsilon)}{\varepsilon} \right)^2 [M(0) - M(2\xi(\varepsilon))] \quad (174)$$

where the function  $M(\xi)$  is defined in Eq.(44). Since  $M(0) \sim \mathcal{V}^\gamma \gg M(2\xi)$ , the variance (174) diverges for an infinite system, and one should consider the distribution function  $W[\rho(\varepsilon, \mathbf{r})]$  for the dimensionless variable

$$\rho(\varepsilon, \mathbf{r}) = \frac{\nu_a(\varepsilon, \mathbf{r})}{\nu(\varepsilon)} \frac{\sqrt{2}\varepsilon}{\xi(\varepsilon)} \quad (175)$$

The distribution function  $W[\rho(\varepsilon)]$  coincides with that of the wavefunction's intensities  $\mathcal{P}(\psi^2)$ , see Eq.(2.33) of the review [78]. It is determined by the "singularity spectrum"  $f(\alpha)$ ; the shape of this function for the 3D Anderson model is similar to the one found for the power-law banded matrix model [92, 72] with the parameter  $b \approx 0.4$ , see Fig.3 of paper[78].

It is clear from the definition (175) that the normalized asymmetric fluctuations  $\nu_a(\varepsilon, \mathbf{r})/\nu(\varepsilon)$  are small for  $\varepsilon \approx \Delta(0)$ , where  $\xi(\varepsilon) \rightarrow 0$ . However, for a generic value of the energy of the order of  $\Delta(0)$ , the asymmetry in the tunneling spectra is strong; we emphasize that it occurs due to mesoscopic fluctuations which do not involve any "regular" mechanism of particle-hole asymmetry.

##### 5.5. Superfluid density and critical current.

We define the superfluid density  $\rho_s$  via the relation  $\mathbf{j} = -\rho_s \mathbf{A}/c$  assuming the transverse gauge with  $\nabla \cdot \mathbf{A} = 0$ . To estimate  $\rho_s(T)$  near  $T_c$ , one can use the expression (108) for the free energy functional, and make there the replacement  $\nabla \rightarrow \nabla - i(2e/\hbar c)\mathbf{A}$ . Then taking the double functional derivative  $\delta^2 F_{GL}/\delta \mathbf{A}^2$  one obtains:

$$\rho_s(T) = 2 \left( \frac{2e}{\hbar} \right)^2 \nu_0 T_c^2 C \Psi^2(T) \quad (176)$$

where  $\Psi(T) = \Psi_{\text{MFA}}^2 = \frac{|a(T)|}{b} = 9.5 \left( 1 - \frac{T}{T_c} \right)$  and the coefficient  $C \sim L_T^2$  is given by Eq.(135).

We also estimate the critical current  $j_c$  in a standard way via the Ginzburg-Landau functional (108). By extrapolating the result of Ginzburg-Landau theory to lower temperatures, one obtains

$$j_c = c \frac{2e}{\hbar} T_c (\nu_0 T_c)^{2/3} \quad (177)$$

Extrapolation (177) of the Ginzburg-Landau result to  $T = 0$  might be wrong by a factor of the order of unity, this factor for the fractal superconductor might be different from the known factor for a conventional "dirty-limit" superconductor.

The results Eqs.(176),(177) do not contain any "fractal" specificity and coincide with estimates of earlier works[2, 3] that used scaling arguments. Yet, as we have demonstrated above, the web of superconductivity is sparse and occupies only a small fraction  $f \sim \lambda \ll 1$  of space. The derivation of Eq.(135) demonstrates that the fractality-independent result for the coefficient  $C$  emerges because of the compensation of the small parameter  $\lambda^2$  by the enhancement factor  $(E_0/T_c)^{2\gamma}$ . We interpret this cancellation as the compensation of the small cross-section area of "superconductive filaments" by a large current that they support.

## 6. Superconductivity with a pseudogap.

In this section we study the superconductivity formed against the background of moderately localized single-electron eigenstates. We demonstrate here the existence of the interesting regime where the local pairing (discussed above in section 3 in relation with the hard-gap insulator) coexists with the long-range superconducting correlations. In this situation the material demonstrates the "pseudo-gap" phenomenology characterized by the insulating behavior of  $R(T)$  in a significant temperature range above the superconducting transition. We provide a semi-quantitative description for the evolution of the pseudo-gap  $\Delta_P$  and  $T_c$  while  $E_F$  moves across the mobility edge  $E_c$ . Surprisingly, we find that  $T_c(E_F)$  curve is non-monotonic, with a maximum reached at the Fermi-level on the localized side of the Anderson transition. The most important outcome of our analysis is the existence of a range of Fermi energies for which superconductor is characterized by relatively high values of  $T_c$  and by a *larger* insulating pseudo-gap  $\Delta_P \gg T_c$ . In this regime the low energy properties such as the formation of the superconductivity can be described by the truncated pseudo-spin model. In this model the effective Hamiltonian is of the form (145) while the Hilbert space contains only the states in which each localized orbital is either empty or populated by a pair of electrons. The effective Hamiltonian (145) does not contain  $\Delta_P$  because the states that differ in energy by  $\Delta_P$  are absent from the truncated Hilbert space. These states, however, appear when single particles are excited, thus the single particle excitations spectrum contains both correlations and local pairing effects. Below we discuss the region of validity of the mean-field treatment of the pseudo-spin Hamiltonian (145) and then turn to analysis of several measurable quantities which may provide one with the "proof of the case" for realization of the pseudo-gap superconductivity in real material: the temperature evolution of the local single-particle density of states  $\nu(\varepsilon, T)$ , the Andreev conductance spectra  $G_A(V)$  at  $T \ll T_c$ , and the temperature dependence of the full spectral weight  $K(T)$ .

### 6.1. Transition temperature and insulating gap as functions of Fermi energy.

We demonstrated in section 5.2 that the transition temperature found by the virial expansion to the third order provides results very close to the ones obtained with the modified MFA. These calculations were performed for the critical case  $E_F = E_c$  where the function  $M(\omega)$  is given by the power law (44). This coincidence implies that the virial expansion to the third order provide the accurate result for the transition temperature. Generally, both methods suffer from the neglect of the off-diagonal matrix elements, these matrix elements mix the odd and even fermionic sectors which might decrease the  $T_c$  below the MFA value by a factor of the order of unity (which would be consistent with the  $G_i \sim 1$  obtained for the critical case in section 4.2.5). While there is no general reasons why the off-diagonal matrix elements can be completely neglected in the metallic and in the critical region, in the region of well localized single-particle states the validity of the spin Hamiltonian (145) is ensured by the large value of the pseudogap  $\Delta_P$ . One thus expects that pseudospin model provides very good description of the pseudogap state and a semi-quantitative description of the crossover from the pseudogap state (where it is exact) to the fractal superconductor (where its results might differ by a factor of the order of unity). Because the superconductivity suppression deep in the insulating regime is due to the decrease in the effective number of neighbors of each pseudospin and this

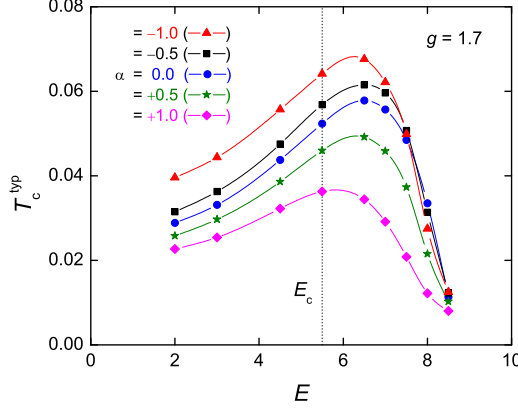


Figure 25: (Color online) Transition temperature as a function of the Fermi-level position, determined by the virial expansion method. Blue dots correspond to the pseudo-spin Hamiltonian Eq.(145) with  $g_{\parallel} = 0$ , whereas other data were obtained after including the Hartree-type terms proportional to  $g_{\parallel}$  of repulsive (red triangles and black squares) and attractive (green stars and violet diamonds) sign (see text for details). All calculations were done at a fixed coupling constant  $g_{\perp} = g$ .

effect is missing in the modified MFA we shall use the virial expansion applied to the spin Hamiltonian (145) to obtain the properties in both the crossover and pseudogap regime.

We begin by applying this method to describe the evolution of  $T_c$  as Fermi-level crosses the mobility edge  $E_c$  and gets into the region of weakly localized states. In this regime, assuming that single electron states are characterized by small participation ratio so that corresponding  $\Delta_P < T_c$ , we can use the simplified version of the virial approach with the distribution function  $\tanh \frac{E_i}{T}$  replaced by  $\tanh \frac{E_i}{2T}$ , as it was done for critical states at  $E_F = E_C$  in Sec. V. The numerical results for the minimal pseudo-spin Hamiltonian Eq.(145) with  $g_{\parallel} = 0$  and coupling matrix  $M_{ij}$  generated by random 3D Anderson model Eq.(21) are shown in Fig.25 by blue points. They correspond to the fixed coupling constant  $g = 1.7$  in the original model and, thus, *dimensionless* coupling constant  $\lambda = g\nu_0$  varying as function of  $E_F$ . The energy dependence of density of states is not negligible around  $E_c$  as can be seen in Fig.4, as a result  $\lambda(E_F)$  drops considerably in the range of Fermi-energies covered in Fig. 25. Nevertheless, the calculation not only confirms our analytical prediction of the enhancement of  $T_c$  near the critical disorder made in section 4.1 but also shows that  $T_c$  continues to increase in a significant interval of Fermi energies corresponding to the localized region. This surprising result can be traced back to the behavior of the correlation function  $M(\omega) = \mathcal{V}M_{ij}$  in the domain of weakly localized states. Indeed, it was found previously (see the discussion at the end of section VIII B of Ref. [77]) that the effective decrease of fractal dimension  $d_2$ , and, thus, the increase of  $\gamma = 1 - d_2/d$  occurs while going further into the insulating domain. For small values of  $\lambda$  it results in the increase of  $T_c \propto \lambda^{1/\gamma}$  evident in Fig.25 in the range of  $E_c < E < 6.5$ . Note that in contrast to Fig.23 the Fig.25 shows the data for the fixed value of system size,  $L = 20$ , with no finite-size scaling adjustment. This is why the

values of  $T_c$  data for the critical states,  $E = 5.5$ , differ slightly between these two data sets.

The generic pseudo-spin Hamiltonian Eq.(145) contains also the Hartree terms

$$H_{\text{Hartree}} = -g_{\parallel} \sum_{ij} M_{ij} S_i^z S_j^z. \quad (178)$$

Moreover, for the short-range  $\delta$ -function two-body interaction, the coupling constant  $g_{\parallel}$  is equal to the Cooper-channel coupling constant  $g_{\perp}$  and, thus, the terms containing the spin-spin interaction in pseudo-spin Hamiltonian (145) become isotropic. Because the full Hamiltonian (145) remains highly anisotropic due to the presence of the single spin terms, the effect of the  $S_i^+ S_j^-$  and  $S_i^z S_j^z$  spin-spin interactions is dramatically different: the former leads to the superconducting instability at low temperatures, while the latter term by itself has only weak effect of spin susceptibility for small  $g_{\parallel}\nu$ . Because the transition temperature depends strongly on the spin susceptibility, in the presence of the  $S_i^+ S_j^-$  the Hartree term can have slightly more significant effect. Below we study the change in the critical temperatures induced by the  $S_i^z S_j^z$  interaction for a generic ratio  $\alpha = g_{\parallel}/g_{\perp}$  using the virial expansion method.

The results are shown in Fig. 25 by green and violet points for  $\alpha = +0.5$  and  $\alpha = +1$ , and by red and black points for  $\alpha = -1$  and  $\alpha = -0.5$ , respectively. We conclude that upon the account for the Hartree terms, all the qualitative features of the original  $T_c(E_F)$  behavior, including the enhancement of  $T_c$  by disorder, are preserved. Therefore below we stick to the simplest version of our model with  $\alpha = 0$ .

With a further shift of  $E_F$  into the localized domain, the two effects become important. First of them is the growth of the inverse participation ratio  $M_j$ , and the related development of the parity gap  $\Delta_P$ , see Eq.(77). In some range of  $E_F$ , as we will see soon, the typical value of  $\Delta_P$  becomes larger than  $T_c$ , which means that the calculations of the virial coefficients should be modified, taking into account *exactly* the effect of "dilution" by the odd states discussed in section 4.4. The necessary modification of the formalism is presented in the Appendix B. The dilution elimination by the pseudo-gap leads to the increase of  $T_c$  values (as compared to the data for  $\Delta_P = 0$  shown in Fig.25, where the maximum effect of dilution was assumed). However, as one can see in Fig. 26 in the region where superconductivity exists this increase is not more than 30%.

The second effect, which takes over sufficiently far in the localized region, is due to the drop of the effective coordination number  $Z_{\text{eff}}$  of the spin model defined by Eq.(145). Indeed, the effective number of states  $k$  that are coupled to a given state  $j$  can be roughly estimated by  $Z \sim \nu_0 T_c L_{loc}^3$  (this estimate misses the important logarithmic factor that we discuss below around Eq.(179)). With decreasing of the localization length  $L_{loc}$ , the coordination number  $Z_{\text{eff}}$  drops down, and eventually becomes less than unity, which makes description in terms of average matrix elements  $\mathcal{V}\overline{M_{ij}} = M(\omega)$  meaningless. When the Fermi energy is increased further,  $T_c$  starts to drop down sharply simply because most individual pseudospins (with a possible exception of rare small spin clusters) become essentially decoupled from each other.

Evolution of both  $T_c$  and  $\Delta_P$  with the Fermi-level position are shown in Fig.26, where we show the results obtained by the virial expansion method, with a finite pseudo-gap  $\Delta_P$  taken into account. The most important feature seen in this plot is the existence of some range of  $E_F$  where superconductivity with an appreciable  $T_c$  exists, but the

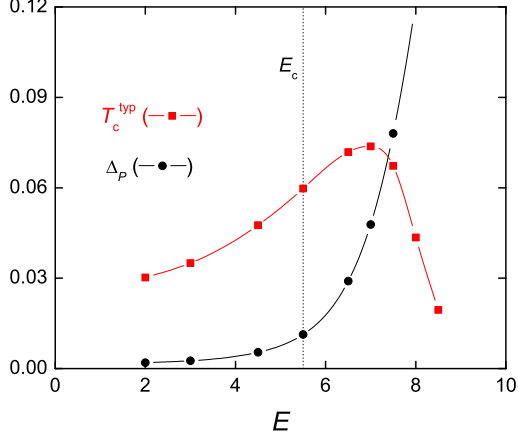


Figure 26: (Color online) Virial expansion results for  $T_c(E_F)$  (red squares) and typical pseudogap  $\Delta_P$  (black dots) as functions of  $E_F$ . The model with fixed value of the attraction coupling constant  $g = 1.7$  was used; pairing susceptibilities were calculated using equations derived in Appendix B.

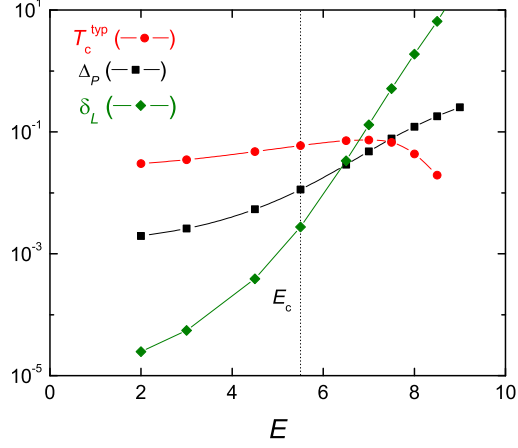


Figure 27: (Color online) Virial expansion results for  $T_c(E_F)$  (red dots), the typical pseudo-gap  $\Delta_P$  (black squares) and the corresponding level spacing  $\delta_L$  (green diamonds), as functions of  $E_F$  in the semi-logarithmic scale.

parity gap  $\Delta_P$  exceeds substantially the superconductive gap  $\Delta \approx 1.7T_c$ . Below we concentrate specifically on this range of parameters (approximately, it corresponds to the range  $E_F \in (7.5, 8.5)$  for the 3D Anderson model studied here), where the specific features of superconductivity developed on top of the pseudo-gap are most pronounced. This is precisely the region of the *pseudo-gap superconductivity* where the pseudo-spin model Eq.(145) provides a quantitatively correct description of superconductivity.

Note that in this range of parameters the typical level spacing  $\delta_L$  inside the localization volume (estimated with the use of Eq.(71)) is much larger than both  $T_c$  and  $\Delta_P$ , as it is demonstrated in Fig.27. The very existence of a nonzero  $T_c$  in this situation is unexpected.<sup>6</sup> It is related to the fact (noticed in Ref. [77] and discussed in section 2.2.5) that the localized states characterized by the localization length  $L_{\text{loc}}$  overlap effectively up to the distance  $R(\omega) \gg L_{\text{loc}}$  between them, where  $\omega \ll \delta_L$  is the relevant energy window  $(-T_c, T_c)$ . In the present context we can put  $\omega \sim T_c$  and estimate the effective interaction range  $R_0$  and coordination number  $Z_{\text{eff}}$  of the spin model (145) using the definition in Eq.(66) in subsection 2.2.5, see also Eqs.(21,25) in the paper [77]. We obtain

$$Z_{\text{eff}} = \nu_0 \frac{4\pi}{3} R_0^3(T_c) \cdot 2T_c \quad (179)$$

where the function  $R_0(\omega)$  should be determined numerically. Using data shown in Fig. 27 for the case of  $E_F = 8$  and similar data for several other values of  $E_F$  in the pseudogap range, where  $T_c \ll \delta_L$ , we obtain the following values for the effective number of neighbors in the energy window  $(-T_c, T_c)$ :

$E_F$	7.75	8.0	8.25	8.5
$T_c$	0.057	0.044	0.030	0.02
$\delta_L$	1.0	1.9	3.5	6.5
$Z_{\text{eff}}$	0.08	0.09	0.09	0.07

(180)

Of course, the numerical coefficient in Eq.(179) is somewhat arbitrary; the main conclusion from Eq.(179) is that (due to a presence of the logarithmic enhancement in  $R_0(\omega)$ ) the effective number of neighbors remains nearly constant in a wide range of small  $T_c/\delta_L \ll 1$ . Together with a weak  $T_c/\delta_L$  dependence this explains why a significant  $T_c$  is found even for  $\delta_L/T_c \sim 300$ , see Fig. 27.

As we explain in more detail below, the possibility to find a pseudogaped superconductive state with a numerically small effective coordination number ( $Z_{\text{eff}} \sim 0.1$ ) is natural. The qualitative reason is that our definition of  $Z_{\text{eff}}$  implies average over all states. Therefore, this average includes the states that overlap strongly with each other and the ones which overlap little with any other states. The former states form an infinite superconducting cluster while the latter do not contribute to superconductivity and are largely irrelevant. In the strongly disordered regime the superconducting cluster occupies a small part of all states, so the average is dominated by the states which overlap very little with each other.

Upon a further increase of the Fermi energy into the localized region the effective number of neighbors slowly decreases leading to a sharp drop in  $T_c^{\text{typ}}(E_F)$ , see Fig. 26.

---

<sup>6</sup>In contrast, superconducting correlations in ultrasmall metall grain are destroyed at  $\delta \sim \Delta$ , see discussion in section 2.1.1.

Finally, when the effective number of neighbors becomes less than some critical value  $Z_c$ , the superconducting instability ceases to occur even at  $T = 0$ . The details of this quantum transition and the qualitative properties of the phase formed at high disorder are discussed in [93]. This work solves the simplified model similar to (145) in which spin are located of a Bethe lattice with coordination number  $Z^{\text{Bethe}}$ , i.e. in this model  $M_{ij} = 1/Z^{\text{Bethe}}$  for  $Z^{\text{Bethe}}$  neighbors and 0 otherwise.<sup>7</sup> The result of the solution [93] which is important for the present discussion is that critical fluctuations become important only in the narrow vicinity of the quantum critical point at which superconductivity disappears completely. In other words, the critical fluctuations become important only in the systems in which transition temperature is already strongly suppressed by disorder. In more detail, the work [93] distinguishes between the high temperature phase where corrections to mean field are small and a low temperature phase where mean field solution becomes qualitatively incorrect due to the strong inhomogeneity of the formed ordered phase. The temperature ( $T_{\text{RSB}}$ ) that separates them corresponds to replica symmetry breaking (RSB) in the formalism, it turns out to be numerically small even for modest number of neighbors as illustrated in Fig. 28. Viewed differently, it means that the effective number of neighbors in this regime is very low (see Fig. 28 insert).

As long as the transition temperature obtained in the mean field approximation is above  $T_{\text{RSB}}$  shown in Fig. 28, the mean field equations are qualitatively correct. Thus, one can use mean-field approximation for the Hamiltonian (145) to get semi-quantitative results for the transition temperature in a large interval of Fermi energies at which  $T_c(E_F)$  decreases significantly from its maximum.

The solution of the Bethe lattice model [93] can be used to estimate critical value of the effective coordination number  $Z_{\text{eff}}^{\text{Bethe}} = \nu_B T_{c0} Z_{\text{RSB}}^{\text{Bethe}}$  which corresponds to the value  $Z_{\text{RSB}}^{\text{Bethe}}$  of the Bethe-lattice coordination number where  $T_c = T_{\text{RSB}}$  and standard mean-field solution becomes qualitatively incorrect. The details of the corresponding calculation will be presented in the extension [94] of the paper [93]; the result, valid in the limit  $Z^{\text{Bethe}} \gg 1$ , is

$$Z_{\text{eff}}^{\text{Bethe}} = \lambda_b e^{1/2\lambda_b} \nu_B T_{c0} = \frac{1}{2} \sqrt{\pi} e^{-\mathbf{C}/2} \frac{\sqrt{\nu_B T_{\text{RSB}}}}{|\log(\nu_B T_{\text{RSB}})|} \ll 1 \quad (181)$$

where  $\lambda_b = \nu_B g_B \ll 1$  is the dimensionless coupling constant for the Bethe lattice model, with  $\nu_B T_{c0} = \frac{4}{\pi} e^{\mathbf{C}} e^{-1/\lambda_b}$ , and  $\mathbf{C} = 0.577..$  is the Euler number. Eq.(181) demonstrates again, that typical number of neighbors with energies within the energy stripe  $\sim T_c$  can be very small in the weak-coupling limit, contrary to naive expectations. Physically, the reason for this is that in this regime a dilute superconducting cluster is formed by a small number of sites. One expects that similar phenomena should happen in physical systems. Although our fractal model differs significantly from the Bethe lattice model due to power-law dependence of the interaction strength  $M(\omega)$ , we expect that qualitative conclusion about  $Z_{\text{eff}}^{\text{min}} < 1$  survives in the fractal model as well.

The significant number of neighbors that persists up to numerically large values of  $\delta_L/T_c \sim 300$  implies that Ginzburg parameter remains of the order of unity in this

---

<sup>7</sup>Notice that this definition of the number of neighbors differs a lot from the (179) that counts the neighbors *only* in the narrow energy interval of  $T_c$ .



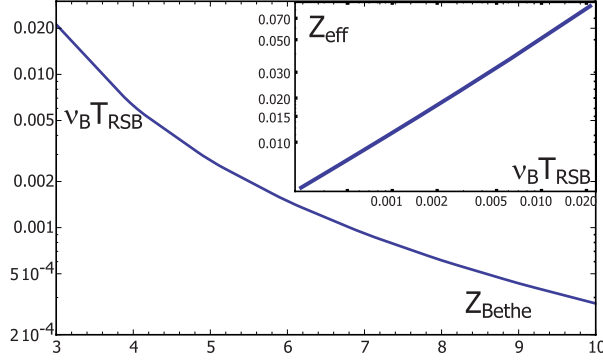


Figure 28: Temperature separating high and low temperature regimes of the simplified pseudospin model (145) on Bethe lattice with  $Z_{\text{Bethe}}$  neighbors, for which  $M_{ij} = 1/Z_{\text{Bethe}}$  and density of states per site  $\nu_B$ . In the high temperature regime  $T > T_{RSB}$  the mean field theory is semi-quantitatively correct, in the low temperature regime it is qualitatively wrong; the value of  $T_{RSB}$  does not depend upon coupling constant  $g$  within the Bethe lattice model. The inset shows the effective number of neighbors in this model defined by  $Z_{\text{eff}}^{\text{Bethe}} = \nu_B T_{c0} Z_{\text{Bethe}}$  at which the mean field solution becomes qualitatively incorrect.

range.<sup>8</sup> In this regime the gap below  $T_c$  can be semi-quantitatively approximated by the solution of the mean field equation:

$$\Delta(\xi) = \frac{\lambda}{2} \int d\zeta \frac{M(\xi - \zeta) \Delta(\zeta)}{\sqrt{\zeta^2 + \Delta^2(\zeta)}} \tanh \frac{\sqrt{\zeta^2 + \Delta^2(\zeta)}}{T} \quad (182)$$

where we used the fact  $\Delta_P \gg T_c$  to replace  $2T \rightarrow T$  and  $M(\omega)$  is given, for localized states, by interpolating formula, Eq.(69).

One of basic results of weak-coupling BCS theory is the universal relation between low-temperature gap value and transition temperature,  $\Delta(0) = 1.76T_c$ . As was shown in section 5.1, the ratio  $\Delta(0)/T_c$  stays about the same within MFA for fractal superconductor with  $\gamma$  exponent near 0.6, corresponding to 3D Anderson model, see Fig.20b. The presence of strong pseudo-gap  $\Delta_P \gg T_c$  leads to the doubling of  $T_c$  for the same value of  $\Delta(0)$ ; on the other hand, thermal fluctuations beyond MFA always lead to suppression of  $T_c$  with respect to  $\Delta(0)$ . We do not attempt here an explicit calculation of the  $\Delta(0)/T_c$  ratio in the pseudo-gap region, which should take into account both the above effects; roughly we may expect  $\Delta(0)/T_c \sim 1.5 - 2$  in this region.

<sup>8</sup>This does not contradict our findings in section 4.2.5 that Ginzburg parameter becomes  $Gi \sim O(1)$  already for the fractal superconductor with the Fermi energy at the mobility edge. It only implies that  $Gi$  grows very slowly and remains  $O(1)$  upon a further increase of the Fermi energy until the transition temperature becomes small. The reason for it is the appearance of a large pseudogap  $\Delta_P \gg T_c$  that suppresses the fluctuational processes that involve off-diagonal terms  $M_{ijkl}$ .

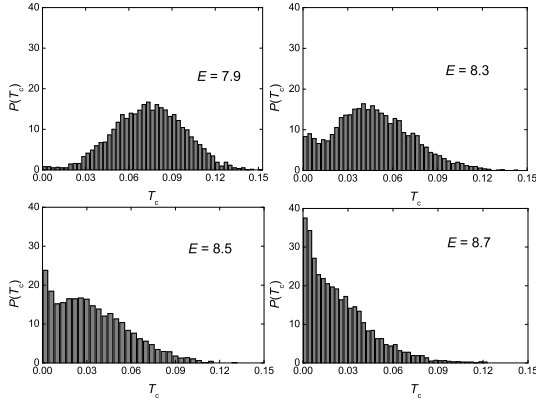


Figure 29: Distribution functions  $P(T_c)$  obtained by the virial expansion for different Fermi energies. All values of  $T_c$  were obtained in the pseudo-spin approximation  $\Delta_P \gg T_c$ , which leads to some overestimation of  $T_c$ 's at the Fermi energy  $E_F = 7.9$  where  $\Delta_P/T_c$  is not very large. The bi-modal character of the distribution for  $8.2 < E_F < 8.7$  indicates on the percolation character of the superconductive transition.

With a further shift of the Fermi energy deeper into the localized region ( $E_F \geq 8.2$  for our model), a remarkable new feature appears in the distribution of "transition temperatures" obtained from the truncated criterion Eq.(150) via the virial expansion. Namely, it acquires two maxima as shown in Fig. 29. One of them is located at  $T_c = 0$  and corresponds to an insulating phase, while another one corresponds to a superconducting phase with a nonzero  $T_c$ . The magnitude of this latter maximum decreases with increasing  $E_F$ , until it disappears completely at about  $E_F = 8.7$ .

Dramatic modification of the character of the distribution of  $T_c$  implies that the qualitative change in the physics of the superconductive transition. The appearance of two maxima in the distribution function means that not-too-large systems available for numerical studies are *either* superconducting or insulating. Larger systems and physical materials become strongly inhomogeneous with some parts becoming superconducting and some insulating at low temperatures. This observation is fully consistent with the result of the analytical theory[93] that predicts a replica symmetry breaking transition upon the decrease of the effective number of neighbors. This transition signals the absence of a local self-averaging and a global behavior which is dominated by rare superconducting paths. Thus, it is likely that for the physical, very large system the transition in this energy interval occurs by a *percolation* scenario.

The inhomogeneity of the superconductor in this regime is very different from that of the "fractal" superconductivity that we discussed in the previous section. The latter is *macroscopically homogeneous* because the strong inhomogeneity corresponding the fractal structure is seen only at scales smaller than  $L_T$ . In this case, the distribution function of transition temperatures *for all macroscopic samples* with  $L > L_T$  appears to be the Gaussian single-peak distribution with the width decreasing to zero as the system size increases, typical of the self-averaging quantities. In contrast the bimodal distribution

observed in numerical simulations and in analytic solution[93] of the pseudospin model signals of the macroscopic inhomogeneity and lack of self averaging.

Finally we note that our treatment above assumed a second-order transition to the superconducting phase, for instance, we have determined the transition temperature as a temperature of Cooper instability. We cannot exclude the first order transition to the superconducting phase although it seems unlikely, especially in the regime of a large disorder.

## 6.2. Tunneling conductance.

Here we analyze in detail the tunneling conductance into the pseudo-gaped state, at temperatures above and below the superconductive transition. We compute the *average* tunneling conductance in these two cases in sections 6.2.1 and 6.2.2. These conductances can be probed by large tunneling junctions. Computation of local tunneling conductance (as measured by scanning tunneling probe) is more complicated, we are able to make only qualitative predictions for this quantity in section 6.2.3.

### 6.2.1. Tunneling in a normal state.

We start by discussing the temperature-dependent differential tunneling conductance  $G(V, T, \mathbf{r})$  in the presence of a pseudo-gap  $\Delta_P$  *above* the superconducting transition. In this case the total tunneling current is given by

$$I(V) = \frac{G_0}{e\nu_0} \int \int d\varepsilon d\varepsilon_1 \nu_0(\varepsilon, \mathbf{r}) \left[ (1 - f(\varepsilon))f(\varepsilon_1)\delta(\varepsilon_1 - \varepsilon + eV - \Delta_P^{(j)}) - (1 - f(\varepsilon_1))f(\varepsilon)\delta(\varepsilon_1 - \varepsilon + eV + \Delta_P^{(j)}) \right] \quad (183)$$

where  $G_0$  is the bare conductance of the tunnel junction,  $\nu_0(\varepsilon, \mathbf{r}) = \sum_j \psi_j^2(\mathbf{r})\delta(\varepsilon - \tilde{\xi}_j)$ , and  $\tilde{\xi}_j \equiv \xi_j - \Delta_P^{(j)}$ . Eq.(183) was obtained by the following arguments. First, we consider the tunneling from the probe to the sample, it is given by the first term in (151). Here the  $j$ -th level in the sample is empty, the probe level is full, which gives rise to the usual factor  $(1 - f(\varepsilon))f(\varepsilon_1)$  involving the Fermi distribution function  $f(\varepsilon)$ . In this case the energy conservation requires  $\varepsilon_1 = \xi_j - eV = \varepsilon + \Delta_P^{(j)} - eV$ . Second, we consider the tunneling from the sample to the probe: the  $j$ -th level in the sample is full, the probe's level is empty, the thermal distribution functions produce the factor  $f(\varepsilon)(1 - f(\varepsilon_1))$ ; in this case the energy of a pair of electrons on the  $j$ -th level contains the binding energy  $-2\Delta_P^{(j)}$ , so that the energy conservation reads:  $\varepsilon_1 = \xi_j - 2\Delta_P^{(j)} - eV = \varepsilon - \Delta_P^{(j)} - eV$ .

Note that this calculation assumes the validity of Fermi Golden Rule for the tunneling rate; it also neglects electron-electron interactions (apart from the local terms leading to the parity gap  $\Delta_P$ ). The simultaneous validity of both these assumptions is not guaranteed when we consider localized states with relatively large typical level spacing  $\delta_L$ ; we will discuss this more below in section 6.2.3.

The differential conductance  $G(V) = dI/dV$  corresponding to Eq.(183) can be represented in the usual form

$$\frac{G(V, T, \mathbf{r})}{G_0} = \nu_0^{-1} \int d\varepsilon \nu(\varepsilon, \mathbf{r}) \left( -\frac{\partial f(\varepsilon - eV)}{\partial \varepsilon} \right) \quad (184)$$

where the density of states in the presence of a pseudo-gap (but above  $T_c$ ) depends explicitly on temperature:

$$\begin{aligned} \nu_n(\varepsilon, \mathbf{r}) = & \sum_j \psi_j^2(\mathbf{r}) \left[ \delta(\varepsilon - \tilde{\xi}_j - \Delta_P^{(j)})(1 - f(\varepsilon - \Delta_P^{(j)})) \right. \\ & \left. + \delta(\varepsilon - \tilde{\xi}_j + \Delta_P^{(j)})f(\varepsilon + \Delta_P^{(j)}) \right] \end{aligned} \quad (185)$$

Note that Eq.(185) cannot be represented in terms of the normal-state DoS,  $\nu_0(\varepsilon, \mathbf{r})$ , due to the correlations between the eigenfunction intensities  $\psi_j^2(\mathbf{r})$  and the local pairing gaps  $\Delta_P^{(j)}$ . The spatial average of the tunneling DoS can be obtained from Eq.(185) by integration over  $\mathbf{r}$  which replaces of  $\mathcal{V}\psi_j^2(\mathbf{r})$  by unity in Eq.(185).

The next (approximate) step in the simplification of this expression is to replace the summation over eigenstates  $j$  by averaging over distribution of pairing gaps  $P(\Delta_P)d\Delta_P$ , see Fig. 14. The distribution function of the normalized gaps  $y = \Delta_P/\Delta_P^{\text{typ}}$  can be fit by analytical expression

$$P(y) = \frac{A}{y^2} \exp\left(-\frac{c}{y} - b_1 y - b_2 y^2\right) \quad (186)$$

where  $c = 1.1$ ,  $b_1 = 0.16$ ,  $b_2 = 0.03$  and  $A = 1.8$  for  $E = 8.0$  (coefficients  $b_1, b_2$  are not universal as can be seen from Fig. 15).

The result for average density of states then reads:

$$\nu_n(\varepsilon) = \nu_0(\varepsilon) \int_0^\infty \frac{e^{-yz} + \cosh \frac{\varepsilon}{T}}{\cosh yz + \cosh \frac{\varepsilon}{T}} \cdot P(y) dy \quad (187)$$

where  $z = \Delta_P^{\text{typ}}/T$  and  $\nu_0(\varepsilon)$  is the average (in general, energy-dependent) DoS in the normal state. In the low-temperature limit Eq.(187) reduces to Eq.(78) from section 3.

Evolution of the average tunneling DoS obtained from Eq.(185) and its approximation Eq.(187) at different temperatures  $T < \Delta_P^{\text{typ}}$  for the 3D Gaussian Anderson model are shown in Fig.30. The asymmetry with respect to the sign of  $\varepsilon$  is due to a non-negligible energy-dependence of the bare DoS  $\nu_0(\varepsilon)$ .

The obtained results for the DoS are translated into the measurable tunneling conductance by Eq.(184). The zero-bias conductances  $G(0, T)$  obtained from the "exact" (Eq.(185)) and the approximate (Eq.(187)) expressions for the DoS are shown in Fig. 31. It is seen from Figs.30 and 31 that the approximation (187) works reasonably well; below we will use this approximation in the further analysis of the average tunneling conductance.

The ensemble-averaged tunneling conductance  $G(V, T)$  as a function of voltage is plotted in Fig. 32 for several temperatures. Remarkably, the curves we obtained demonstrate nearly exact crossing at  $eV \approx \Delta_P^{\text{typ}}$ . In other terms, the tunneling conductance at this voltage is nearly  $T$ -independent. This unexpected feature provides a simple way for experimental determination of  $\Delta_P^{\text{typ}}$ . Note that at very low temperatures  $T \ll \Delta_P^{\text{typ}}$  the crossing point moves to somewhat lower voltages. Indeed, a simple analysis of the integral in Eq.(187) shows that in the  $T \rightarrow 0$  limit the derivative  $d\nu(\varepsilon)/dT \propto dP(\varepsilon)/d\varepsilon$  vanishes at  $\varepsilon = \varepsilon_0$  corresponding to the maximum of the function  $P(\varepsilon/\Delta_P^{\text{typ}})$ , i.e.  $\varepsilon_0 \approx 0.5\Delta_P^{\text{typ}}$ , see Eq.(186) and Fig. 14.

The averaged tunneling conductance can be measured in the normal state by a large-area tunnel junction contact. It is important that the temperatures are not too low

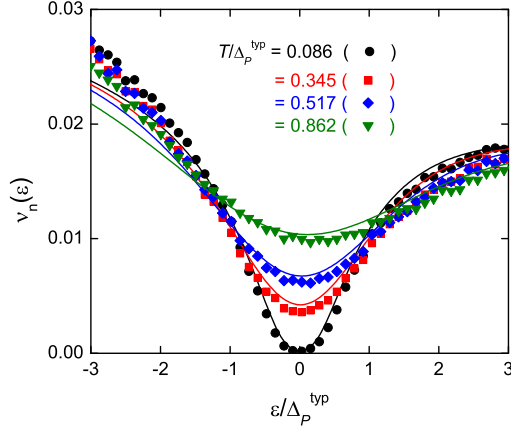


Figure 30: (Color online) Global tunneling density of states for the 3D Gaussian Anderson model at  $E_F = 8$  and the system size  $20^3$  for different temperatures normalized to the typical value of the local gap  $\Delta_P^{\text{typ}}$ . The data points stand for the all-numerical evaluation of Eq.(185) whereas the lines were calculated by means of Eqs.(187) and (186).

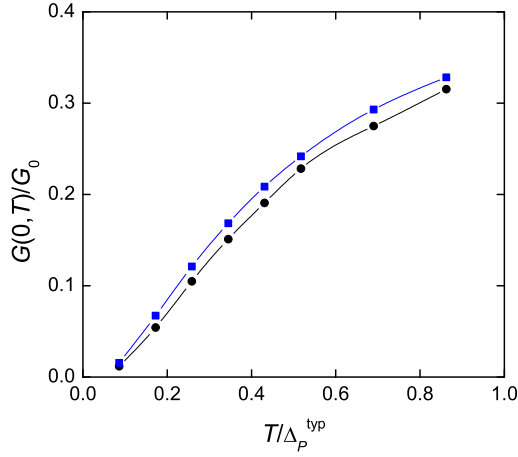


Figure 31: (Color online) Zero-bias tunneling conductance as a function of temperature below the typical pseudo-gap value; results obtained with exact formula (185) are shown by black dots, whereas blue squares correspond to the approximate formula (187).

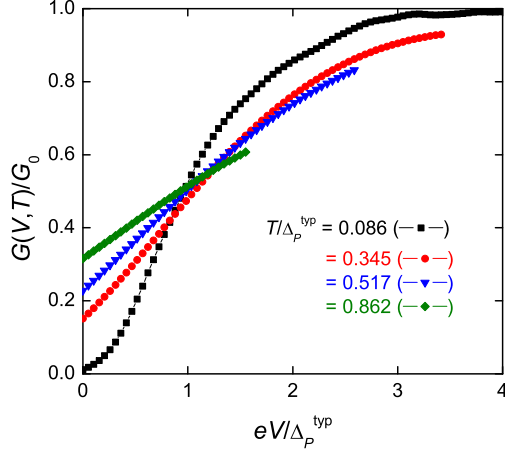


Figure 32: (Color online) Ensemble-averaged tunneling conductance, Eq.(184), for several values of temperature below the typical local gap  $\Delta_P^{\text{typ}}$ .

with respect to the typical  $\Delta_P$  because as temperature drops down, the bulk resistivity grows exponentially, leading to development of a strong Coulomb gap (not taken into the account above) which makes tunneling measurement unfeasible. The same problem becomes even more severe for the STM measurements at low temperatures.

### 6.2.2. Tunneling in a superconductor.

Provided that Fermi Golden Rule remains valid the tunneling current in the superconductive state is given by the formula similar to Eq.(183). We only need to replace in Eq.(183) the bare normal-state DoS  $\nu_0(\varepsilon, \mathbf{r})$  by its superconductive counterpart given by Eq.(172). Then, repeating the derivation of Eq.(185), we come to the expression for the tunneling density of states in presence of both pseudo-gap and the superconducting correlations:

$$\begin{aligned} \nu_{sc}(\varepsilon, \mathbf{r}) = & \frac{1}{2} \sum_j \psi_j^2(\mathbf{r}) \left\{ \left( 1 + \frac{\tilde{\xi}_j}{\varepsilon - \Delta_P^{(j)}} \right) \left[ \delta(\varepsilon - \varepsilon_j - \Delta_P^{(j)}) + \delta(\varepsilon + \varepsilon_j - \Delta_P^{(j)}) \right] \right. \\ & \times (1 - f(\varepsilon - \Delta_P^{(j)})) + \\ & \left. \left( 1 + \frac{\tilde{\xi}_j}{\varepsilon + \Delta_P^{(j)}} \right) \left[ \delta(\varepsilon - \varepsilon_j + \Delta_P^{(j)}) + \delta(\varepsilon + \varepsilon_j + \Delta_P^{(j)}) \right] f(\varepsilon + \Delta_P^{(j)}) \right\} \end{aligned} \quad (188)$$

where  $\varepsilon_j = \sqrt{\tilde{\xi}_j^2 + \Delta^2(\tilde{\xi}_j)}$  and the function  $\Delta(\xi)$  has to be determined by solving the gap equation (182). Below we use Eq.(188) in order to derive an expression for the *averaged* tunneling conductance; situation with the *local* tunneling conductance is more complicated and cannot be described this way, as explained in subsection 6.2.3.

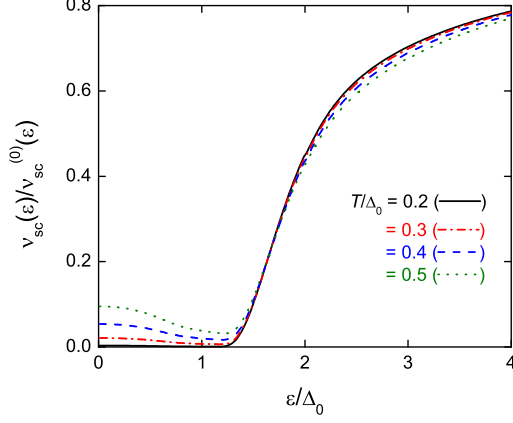


Figure 33: (Color online) Ensemble-averaged tunneling DoS, Eq.(189), for several values of temperature much below the value of the superconductive gap  $\Delta_0 \equiv \Delta_0(\xi = 0)$ . The latter is chosen to be  $\Delta_0 = 0.5\Delta_P^{\text{typ}}$ , where  $\Delta_P^{\text{typ}}$  is the parity gap.

The averaged density of states in the superconductive state with a pseudo-gap,  $\nu_{sc}(\varepsilon)$ , can be obtained in the same way as it was done above for the normal state, see Eq.(187). The odd terms in  $\tilde{\xi}_j$  proportional to  $\tilde{\xi}_j/(\varepsilon \pm \Delta_P^j)$  in Eq.(188) cancel out upon summation over  $\tilde{\xi}_j = \pm|\tilde{\xi}_j|$ , provided we neglected the energy-dependence of typical  $\Delta_P(E)$  inside the energy band of the width  $\Delta E \sim \Delta_P$ . We get

$$\nu_{sc}(\varepsilon) = \int_0^\infty P(y) \left[ \frac{\nu_{sc}^{(0)}(\varepsilon - yzT)}{e^{yz - \varepsilon/T} + 1} + \frac{\nu_{sc}^{(0)}(\varepsilon + yzT)}{e^{yz + \varepsilon/T} + 1} \right] dy \quad (189)$$

where  $z = \Delta_P^{\text{typ}}/T$  and  $\nu_{sc}^{(0)}(\varepsilon)$  is the DoS in the superconductive state without a pseudo-gap, defined by  $\nu_{sc}^{(0)}(\varepsilon) = \nu_0(\varepsilon)|d\xi(\varepsilon)/d\varepsilon|$  (173), similar to the one shown in Fig. 24 for the case of critical superconductor. Note that the function  $\xi(\varepsilon)$  that we need here differs slightly from the one shown in Fig. 24 due to the different form of the correlation function  $M(\omega)$  entering modified MFA equation (182) in the case of pairing between localized states. However, the effect of this difference reduces to an overall prefactor, as is seen from Fig. 5. We thus do not expect significant difference between the solution  $\Delta(\xi)$  and the corresponding  $\xi(\varepsilon)$  functions calculated within the modified MFA approximation in the mildly localized region considered here and for the "critical" case studied in section 4. Thus we use  $d\xi(\varepsilon)/d\varepsilon|$  as it was found in section 5.4 but take into account a smooth energy-dependent DoS pre-factor  $\nu_0(\varepsilon)$ , as it was done above when computing Eq.(187) and Fig. 30.

Evolution of the  $\nu_{sc}(\varepsilon)$  shapes as function of temperature in the low-temperature range  $T < 0.5T_c$  is shown in Fig.33 where we use the analytic interpolation formula Eq.(186) for the distribution function  $P(y)$ , and the  $T = 0$  solution for the gap function  $\Delta(\xi)$ . The average tunneling conductance  $G(V, T)$  obtained with this DoS from Eq.(184)

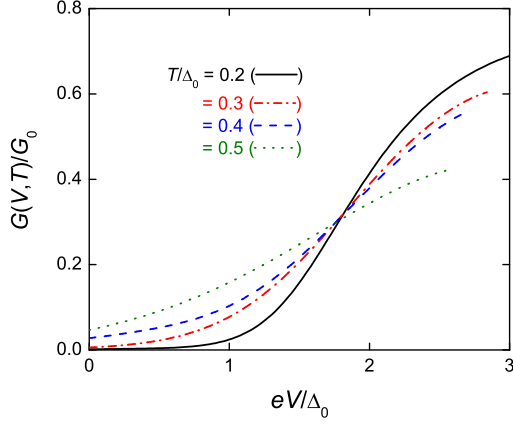


Figure 34: (Color online) Average tunneling conductance in the superconductive state for several values of temperature much below the value of the superconductive gap  $\Delta_0 = 0.5\Delta_P^{\text{typ}}$ .

is shown in Fig. 34. The crossing point at this plot, i.e. the  $T$ -independent conductance at some specific value of voltage, corresponds to  $eV - \Delta_0 \approx 0.5\Delta_P^{\text{typ}}$ . In zero energy limit the expression for the density of states simplifies to

$$\nu_{sc}(0) = \int_0^\infty P(y) \frac{2\nu_{sc}^{(0)}(y)}{e^{y/T} + 1} dy \quad (190)$$

The temperature dependence of the corresponding zero bias tunneling conductance  $G(0, T)$  is shown in Fig.35.

The averaged DoS and the tunneling conductance presented in Figs. 34, 35 do not show any coherence peaks similar to the one presented in Fig. 24 for the critical superconductive state (section 5.4). This is due to the averaging of the peak position  $eV = \Delta_0 + \Delta_P^{(j)}$  over a broad distribution  $P(\Delta_P)$  of the local pairing gaps  $\Delta_P^{(j)}$ . Note that the non-monotonic behavior of the DoS curve in Fig. 33 reflects the (smeared) edges at  $\varepsilon = \Delta_P^{\text{typ}} \pm \Delta_0$  of the  $\nu_{sc}^{(0)}(\varepsilon)$  function shifted by the pairing gap  $\Delta_P^{\text{typ}} > \Delta_0$  and weighted by the temperature-dependent distribution functions in Eq.(189).

We emphasize again that the results obtained in this section give the averaged tunneling conductance which can be measured with a large-area junctions, such as the ones used in [41]. They may differ significantly from the local tunneling conductance measured by a small tip and discussed in the following subsection.

### 6.2.3. Point contact tunneling.

The equation (183) can be easily generalized to describe point conductance. One gets using the perturbation theory in the tunneling amplitude,  $t$  (which is equivalent to Fermi Golden Rule) that the most general case the point conductance is given by



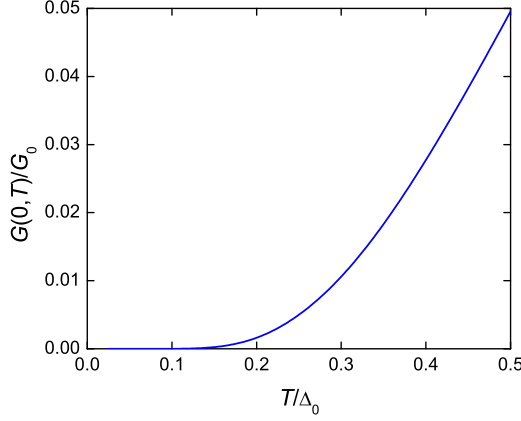


Figure 35: Zero-biased conductance as function of temperature for the case of  $\Delta_0 = 0.5\Delta_P^{\text{typ}}$ .

equation (183) where  $\nu_0(\varepsilon, \mathbf{r})$  is replaced by the exact single particle Green function at the tunneling position,  $\text{Im}G_R(\varepsilon, r)$ . In a poor conductor in which single particle states are localized or almost localized one expects that  $\text{Im}G_R(\varepsilon, r)$  shows a series of peaks corresponding to the single particle states located in the vicinity of the tunneling point. Applying this reasoning to the superconductor-insulator transition in a situation when  $E_F$  corresponds to a well developed pairing gap  $\Delta_P$  and repeating the arguments of the previous subsection one expects to observe the peaks in the tunneling conductance with width  $T$  and separation  $\delta_L$ .

These arguments do not take into account the effect of the collective modes of the superconductor which smear the peaks in the tunneling conductance. In fact, the presence of the collective modes make the observation of the peak structures in the density of states difficult. Briefly, the experimental observation of tunneling is possible only in the superconducting state, but in this state the effect of the collective modes on the single particle density of states is large. We estimate this effect within a simplified model, namely we use the pseudospin Hamiltonian (145) to which we add the possibility of having single particle excitation at the single site 0:

$$H = \xi_0 n + \Delta_P(1 - n^2) - g \left[ c_{\uparrow}^{\dagger} c_{\downarrow}^{\dagger} \sum_j M_{0j} S_j^{-} + c_{\downarrow} c_{\uparrow} \sum_j M_{0j} S_j^{+} \right] + H_{PS}(S) \quad (191)$$

where  $n = \sum_a c_a^{\dagger} c_a - 1$  where  $a = \uparrow, \downarrow$  are two spin components, and the sum over  $j$  runs over the neighbors of the site 0. This model describes the process of electron tunneling in a single localized state; in a more realistic case the electrons tunnel in few such states with an amplitude proportional to  $\psi_{\alpha}^2(r)$  where  $r$  is a tunneling point. These processes are incoherent due to randomness of local binding energies  $\Delta_P^{(j)}$ , so the physical tunneling conductivity is the sum of the contributions from different eigenstates.

In a good BCS-like superconductor characterized by a large number of neighbors one can replace pairing field  $h_\perp = g \sum_j M_{0j} S_j^\perp$  by their average values  $\langle h_\perp \rangle = \Delta$ . In this case the Green function of the electron at site 0 obeys Dyson equation

$$G_R(\epsilon) = \frac{1}{G_{0R}^{-1}(\epsilon) - \Delta^2 G_{0A}(-\epsilon)} \quad (192)$$

$$G_{0R}(\epsilon) = \frac{1}{\epsilon - \xi_0 - \Delta_P \text{sgn}(\xi_0) + i0}. \quad (193)$$

The resulting single electron Green function has a pole at  $\epsilon_0 = \sqrt{(\xi_0 + \Delta_P \text{sgn}(\xi_0))^2 + \Delta^2}$  which shows the combined effect of the pseudogap and superconducting order parameter on the electron. As one expects, in the case of a large number of neighbors the electron density of states has a sharp peak at the pole energy  $\epsilon_0$  which is smeared only by thermal effects by  $\delta\epsilon \sim T$ . As the disorder is increased the effective number of neighbors goes down and fluctuations of the pairing field become relevant. This leads to two physical effects. The first effect is that tunneling of the electrons removes the spin from site 0 which changes the effective spin Hamiltonian. The new ground state spin wave function is orthogonal to the one realized before the tunneling process. This leads to a suppression of the tunneling of the electron with the energy exactly equal to  $\epsilon_0$ . The second effect is that tunneling might be accompanied by the emission of the pseudospin excitations. This leads to non-zero tunneling density of states at energies larger than  $\epsilon_0$ . Both effects are controlled by the same parameter, the effective number of neighbors which determines the strength of the quantum fluctuations of the pairing field and both round the peaks in the observed spectrum. In order to compute local tunneling conductance one needs the full description of the spin fluctuations in the regime of the small  $Z_{eff}$  which is not presently available.

Below we estimate the second effect, i.e. the magnitude of the level broadening in the framework of the perturbation theory. In perturbation theory the emission of the pseudospin excitations is described by the inclusion of the self energy part in the Dyson equation (192):

$$G_R(\epsilon) = \frac{1}{\tilde{G}_R^{-1}(\epsilon) - \Delta^2 \tilde{G}_A(-\epsilon)}, \quad \tilde{G}_R(\epsilon) = \frac{1}{\epsilon - \xi_0 - \Delta_P \text{sgn}(\xi_0) - \Sigma_R(\epsilon)} \quad (194)$$

$$\text{Im}\Sigma_R(\epsilon) = g^2 \sum_j M_{0j}^2 \int_0^\epsilon \frac{d\omega}{2\pi} \text{Im}\tilde{G}_A(\omega - \epsilon) \text{Im}D_R(\omega) \quad (195)$$

where  $D(\omega) = \langle\langle S^\perp S^\perp \rangle\rangle_\omega$  is irreducible correlator of the pairing field. Even in a weakly superconducting phase the pseudospin excitations are delocalized and thus have a continuous spectrum. Here we focus on the large energy scale  $E \sim \Delta_P$  properties of the spectrum, we do not discuss here the structure of tunneling conductance very close to the edge, where coherence peaks are expected. At these large energies, the density of collective modes is featureless, so we estimate the  $\text{Im}D(\omega) = \nu_B \theta(\omega)$ .

As it is clear from (194), the interaction with pseudospins lead to the decay rate of the single particle excitations,  $\Gamma_{el}$ , which smears the peak structure of  $\text{Im}G(\epsilon)$  replacing it with the threshold behavior. In the leading order of perturbation theory we replace  $\tilde{G}(\omega - \epsilon)$  in (194) by  $G_0(\omega - \epsilon)$  and get for the level width  $\Gamma_{el} = g^2 \nu_B \sum_j M_{0j}^2$ .

Because the expression for the level width,  $\Gamma_{el}$  contains the square of the interaction constant,  $g^2$ , but only one sum over neighboring sites, it is small in a good superconductor (where  $gM \propto 1/Z$ ) but may become large in a weak superconductor close to superconductor-insulator transition. We estimate it in the framework of the Bethe lattice model for this transition discussed in section 6.1. In this model  $M_{0j} = 1/Z_{\text{Bethe}}$ , so we get  $\Gamma_{el} = g^2\nu_B/Z_{\text{Bethe}}$ . In order to express it in terms of the physical parameters, we use the equation (181) that relates the transition temperature to the effective number of neighbors  $Z_{\text{Bethe}}$  at the onset of the weak superconductor regime. The onset of this regime can be defined (and determined experimentally) by the beginning of the sharp decrease of  $T_c$  with the increase of disorder. We get:

$$\Gamma_{el} \sim (g\nu_B)^2 \sqrt{T_c E_F} \gg T_c. \quad (196)$$

The apparently large value of the level width in this regime implies that distinct peaks become absent, being replaced by the threshold. For a tunneling leading to a single state,  $\alpha = 0$ , the threshold coincides with the value of energy  $\epsilon_\alpha \approx [\xi_\alpha^2 + \Delta^2]^{1/2} + \Delta_P^{(\alpha)}$ . This discussion assumed that tunneling happens only in one localized state; in a more realistic situation when tunneling amplitudes proportional to  $\psi_\alpha^2(r)$  are significant for a few states, the threshold energy is equal to  $\Delta$  plus a minimal value of  $\min \Delta_P^\alpha$  available for a contact tunneling process at a given point.

We conclude that the model Hamiltonian Eq. (191) results in the threshold dependence of the tunneling conductance. The threshold distribution (observed when scanning along the surface) is expected to be similar to  $P(\Delta_P)$  distribution shown in Fig. 14 whereas the tunneling conductance  $G(V)$  should be similar to the integral of that distribution shown in Fig. 15. These conclusions are in a qualitative agreements with the data presented in [42, 95].

The model (191) neglects the off-diagonal matrix elements of the form

$$\sum_j c_{\alpha\uparrow} c_{j\downarrow} \sum_k M_{\alpha j k k} \langle c_{k\uparrow}^+ c_{k\downarrow}^+ \rangle$$

that are present in the full Hamiltonian and might be important for the quantitative description of the data. Physically these terms lead to the possibility of non-local process in which electron is converted into a hole in the adjacent state and emits a collective mode quantum. The presence of a sum over many states  $j$  connected with a pre-selected state  $\alpha$  leads to a partial average over the gap distribution  $P(\Delta_P)$ ; this suppresses the relative magnitude of spatial fluctuations of the local thresholds. As a result, we expect that the threshold voltage is given by

$$eV_{\text{th}} = \alpha_{\text{th}} \overline{\Delta_P} + \Delta \quad (197)$$

with  $\alpha_{\text{th}} < 1$  being numerical factor of order unity, with a moderate spatial fluctuations.

The arguments leading to an estimate Eq.(196) imply that peak structure of the density of states might be only observed in a narrow transient regime that corresponds to a well developed pseudogap combined with a strong superconductor. It is not clear that this regime can be realized in physical systems. In particular, it is very likely that experiment [42, 95] which reported the gap in the density of states but no obvious peak structure were performed in a weakly superconducting state close to the transition into the insulator. As explained above, in this regime one expects that at a typical point

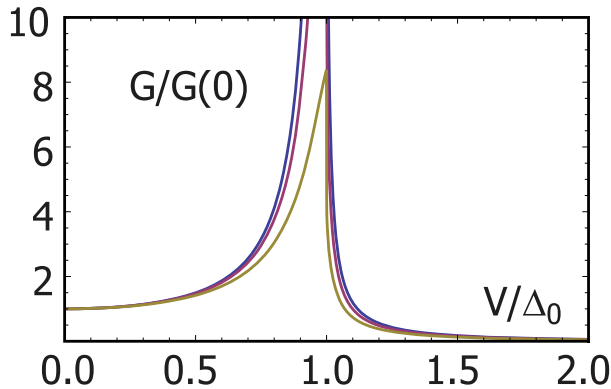


Figure 36: (Color online) Andreev point-contact conductance (normalized by its value at zero bias) is calculated within zero-temperature BTK approximation, Eq.(198), for three different values of the contact transparency,  $\mathcal{T} = 0.2$  (blue line),  $0.4$  (red) and  $0.6$  (yellow). Voltage  $eV$  is normalized by the maximum value  $\Delta_0$  of the gap function  $\Delta(\xi)$ . It is assumed that single-electron tunnelling is fully suppressed by large gap  $\Delta_P \gg \Delta_0$ .

the spectrum of collective modes is continuous and featureless resulting in the tunneling conductance characterized by a threshold that corresponds to the minimal value of  $\epsilon_0$ . However, large inhomogeneity of the ordered state (discussed in a different context in the section 6.1) implies that at some locations the spectrum of collective modes might develop large peaks leading to the peak structures in the tunneling conductance.

Qualitatively, interaction of single electron with pseudospin collective modes plays the same role as its interaction with other electrons in zero bias anomaly and Fermi-edge singularity problem [96]. The quantitative theory of these effects and in particular, the predictions for the shape of the pseudogap require the full theory of the collective modes appearing in the vicinity of superconductor-insulator transition, this is beyond the approach developed in this paper.

### 6.3. Andreev contact conductance at low temperatures.

In the regime of a strong pseudo-gap  $\Delta_P \geq \Delta_0$  a peculiar situation occurs: the energy gap for a single-particle excitation  $\Delta_1 = \Delta_P + \Delta_0$  is *larger* than the two-particle excitation gap  $2\Delta_0$ . The crucial point here is that the *local* pairing energy  $\Delta_P$  drops out of the expression for the two-particle excitation gap which is determined only by the *collective* superconductive gap  $\Delta_0$ . Local pairing energy becomes important only when we have to break the pair to produce the single-particle excitation. This allows to experimentally distinguish between the two types of gaps: the pairing gap  $\Delta_1$  seen in the *single-electron* tunneling and the collective gap  $\Delta_0$  which can be observed in the experiments where the entire pair is transferred through the tunnel junction. This type of tunneling experiments is called Andreev-contact spectroscopy (see [97] for the review of its application to similar studies in high- $T_c$  cuprates). Since the probability to transfer a pair is proportional to the square of the tunnel contact transparency  $\mathcal{T}$ , the latter should be not too small for the Andreev conductance to be observable.

Below we provide simplest estimates of Andreev conductance for the pseudogapped fractal superconductor, based upon Blonder-Tinkham-Klapwijk (BTK) approach [98].

We consider the case of moderately large parameter of normal reflection  $Z \geq 1$ . Charge transport within BTK approach is characterized by (energy-dependent) probabilities  $A$ ,  $B$ ,  $C$  and  $D$  of four processes which may occur when normal incident electron approaches N-S boundary:  $A(\varepsilon)$  is the probability of Andreev reflection,  $B(\varepsilon)$  corresponds to normal reflection,  $C(\varepsilon)$  and  $D(\varepsilon)$  correspond to two different processes of single-electron transmission into superconductor. We are interested here in the low-temperature limit  $T \ll T_c \ll \Delta_P$  and relatively low voltages  $eV < \Delta_P$ , thus the processes of electron transmission into superconductor can be neglected and the full sub-pseudogap current can be written as

$$I_{NS}(V) \propto \int d\varepsilon 2A(\varepsilon)[f(\varepsilon - eV) - f(\varepsilon)]$$

This expression is obtained from Eq.(17) of the BTK paper by the substitution of the integrand  $1 + A - B \equiv 2A + C + D$  for  $2A$ , due to vanishing of normal current. Therefore differential conductance is proportional to the Andreev reflection probability  $A(\varepsilon)$ , which we will write using BTK results, see Table II of Ref. [98], but in slightly different notations. To begin with, we introduce normal transmission coefficient  $\mathcal{T} = 1/(1 + Z^2)$  and write NS differential conductance in BTK approximation (at  $T = 0$ ) for usual superconductor as

$$\begin{aligned} \frac{dI_{NS}}{dV} &= G_{NS}(V) \\ &= 2G_0\mathcal{T} \left( \frac{\Delta(eV)}{eV} \right)^2 \frac{n_0^2(eV)}{\mathcal{T}^2 n_0^2(eV) + (2 - \mathcal{T})^2 + 2n_0(eV)(2 - \mathcal{T})\theta(eV - \Delta)} \end{aligned} \quad (198)$$

where  $G_0 = 2\mathcal{T}N_{ch}$  is the normal-state conductance of the contact,  $N_{ch}$  is the number of orbital conductance channels (in BTK approach all channels are characterized by the same transmission coefficient  $\mathcal{T}$ ), and  $n_0(\varepsilon) = \varepsilon/|\varepsilon^2 - \Delta^2|^{1/2}$ .

In order to generalize Eq.(198) for the case of fractal superconductor, we consider subgap region  $\varepsilon < \Delta_0$  and region of real excitations  $\varepsilon > \Delta_0$  separately. In the subgap region we introduce function  $n_-(\varepsilon)$  defined by

$$n_-(\varepsilon) = \frac{1}{\pi} \int d\xi \frac{\Delta(\xi)}{-\varepsilon^2 + \xi^2 + \Delta^2(\xi)} \quad (199)$$

where  $\Delta(\xi)$  is the solution to the gap equation (182). Then NS conductance in the subgap region is:

$$G_{NS}^-(V) = 2G_0\mathcal{T} \frac{n_-^2(eV)}{(n_-^2(eV) - 1)\mathcal{T}^2 + (2 - \mathcal{T})^2} \quad (200)$$

For the region above the gap one should introduce function  $\hat{\Delta}(\varepsilon) \equiv \Delta(\xi(\varepsilon))$ , and replace in Eq.(198) the function  $n_0(\varepsilon)$  by the actual normalized density of states  $n_+(\varepsilon) = \nu(\varepsilon)/\nu_0$ , defined by Eq.(173):

$$G_{NS}^+(V) = 2G_0\mathcal{T} \frac{(\hat{\Delta}(eV)/eV)^2 n_+^2(eV)}{\mathcal{T}^2 n_+^2(eV) + (2 - \mathcal{T})^2 + 2n_+(eV)(2 - \mathcal{T})} \quad (201)$$

The comment is in order here: we do not expect Eqs.(200,201) to be quantitatively exact for the problem considered, due to a number of oversimplifying assumptions borrowed

from the BTK approach (it was developed for clean superconductors in a contact with clean metal). However, comparison of BTK expression for  $A(\varepsilon)$  with exact calculations done for dirty NS junctions (see Appendix to the paper [99] and references in that paper, and also paper [100] ) shows that the key feature of the result (200,201), that is, the peak of differential conductance at  $eV = \Delta_0$ , is reproduced by these more adequate calculations; thus we hope it will survive for very strongly disordered pseudogaped superconductor as well.

In Fig. 36 we present the results of the computation of the  $T = 0$  differential Andreev conductivity based on Eqs.(200,201) for several values of the contact transparency. Note that we give here the data for Andreev conductivity normalized to its value at zero voltage  $G(0)$ , which scales itself as  $\mathcal{T}^2$ . Therefore the plots presented in Fig.36 illustrate variation of the  $G(V)$  peak shape, but do not show the overall scale of  $G(V)$  as function of  $\mathcal{T}$ . The gap function  $\hat{\Delta}(\varepsilon)$  was computed using the  $T = 0$  limit of the solution to the modified MFA equation (182) for the "critical"  $M(\omega)$ , Eq.(44). Voltage is normalized by the maximum value  $\Delta_0$  of the gap function  $\Delta(\xi)$ .

Note that the plots in Fig.36 illustrate the limit of a very large paring gap  $\Delta_P \gg \Delta_0$ . In the case of parity gap  $\Delta_P$  comparable to the superconductive gap  $\Delta(0)$ , the point-contact conductance should contain two peaks: at  $eV_1 = \Delta(0)$  due to Andreev processes, and at  $eV_2 = \Delta_P + \Delta(0)$  due to single-electron tunnelling. These two voltage values behave differently with change of temperature and location of the point contact. The voltage  $V_1$  is determined by the *collective superconductive gap*  $\Delta_0$  and, therefore, is position-independent but goes to zero as  $T \rightarrow T_c$ . In contrast,  $V_2$  fluctuates strongly between different contact locations due to the local paring gap  $\Delta_P$  but does not vanish as  $T$  approaches  $T_c$  from below. Recent experimental results [101] seem to support the above predictions.

#### 6.4. Spectral weight of high-frequency conductivity and superconducting density.

The studies[102] of high  $T_c$  superconductors has shown that the unconventional physics of these materials can be probed by the temperature dependence of the spectral weight  $K^{tot}(T)$  of the high-frequency conductivity defined by

$$K^{tot}(T) = \frac{2}{\pi} \int_0^{\Omega_{max}} \Re \sigma(\omega, T) d\omega + \rho_s(T) \equiv K(T) + \rho_s(T). \quad (202)$$

Here  $\sigma(\omega, T)$  denotes the regular part of conductivity, whereas the contribution  $\rho_s = -c\delta\mathbf{j}/\delta\mathbf{A}(\omega = \mathbf{0})$  of superconductive part (proportional to  $\delta(\omega)$ ) is explicitly separated in the last term of Eq.(202); the high-frequency cutoff  $\Omega_{max}$  is chosen a several times larger than  $T_c$ .

In agreement with the data on conventional superconductors, BCS theory and its strong coupling generalizations predict that  $K^{tot}(T)$  does not change as temperature decreases below the superconducting transition temperature  $T_c$ : the appearance of  $\rho_s(T)$  is compensated by the decrease of the regular part. In contrast, for underdoped cuprates the regular part  $K(T)$  of the c-axis spectral weight changes below  $T_c$  by one half of  $\rho_s(T)$  only, so that  $K^{tot}(0) - K^{tot}(T_c) = \frac{1}{2}\rho_s(0)$ . [102]

The observation [102] was explained by Ioffe and Millis [103] as being caused by formation of a pseudo-gap that survives up to a temperature  $T_{PG}$  well above  $T_c$ , and at the same time by the absence of the inter-layer coherence in the range  $T_c < T < T_{PG}$  due

to strong quantum and thermal fluctuations. The weight non-conservation occurs only for the c-axis conductivity, whereas the in-plane conductivity behaves in a usual way in all cuprates.[102] The theory [103] attributes to the large phase fluctuations between weakly coupled layers and a tunneling nature of c-axis transport, in contrast with the smooth phase variations and the continuous electron motion in the planes.

We expect that pseudogapped superconductivity formed near superconductor-insulator transition shows similar anomaly in the behavior of the spectral weight  $K_{tot}(T)$ . In particular, we show that inside the strong pseudo-gap region  $T_c \ll \Delta_P$  the effect of the  $K^{tot}(T)$  non-conservation is even stronger: its variation  $\Delta K^{tot}(T)$  is equal (within the mean field approximation) to  $\rho_s(T)$ , whereas the variations of the regular part of spectral weight  $\Delta K(T)$  are smaller by  $\sim 1/Z_{\text{eff}}$  factor. In this derivation we shall assume that pseudogap sets the largest scale in the problem, i.e. that the upper frequency cutoff  $\Omega_{max}$  satisfies  $T_c \ll \Omega_{max} \ll \Delta_P$ . This assumption allows us to neglect completely single electron processes (which do not contribute for  $\omega < \Delta_P$ ) and use pseudospin model for the computation of the conductivity in the entire frequency range. Furthermore, because, as we shall show below the conductivity in the pseudospin model decreases fast at frequencies above  $T_c$ , we can replace the upper cutoff  $\Omega_{max} \rightarrow \infty$  when evaluating the spectral weight in this model.

In order to compute the conductivity in the pseudospin model we need to include in the spin Hamiltonian (145) the effect of the vector potential  $\mathbf{A}$ :

$$H = \sum_j 2\xi_j S_j^z - \frac{g}{2} \sum_{ij} M_{ij} (S_i^+ S_j^- e^{i\phi_{ij}} + h.c.), \quad (203)$$

where  $\phi_{ij} = \frac{2e}{\hbar c} \int_{\mathbf{r}_i}^{\mathbf{r}_j} \mathbf{A} d\mathbf{r}$ . Here  $i, j$  denote localized single-particle states (orbitals) with wavefunctions  $\psi_{i,j}(\mathbf{r})$ . The Hamiltonian in the form (203) is applicable provided that the typical distance  $R_0$  between centers of localization of the relevant eigenstates is much longer than the localization length  $L_{loc}$  (the same assumption is used everywhere in this section, see Eq.(179)). Then  $i, j$  can also be viewed as sites characterized by the position vectors  $\mathbf{r}_i, \mathbf{r}_j$  of centers of localization of the corresponding orbitals. The assumption  $R_0 \gg L_{loc}$  implies that the theory is not sensitive to an exact definition of "center of localization" inside the localization radius. It is this assumption that allows to define the phase  $\phi_{ij}$  in Eq.(203). Another assumption implied in (203) is that the magnetic field is weak enough so that its effect reduces to the introduction of the phase factors  $e^{i\phi_{ij}}$  and does not change the matrix elements  $M_{ij}$ .

The electrical current across each link ( $ij$ ) that corresponds to the Hamiltonian Eq.(203) is

$$\hat{\mathcal{I}}_{ij} = \frac{g}{2} M_{ij} i (S_i^+ S_j^- e^{i\phi_{ij}} - h.c.). \quad (204)$$

The response of the superconductor to the slowly spatially varying electromagnetic field is fully characterized by  $Q(\omega) = -c\delta/\delta A_{k=0}(\omega) = Q_0 + \tilde{Q}(\omega)$  where we separated the constant part  $Q_0$  and the frequency dependent one  $\tilde{Q}(\omega)$  that satisfies  $\tilde{Q}(\omega \rightarrow \infty) = 0$ . At high frequencies the conductivity is purely imaginary with  $\text{Im}\sigma(\omega) = Q_0/\omega$ , expressing  $\text{Im}\sigma(\omega)$  through the real part by Kramers-Kronig relations one gets that  $K^{tot}(T) = Q_0$ .

The constant term  $Q_0$  originates from the direct expansion of the expression for the

current (204) in  $\phi_{ij}$ :

$$K^{tot}(T) = Q_0(T) = \frac{g}{2\mathcal{V}} \sum_{ij} \left( \frac{2e}{\hbar} x_{ij} \right)^2 M_{ij} Q_{ij}^{(0)} \quad (205)$$

where  $Q_{ij}^{(0)} = \langle S_i^+ S_j^- + h.c. \rangle$ .

The equation (205) implies that in the general case  $Q_0$  cannot be temperature independent because  $\langle S_i^+ S_j^- + h.c. \rangle$  is generally temperature dependent. Furthermore, one expects a strong temperature dependence to appear below  $T_c$  where order parameter induces large spin-spin correlator. In the leading order in  $1/Z_{eff}$  one can replace  $\langle S_i^+ S_j^- \rangle \approx \langle S_i^+ \rangle \langle S_j^- \rangle$  and conclude that the spectral weight is constant above  $T_c$  but acquires temperature dependence below  $T_c$ :

$$K^{tot}(T) = \frac{1}{4\mathcal{V}} \sum_{ij} g M_{ij} \left( \frac{2e}{\hbar} x_{ij} \right)^2 \frac{\Delta_i \Delta_j \tanh \beta \varepsilon_i \tanh \beta \varepsilon_j}{\varepsilon_i \varepsilon_j}. \quad (206)$$

where  $\varepsilon_i = \sqrt{\xi_i^2 + \Delta_i^2}$ .

We now compute the leading correction in  $1/Z_{eff}$  to  $\langle S_i^+ S_j^- \rangle$  above  $T_c$ , we find that it does not result in the spectral weight temperature dependence in this temperature range. This result does not preclude that temperature dependence appears in high orders in  $1/Z_{eff}$  but it implies that the temperature dependence is very small in this regime. Note that in this temperature range the superconducting response is absent, so temperature independence of the full weight implies temperature independence of its regular part. To compute the leading contribution to  $\langle S_i^+ S_j^- \rangle$  it is sufficient to diagonalize two spin problem with the Hamiltonian

$$H = \xi_j \sigma_j^z + \xi_i \sigma_i^z - \frac{g}{2} M_{ij} (S_i^+ S_j^- + S_j^+ S_i^-), \quad (207)$$

which mixes states pairwise. We get

$$\langle S_i^+ S_j^- + S_j^+ S_i^- \rangle = \frac{g}{2} M_{ij} \left[ \frac{\tanh(\beta \xi_i) - \tanh(\beta \xi_j)}{4(\xi_i - \xi_j)} + \frac{\tanh(\beta \xi_i) + \tanh(\beta \xi_j)}{4(\xi_i + \xi_j)} \right]$$

Inserting this expression in (205) and averaging over distribution of  $\xi$ , assuming that it is not correlated with the values of  $M_{ij}$  and  $x_{ij}$  we get

$$\begin{aligned} Q_0 &= \sum_{ij} \overline{\left( \frac{2e}{\hbar} x_{ij} \right)^2} \overline{\left( \frac{g}{2} M_{ij} \right)^2} R \\ R &= \frac{\overline{\tanh(\beta \xi_i) - \tanh(\beta \xi_j)}}{2(\xi_i - \xi_j)} \end{aligned}$$

The temperature enters only in the last factor in this product, differentiating it over the inverse temperature we find

$$\frac{dR}{d\beta} = \int d\xi_1 d\xi_2 \frac{\nu(\xi_1) \nu(\xi_2)}{\xi_1 - \xi_2} \left[ \frac{1}{\cosh^2 \beta \xi_1} - \frac{1}{\cosh^2 \beta \xi_2} \right]$$



The integrand decreases exponentially fast for  $\xi \gg T$ , neglecting the contribution from these regions and assuming, as usual, that  $\nu(\xi \lesssim T) = \nu$  is constant at low energies we perform integration and get the result announced earlier:  $dR/d\beta = 0$ .

We now discuss the regular and superconducting contributions to the spectral weight below  $T_c$ . The computation above demonstrates that leading terms in  $1/Z_{eff}$  involve only pairs of spins. This remains true below  $T_c$  as well and allows us to compute easily the regular part of the spectral weight in this temperature range. We begin by using the Kubo formula to express it through the spin-spin correlators

$$K(T) = \frac{1}{\mathcal{V}} \sum_{ij} \left( \frac{2e}{\hbar} x_{ij} \right)^2 \left( \frac{g}{2} M_{ij} \right)^2 \int_0^\infty \frac{d\omega}{\omega} \text{Re} R_{ij}(\omega) \quad (208)$$

where  $R_{ij}(\omega)$  is current-current correlator

$$R_{ij}(\omega) = i \int_0^\infty dt e^{i\omega t} \left\langle \left[ \hat{I}_{ij}(t), \hat{I}_{ij}(0) \right] \right\rangle \quad (209)$$

evaluated in the absence of the external field:  $\hat{I}_{ij}(t) = i(S_i^+ S_j^- - S_i^- S_j^+)t$ . The equation (208) can be simplified by using the Kramers-Kronig relation for the correlator  $R_{ij}(\omega)$ :

$$K(T) = \frac{1}{\mathcal{V}} \sum_{ij} \left( \frac{ge}{\hbar} x_{ij} M_{ij} \right)^2 \text{Im} R_{ij}(0) \quad (210)$$

$$\begin{aligned} K(T < T_c) = \frac{1}{8\mathcal{V}} \sum_{ij} \left( \frac{2e}{\hbar} x_{ij} \right)^2 \left( \frac{g}{2} M_{ij} \right)^2 & \left[ \left( \frac{\xi_i}{\varepsilon_i} + \frac{\xi_j}{\varepsilon_j} \right)^2 \frac{\tanh(\varepsilon_i/T) - \tanh(\varepsilon_j/T)}{\varepsilon_i - \varepsilon_j} \right. \\ & \left. + \left( \frac{\xi_i}{\varepsilon_i} - \frac{\xi_j}{\varepsilon_j} \right)^2 \frac{\tanh(\varepsilon_i/T) + \tanh(\varepsilon_j/T)}{\varepsilon_i + \varepsilon_j} \right]. \end{aligned} \quad (211)$$

One can immediately see that the regular part (211) contains an extra factor  $\sim \frac{gM_{ij}}{\varepsilon}$  compared to the total spectral weight  $K^{tot}(T)$  in (206). Thus we conclude that variation of the regular spectral weight below  $T_c$  is smaller than total spectral weight:

$$\frac{K(T_c) - K(T)}{K^{tot}(T)} \sim \frac{gM_{ij}}{T_c} \sim \frac{1}{Z_{eff}}. \quad (212)$$

The last estimate in Eq.(212) may be considered as a practical definition of  $Z_{eff}$ . Indeed, in lattice spin models where each spin is coupled to  $Z_{eff}$  other spins by a coupling constant  $gM$  the transition temperature can be estimated from  $gMZ_{eff} \sim T_c$ . As we argued above (see Eqs.(179,181) and the corresponding discussion in section 6.1), the effective coordination number  $Z_{eff}$  is not too small (and superconductivity survives) in a wide region of localized single-particle states where  $\delta_L/T_c$  is larger than 1. Eq.(212) implies that at  $Z_{eff} \gg 1$  the temperature dependence of the total spectral weight at  $T < T_c$  is almost entirely related with the variation of the superconducting density:

$$\delta K^{tot} = K^{tot}(T) - K^{tot}(T_c) \approx \rho_s(T)$$

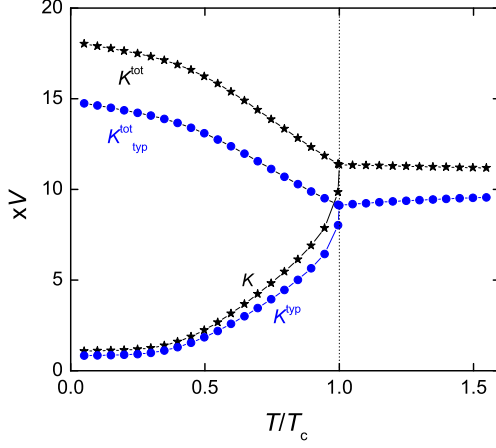


Figure 37: (Color online) Temperature dependence of regular spectral weight  $K(T)$  and full spectral weight  $K^{tot}(T)$  computed numerically (with 3D Gaussian AM of lattice size  $L = 20$ ) in the region of pseudogap superconductivity at  $E_F = 7.9$ . We used Eqs.(211) and (206), correspondingly, and employed approximate expression for the gap function  $\Delta(\xi, T)$  in the factorized form  $\Delta(\xi, T) = \Delta_c(\xi)\sqrt{1 - T/T_c}$ , where  $\Delta_c(\xi)$  is the critical-point solution shown in Fig. 19. Black stars stand for the simple averaging, whereas blue circles correspond to typical averages.

which is thus described by Eq.(205).

We now compute  $\rho_s(T)$  and  $K^{tot}(T)$  as given by (206) in the mean field approximation developed in this paper. We use modified MFA equation for the gap function in the form (182) and replace  $x_{ij}^2$  under the sum by its average value  $\frac{1}{2}R_0^2$  determined in Eq.(179) in (206). The result is

$$\rho_s(T) \approx \frac{2\nu_0 e^2 R_0^2}{\hbar^2} \int_0^\infty \frac{d\xi \Delta^2(\xi)}{\sqrt{\xi^2 + \Delta^2(\xi)}} \tanh \frac{\sqrt{\xi^2 + \Delta^2(\xi)}}{T} \quad (213)$$

which can be further simplified at  $T \rightarrow 0$ :

$$\rho_s \approx \frac{2e^2 R_0^2}{\hbar^2} \int_\Delta^\infty \frac{\nu(\varepsilon) d\varepsilon}{\varepsilon} \hat{\Delta}^2(\varepsilon) \sim \frac{2\nu_0 e^2 R_0^2}{\hbar^2} \Delta^2 \quad (214)$$

This expression allows one to extract the effective interaction range  $R_0$  from the data on the superconducting density in the combination with the gap  $\Delta$  and DoS  $\nu(\varepsilon)$  found from the Andreev spectroscopy measurements (see section 6.3).

In the above discussion we assumed that effective number of neighbors  $Z_{\text{eff}}$  for the pseudospin model is large. It is not always the case because, as discussed in the end of section 6.1, the superconducting state survives in the strongly spatially fluctuating form in the regime  $Z_{\text{eff}} < 1$ . Qualitative picture of the spectral weight temperature dependence in the pseudogap range of the Anderson model formulated in section 6.1 can be obtained from the numerical evaluation of the regular part  $K(T)$  given by (211) and

the total weight  $K^{tot}(T)$  given by (206). The results are shown in Fig.37 for  $E_F = 7.9$ . We emphasize that the expressions (206,211) give the leading orders in  $1/Z_{\text{eff}}$  expansion only, which is the *zero order* for Eq.(206), and the *first order* for Eq.(211). As one sees in Fig.37, both  $K(T)$  and  $K^{tot}(T)$  change by a similar amounts, so in this example  $Z_{\text{eff}} \sim 1$ . We expect that Fig.37 provides a qualitatively good description of the spectral weight behavior in pseudogapped superconductors.

## 7. Summary of results and unsolved problems.

We presented a generalization of the BCS-like theory of superconductivity that is appropriate for poor three-dimensional conductors in which Fermi level is located in the vicinity of the mobility edge. The developed theory neglects the effects of Coulomb repulsion. The reasons why this approximation is appropriate to describe many disordered films were discussed in section 1.2.

The model with BCS-like attraction and no Coulomb repulsion solved in the bulk of the paper can be also realized by ultra-cold fermionic atomic gases in optical traps [6, 104] with controlled disorder [105]. The enhancement of  $T_c$  by disorder predicted theoretically might turn out to be a useful tool to observe BCS state in these systems because without such enhancement  $T_c$  is often too low to be reached experimentally for the small values of the interaction constant  $\lambda$ . Such experiments may be also important for the understanding of superconductor-insulator transition in general.

The control parameter of the model is position of the Fermi level  $E_F$  with respect to the mobility edge  $E_c$ . The major new (with respect to the old works[2, 3, 4]) ingredient of the developed theory is the full account of the critical and weakly off-critical wave-function's fractality. We identified three qualitatively different regimes: the hard-gap insulator realized at large disorder, the pseudogap superconductor that appears when the phase correlations develop between well localized Cooper pairs and the "fractal" superconductor that appears against the background of fractal single particle states. Upon a further decrease of disorder the fractal superconductor smoothly crosses over to a conventional one.

For the insulating state, our main result is the computation of the activation energy  $T_I$  in the Arrhenius temperature dependence of resistivity,  $\ln R(T) \sim T_I/T$ , at low temperatures. The hard-gap character of this insulating state is due to the local attractive electron-electron interaction which leads to formation of localized Cooper pairs with nonzero binding energies  $\Delta_P^{(j)}$ , specific for each  $j$ -th localized orbital. The probability distribution of these energies is similar to the distribution of inverse participation ratios for localized eigenstates of the 3D Anderson model; it drops exponentially fast at low energies, imitating a hard gap. The estimate for the activation energy  $T_I$  as a function of  $E_F - E_c$  is in a reasonable agreement with experimental data [46].

The fractal superconducting state (realized for  $E_F$  very close to  $E_c$ ) is characterized by the following features:

1. In the weak coupling limit,  $\lambda \ll 1$ , the transition temperature,  $T_c$ , becomes a power law function of the interaction constant,  $\lambda$ . This leads to the parametric enhancement of  $T_c$  with respect to its value deep in the metal state. This conclusion is different from previous works [2, 3, 4] which assumed the validity of the "Anderson theorem" in the  $E_F$  region very close to mobility edge. The power law exponent in

the  $T_c(\lambda) \propto \lambda^{3/(3-d_2)}$  dependence is determined by the fractal dimension  $d_2 \approx 1.3$  of the critical eigenfunctions.

2. Strong local fluctuations of the pairing amplitude  $\Delta(\mathbf{r})$  coexist with a unique and well-defined critical temperature  $T_c$  below which a macroscopically coherent state appears.
3. The thermal Ginzburg parameter  $Gi$  of this transition is a universal quantity of the order of unity which is independent of the interaction constant  $\lambda$ , the same holds for the mesoscopic Ginzburg number  $Gi_d$ . This implies that thermal and mesoscopic fluctuations may change the pre-factor in the power law  $T_c(\lambda)$  by a factor  $\sim O(1)$  but cannot change the power-law itself.
4. Local single-particle density of states  $\nu(\varepsilon, \mathbf{r})$  fluctuates strongly in real space; these fluctuations lead to a strong random asymmetry of the tunneling conductance,  $G_T(V, \mathbf{r}) \neq G_T(-V, \mathbf{r})$ .
5. The value of the superfluid response, Eq.(176), coincides with result of [2] (Equation (4.1) in this paper), provided that one inserts in it the correct values of  $T_c$  and  $\Delta_0$  given above.

The pseudogap superconductor is predicted to occur when the Fermi energy  $E_F$  is deep inside the localized band of single-particle states. Its major feature is the presence of two distinct energy scales, both originating from the Cooper attraction between weakly localized electrons: the collective superconductive gap  $\Delta(0)$  and the local binding energy of a Cooper pair  $\Delta_P$ . The most unusual behavior is expected to occur in the regime of a strong pseudo-gap  $\Delta_P \gg (\Delta(0), T_c)$ . The very existence of superconducting correlations and a nonzero  $T_c$  in this regime is unexpected because it is characterized by a typical level spacing  $\delta_L = (\nu_0 L_{loc}^3)^{-1}$  which is larger than  $T_c$  and  $\Delta(0)$ :  $\delta_L/T_c \propto (\Delta_P/T_c)^{3/d_2}$  (81,82). The appearance of this regime was not expected in previous studies[2, 3, 4] which concluded that the superconducting state is stable only up to  $\delta_L \leq T_c$ . The perseverance of superconducting coherence much deeper in the localized region than was expected previously is the result of the enhancement of the correlations between the wave-functions intensities [77], which occurs due to the Mott's mechanism of resonant mixing of localized states. The key features of the pseudo-gap superconductor (in addition to the features of fractal superconductor listed above) are the following:

1. Insulating behavior of the resistivity in a wide range of temperatures above  $T_c$ .
2. Formation of almost hard gap without coherence peaks in the density of states above  $T_c$  with the gap value of the gap that fluctuates significantly from point to point.
3. Growth of coherence peaks below a global  $T_c$ . The magnitude of the coherence peaks (proportional to the local value of the superconducting order parameter) fluctuates from point to point, these fluctuations become very large close to the superconductor-insulator transition.
4. Two-peak feature in differential conductance at moderate transmission probabilities as measured by the Andreev point-contact spectroscopy below  $T_c$ . The lower peak voltage  $V_1(T, \mathbf{r})$  is expected to be  $\mathbf{r}$ -independent, but vanishing as temperature approaches  $T_c$  from below. In contrast, the higher peak voltage  $V_2(T, \mathbf{r})$  is expected to be almost  $T$ -independent, but strongly  $\mathbf{r}$ -dependent.

5. Strong temperature dependence of the total spectral weight  $K^{tot}(T)$  of the high-frequency conductivity which shows with a loss of major part of  $K^{tot}(T)$  at temperatures  $T \leq \Delta_P$ , and its re-appearance below  $T_c$ . The regular part  $K(T)$  of the spectral weight is smaller than the superconducting response  $\rho_s$ , see Eq.(212).

We now briefly discuss possible extensions of the developed theory and open questions. We begin with purely theoretical questions.

An obvious extension of the present theory would be a consistent account of Coulomb interaction effects in fractal superconductors near the 3D mobility edge. Here one should distinguish the effects of short range part of the Coulomb repulsion that competes with the phonon attraction and the long range part which might become very important in the insulator resulting in the formation of the Cooper pair glass and qualitatively new physics. Decreasing the dielectric constant in a real material would change it from the fractal superconductor discussed in this paper to the material in which superconductivity is suppressed by Coulomb interaction. Furthermore, increasing only the short range part of the Coulomb interaction leads to the 'fermionic' mechanism while increase in the long range part leads to the Coulomb blockade with completely different properties. The transition between all these regimes are currently not understood, neither theoretically nor experimentally. It seems likely that at least one of these crossovers was observed as the 'region of poor scaling' in [62].

The character of the quantum critical point that separates the fractal superconductivity and the insulator at  $T = 0$  deserves a further study. As discussed in section 6 on both sides of this transition electrons are bound in the localized pairs, and the transition itself consists in development of phase correlations, well described in terms of the XY ordering of the Anderson pseudo-spins  $\mathbf{S}_j$ . This scenario is different from both "bosonic" and the "fermionic" mechanisms of superconductor-insulator transition, so we suggest the name "pseudo-spin" mechanism. The cavity approach to the study of such transitions was developed recently in [93]; the main qualitative conclusion of this study is self-organized inhomogeneity of the resulting superconductor in which phase correlations are dominated by the rare, almost one-dimensional paths. This conclusion is supported by the results of the virial expansion method shown in Fig. 29 that point out to a percolation-like transition between the pseudo-gap superconductor and an insulator. Another feature of this solution is a very rapid decrease in the transition temperature beyond certain value of disorder which might be seen experimentally as the apparent existence of the lowest nonzero  $T_c \approx 0.5\text{K}$  found in amorphous  $\text{InO}_x$  system [42].

We now turn to experimental findings that lack (partially or entirely) theoretical explanation.

As discussed in section 6.2.3 the quantitative description of point contact tunneling requires the theory of collective modes in the fractal superconducting state. In the absence of such theory the spectacular, nearly rectangular shape of the *local* tunneling conductance  $G(V)$  at low temperatures[42] cannot be explained quantitatively.

The theory of the hard-gap insulating state presented in section 3 neglects the transport by Cooper pairs and takes into account only single electron transport. It is therefore limited to the region relatively far from the transition such as studied in Ref.[46]. Theory of the incoherent transport by Cooper pairs close to the transition was discussed in the recent papers [93, 106], the main conclusion of these studies is that very close to the transition the behavior of Cooper pairs is controlled by the many body mobility edge

which becomes zero exactly at the transition. Away from the transition the theory predicts activated behavior at the lowest temperatures with the gap that increases fast away with disorder and becomes infinite a short distance away from the transition signalling the absence of incoherent transport by Cooper pairs [93].

Recently the experimental paper [107] reported the anomalous size-dependence of the superconductor-insulator transition for extremely wide range of sizes between 1 and 150 microns. In particular, the workers observed a slow but significant dependence of the activation energy  $T_0(L)$  on the system size  $L$  (the distance between the metal contacts) on the insulating side of the transition. In one case  $T_0(L)$  decreased from 13.5 K to 9.6 K while  $L$  was changed from 145 to 12 microns at a fixed width. Although the theory of the incoherent transport by Cooper pairs close to the transition [93] predicts a strong size dependence at mesoscopic scales due to inhomogeneities, the size dependence at the huge scales observed experimentally are very difficult to explain. The explanation of this effect seems currently to be beyond the reach of a theory and presents a real challenge.

A different set of challenges is presented by the superconductor-insulator transition induced by magnetic field for strongly disordered (almost insulating) superconducting samples. As one would expect, the critical field,  $H_c$  (which corresponds to superconductor-insulator transition at  $T = 0$ ) is a strong function of disorder, for instance, it varies over two orders of magnitude in the experiments[53]. Surprisingly, there are indications that phenomenology of the transitions driven by disorder and by magnetic field look differently [46, 61, 44, 45, 62, 65]. Namely, the critical point in disorder is characterized by the activated behavior of the resistance,  $R \sim \exp(T_0/T)$ , with a large gap  $T_0$  even very close to the superconductor-insulator transition. In contrast, activated behavior,  $R \sim \exp(T_I(H)/T)$ , observed at fields above critical  $H_c$  is characterized by a small  $T_I(H)$  which extrapolates to zero at  $H_c$ . In other words, the region in  $(H, T)$  plane where transport is characterized by activated behavior with a small gap has a peculiar wedge like shape as sketched in Figure 1). Generally, one expects that very close to the critical line the transport is dominated by Cooper pairs; this expectation was experimentally confirmed for ultrathin Bi films [68]. In this case the experimental phase diagram implies that the regime of Cooper pair dominated transport is narrow in disorder but wide in field. Qualitatively this is likely to be due to the fact that the effect of a small magnetic field is limited to the generation of local phase differences which have a large effect of the superconducting state but does not affect the incoherent transport of the pairs. However, there is currently no consistent theory of this effect. On the experimental side, it would be important to verify that the transport in this regime is due to Cooper pairs for the InO and TiN films.

Furthermore, strongly disordered superconductors show puzzling behavior in very large magnetic fields: their resistivity become temperature independent and approaches the quantum limit,  $h/e^2$ . The field scale,  $H_P$ , at which this behavior sets in is not sensitive to the disorder in contrast to the critical field,  $H_c$ . The second field scale appears first in the fractal superconductor: it is the field that destroys local Cooper pairs and suppresses the hard gap  $\Delta_P$ . In this regime, the parametric difference between  $H_P$  and  $H_c$  is due to the low fractal dimension  $d_2 \approx 1.3$  of a single-particle wave-function that suppresses the orbital effect of magnetic field on the pairing of two electrons localized on this eigenstate, similarly to a very thin wire. In contrast, long-range coherence requires the existence of large loops involving many localized Cooper pairs. The typical size of these loops is larger than the localization length  $L_{loc}$ , leading to relatively small magnetic

field scale  $H_c \leq \Phi_0/L_{loc}^2 \ll H_P$ . In the pseudogap superconductor the second field scale is associated with the suppression of a large gap,  $\Delta_P$ , responsible for Cooper pair formation whereas the critical field is associated with the frustration of a weak pseudospin coupling. Thus, one expects even larger difference between the field scales in this regime. However, the universal value of the conductance in the regime  $B \gg H_P$  is not expected theoretically and remains mysterious.

Nernst effect can be potentially a very sensitive probe of the nature of the superconducting state.[108] These experiments were performed recently on  $\text{InO}_x$  samples and show [109] Nernst signal which scales as  $N(T) \propto T^{-n}$ , with the "Nernst exponent"  $n \approx 7.5$  at low magnetic fields. Application of the conventional theory [89] of the superconducting fluctuations to the Nernst effect in 2D superconductors [110, 111] gives Nernst signal that scales as  $1/T \ln T$  at high temperatures. This behavior was indeed observed in conventional superconductor NbSi [112]. Because Nernst effect requires a motion of the electrical charge around the plaquette, the temperature dependence is expected to be different in discrete systems where motion around the minimal plaquette involve a large number of hops and each hop implies an extra power of  $1/T$  in the high temperature expansion [113]. For instance, because minimal plaquette on the hexagonal lattice contains six sites, one expects that  $N(T) \propto T^{-6}$  in this case. The striking difference between NbSi and  $\text{InO}_x$  behavior observed in [109] on very low  $T_c$  (very disordered) samples indicates, in our opinion, the importance of Cooper pair hopping between localized sites. This behavior should get less pronounced further away from the transition, thus we expect that slightly less disordered samples will show more 'conventional' exponent in Nernst effect.

A number of papers noted the apparent similarity between phenomenology of disordered films of conventional superconductors discussed in this paper and that of high  $T_c$  oxides.[53, 114] Very briefly, the transport and magnetic measurements show the formation of pseudogap at temperatures much higher than superconducting  $T_c$  in underdoped materials,[115] while STM measurements display highly inhomogeneous order parameter (as measured by coherence peaks) combined with modestly homogeneous tunneling gap.[116, 117, 118, 119] Furthermore, a number of indirect evidences points out to the superconducting nature of the pseudogap in these materials [120, 121, 122], similar to the situation discussed in this paper. The crucial difference between s-wave and d-wave pairing characterizing high  $T_c$  oxides is that, in contrast to s-wave pairing, modest elastic scattering with mean free path of the order of superconducting coherence length suppresses the d-wave superconductivity. Thus, localization of the wave functions is incompatible with generic d-wave superconductivity. This conclusion might need to be revised for the special case of superconductivity which is due to pairing of electrons in a small area of the full Brillouin zone which might be the case of cuprates [123, 124]. In this case, the electrons that are responsible for the pairing belong to two well separated patches on the Fermi surface with each patch characterized by a small momentum  $p_0$ . The density of states in these patches is large which makes scattering of these electrons strong. Furthermore, because most impurities are located far from the conducting copper oxide planes, it is likely that the elastic scattering, though strong, does not mix different patches and thus does not inhibit d-wave pairing. In this situation, single electron states inside each patch may become very similar to the localized states discussed in this work making the developed theory qualitatively correct. This would explain the main phenomenological features mentioned above: formation of pseudogap far above  $T_c$ ,



highly inhomogeneous order parameter observed in tunneling data, insulating behavior of LaSrCuO superconductors in high magnetic fields, etc.

Finally, it is not clear why the phenomenology displayed by Josephson junction networks[9, 50] was not observed in any disordered film. In particular, Josephson junction networks close to superconductor-insulator transition are characterized by the appearance of a wide region of magnetic fields where resistivity has no temperature dependence but varies by many orders of magnitude as a function of magnetic field. This is in a sharp contrast with the films that show more or less good crossing point of  $R(B)$  isotherms. There is very little doubt that Josephson networks are described by model Hamiltonian (2), so one has to conclude that it is not the appropriate model for most films. One possible source of difference discussed above might be that many films are characterized by a large value of the dielectric constant, while another reason, relevant for the films with small dielectric constant, might be the capacitance matrix is not dominated by nearest neighbors in these films. Nearest neighbor capacitance matrix translates into the Coulomb interaction that decreases only logarithmically with distance in the Josephson network as opposed to  $1/r$  expected in a film. The physical result might be the formation of the Cooper pair glass in the Josephson network but not in the disordered film or vice versa. If true, one expects that Josephson networks with the Coulomb interaction screened by the ground plate might display properties more similar to those of the films. Another difference might be due to the fluxes produced by magnetic field are completely random in a disordered films but are (almost) identical on the plaquettes of the Josephson lattice. In this case one expects to see film behavior in randomized Josephson network.

We are grateful to B. L. Altshuler, T. I. Baturina, C. Chapelier, T. Dubouchet, A. M. Finkelstein, V. F. Gantmakher, A. S. Ioselevich, I. V. Lerner, A. Millis, A. D. Mirlin, M. Mueller, Z. Ovadyahu, V. V. Ryazanov, B. Sacepe, V. Schmidt, D. Shahar, M. A. Skvortsov and V. I. Yudson for useful discussions. This research was supported by Triangle de la physique 2007-36, grants ANR-06-BLAN-0218, ARO 56446-PH-QC and DARPA HR0011-09-1-0009, by the grant 07-02-00310 from Russian Foundation for Basic Research, and by the program "Quantum physics of condensed matter" of Russian Academy of Sciences. We thank the FEDER and the Spanish DGI for financial support through Project No. FIS2007-62238. V.E.K acknowledges a hospitality of the Institute for Nuclear Theory at the University of Washington and the DOE for partial support during the completion of this work.

## Appendix A. Virial expansion in pseudospin subspace

The two-spin susceptibility  $\chi_{12}^{(2)} = \chi_{12}^{(2a)} + \chi_{12}^{(2b)}$  is computed as explained in section 4.4 and can be easily written analytically even for nonzero Hartree terms. It is a sum of



two terms, one of which does not explicitly depend on  $J_{12}^\perp$ :

$$\begin{aligned} \chi_{12}^{(2,a)} = & Z_0^{-1} \left[ \frac{\sinh\left(\frac{E_+}{T} + \frac{J_{12}^\parallel}{2T}\right)}{\left(E_+ + \frac{J_{12}^\parallel}{2}\right)} e^{E_-/T} + \frac{\sinh\left(\frac{E_+}{T} - \frac{J_{12}^\parallel}{2T}\right)}{\left(E_+ - \frac{J_{12}^\parallel}{2}\right)} e^{-E_-/T} \right. \\ & \left. + \frac{\sinh\left(\frac{E_-}{T} + \frac{J_{12}^\parallel}{2T}\right)}{\left(E_- + \frac{J_{12}^\parallel}{2}\right)} e^{E_+/T} + \frac{\sinh\left(\frac{E_-}{T} - \frac{J_{12}^\parallel}{2T}\right)}{\left(E_- - \frac{J_{12}^\parallel}{2}\right)} e^{-E_+/T} \right], \end{aligned} \quad (\text{A.1})$$

where

$$Z_0 = 4 \cosh\left(\frac{E_+}{T}\right) \cosh\left(\frac{E_-}{T}\right) \cosh\left(\frac{J_{12}^\parallel}{2T}\right) + 4 \sinh\left(\frac{E_+}{T}\right) \sinh\left(\frac{E_-}{T}\right) \sinh\left(\frac{J_{12}^\parallel}{2T}\right)$$

The other term is proportional to  $J_{12}^\perp$ :

$$\begin{aligned} \chi_{12}^{(2,b)} = & \frac{Z_0^{-1} J_{12}^\perp}{(E_+ - E_-)} \left[ \frac{\sinh\left(\frac{E_+}{T} - \frac{J_{12}^\parallel}{2T}\right) e^{-E_-/T}}{\left(E_+ - \frac{1}{2} J_{12}^\parallel\right)} - \frac{\sinh\left(\frac{E_+}{T} + \frac{J_{12}^\parallel}{2T}\right) e^{E_-/T}}{\left(E_+ + \frac{1}{2} J_{12}^\parallel\right)} \right. \\ & \left. + \frac{\sinh\left(\frac{E_-}{T} + \frac{J_{12}^\parallel}{2T}\right) e^{E_+/T}}{\left(E_- + \frac{1}{2} J_{12}^\parallel\right)} - \frac{\sinh\left(\frac{E_-}{T} - \frac{J_{12}^\parallel}{2T}\right) e^{-E_+/T}}{\left(E_- - \frac{1}{2} J_{12}^\parallel\right)} \right] \end{aligned} \quad (\text{A.2})$$

Here we present the details of the formalism for computing the three-spin susceptibility. It is developed with the goal to use for numerical computation rather than being a full-analytical approach. The even Hilbert subspace of the problem of three sites with 2 or 0 electron on each site (equivalent to the spin- $\frac{1}{2}$  problem with three coupled spins) consists of 8 basic states classified by the total spin. The corresponding Hamiltonian has a block structure corresponding to the total spin  $\frac{3}{2}$ ,  $0$ ,  $\frac{1}{2}$ ,  $-\frac{1}{2}$ . The first two blocks are just numbers:

$$\pm (\xi_1 + \xi_2 + \xi_3) - \frac{1}{2} (J_{12}^\parallel + J_{13}^\parallel + J_{23}^\parallel). \quad (\text{A.3})$$

The last two blocks are  $3 \times 3$  matrices:

$$A = \begin{pmatrix} \xi_{23}^1 + \frac{J_{12}^\parallel + J_{13}^\parallel - J_{23}^\parallel}{2} & -J_{12}^{\perp*} & -J_{13}^{\perp*} \\ -J_{12}^\perp & \xi_{13}^2 + \frac{J_{12}^\parallel - J_{13}^\parallel + J_{23}^\parallel}{2} & -J_{23}^{\perp*} \\ -J_{13}^\perp & -J_{23}^\perp & \xi_{12}^3 + \frac{-J_{12}^\parallel + J_{13}^\parallel + J_{23}^\parallel}{2} \end{pmatrix}. \quad (\text{A.4})$$

$$B = \begin{pmatrix} -\xi_{12}^3 + \frac{-J_{12}^\parallel + J_{13}^\parallel + J_{23}^\parallel}{2} & -J_{23}^{\perp*} & -J_{13}^{\perp*} \\ -J_{23}^\perp & -\xi_{13}^2 + \frac{J_{12}^\parallel - J_{13}^\parallel + J_{23}^\parallel}{2} & -J_{12}^{\perp*} \\ -J_{13}^\perp & -J_{12}^\perp & -\xi_{23}^1 + \frac{J_{12}^\parallel + J_{13}^\parallel - J_{23}^\parallel}{2} \end{pmatrix}. \quad (\text{A.5})$$

where  $\xi_{bc}^a = \xi_b + \xi_c - \xi_a$ . Such structure suggests that the eigenvalues of the 3-spin problem are also grouped:

$$\lambda_{1,2}^{(0)} = \pm(\xi_i + \xi_j + \xi_k) - \frac{1}{2}(J_{12}^{\parallel} + J_{13}^{\parallel} + J_{23}^{\parallel}), \quad (\text{A.6})$$

and two groups of eigenvalues  $\lambda_{3,4,5}^{(0)}$  and  $\lambda_{6,7,8}^{(0)}$  are found from the solution of the two cubic characteristic equations  $\det(A - \lambda_{3,4,5}^{(0)} I) = 0$ , and  $\det(B - \lambda_{6,7,8}^{(0)} I) = 0$ .

One can find the solutions to these equations either numerically or from the Cartan formula for the roots of cubic equations, the former being more efficient in the numerical calculations.

The 8-eigenvectors  $X_1 = (1, 0, 0, 0, 0, 0, 0, 0)$  and  $X_2 = (0, 0, 0, 0, 0, 0, 0, 1)$  are simple: they contain unity in the first and eight row respectively, and all the other elements being zero; the structure of the nontrivial eigenvectors of the  $3 \times 3$  matrices is as follows:

$$\begin{aligned} X_{\alpha=3,4,5}^T &= (0, u_{\alpha}, v_{\alpha}, w_{\alpha}, 0, 0, 0, 0) \\ X_{\alpha=6,7,8}^T &= (0, 0, 0, 0, u'_{\alpha}, v'_{\alpha}, w'_{\alpha}, 0) \end{aligned} \quad (\text{A.7})$$

where  $(u_{\alpha}, v_{\alpha}, w_{\alpha})$  is the normalized 3-eigenvector of the matrix  $A$  that corresponds to the eigenvalue  $\lambda_{\alpha=3,4,5}^{(0)}$  and  $u'_{\alpha}, v'_{\alpha}, w'_{\alpha}$  is the normalized 3-eigenvector of the matrix  $B$  that corresponds to the eigenvalue  $\lambda_{\alpha=6,7,8}^{(0)}$ .

The perturbation matrix in the same basis takes the form:

$$V^{(3)} = \begin{pmatrix} 0 & \Delta & \Delta & \Delta & 0 & 0 & 0 & 0 \\ \Delta^* & 0 & 0 & 0 & \Delta & \Delta & 0 & 0 \\ \Delta^* & 0 & 0 & 0 & \Delta & 0 & \Delta & 0 \\ \Delta^* & 0 & 0 & 0 & 0 & \Delta & \Delta & 0 \\ 0 & \Delta^* & \Delta^* & 0 & 0 & 0 & 0 & \Delta \\ 0 & \Delta^* & 0 & \Delta^* & 0 & 0 & 0 & \Delta \\ 0 & 0 & \Delta^* & \Delta^* & 0 & 0 & 0 & \Delta \\ 0 & 0 & 0 & 0 & \Delta^* & \Delta^* & \Delta^* & 0 \end{pmatrix} \quad (\text{A.8})$$

With the eigenvalues  $\lambda_{\alpha}^{(0)}$  and the eigenvectors  $X_{\alpha}$  ( $\alpha = 1 \dots 8$ ) obtained, one can compute  $\gamma_{\alpha}$  from Eq.(45) (the field  $\Delta$  cancels out):

$$\begin{aligned} \gamma_1 &= \sum_{\beta=3,4,5} \frac{(u_{\beta} + v_{\beta} + w_{\beta})^2}{\lambda_1^{(0)} - \lambda_{\beta}^{(0)}} & \gamma_2 &= \sum_{\beta=6,7,8} \frac{(u'_{\beta} + v'_{\beta} + w'_{\beta})^2}{\lambda_2^{(0)} - \lambda_{\beta}^{(0)}} \\ \gamma_{\alpha=3,4,5} &= \sum_{\beta=6,7,8} \frac{u_{\alpha} u'_{\beta} + w_{\alpha} w'_{\beta} + u_{\alpha} v'_{\beta} + v_{\alpha} u'_{\beta} + v_{\alpha} w'_{\beta} + w_{\alpha} v'_{\beta}}{\lambda_{\alpha}^{(0)} - \lambda_{\beta}^{(0)}} + \frac{(u_{\alpha} + v_{\alpha} + w_{\alpha})^2}{\lambda_{\alpha}^{(0)} - \lambda_1^{(0)}} \\ \gamma_{\alpha=6,7,8} &= \sum_{\beta=3,4,5} \frac{u'_{\alpha} u_{\beta} + w'_{\alpha} w_{\beta} + u'_{\alpha} v_{\beta} + v'_{\alpha} u_{\beta} + v'_{\alpha} w_{\beta} + w'_{\alpha} v_{\beta}}{\lambda_{\alpha}^{(0)} - \lambda_{\beta}^{(0)}} + \frac{(u'_{\alpha} + v'_{\alpha} + w'_{\alpha})^2}{\lambda_{\alpha}^{(0)} - \lambda_2^{(0)}}. \end{aligned} \quad (\text{A.9})$$

and then compute  $\chi_{ijk}^{(3)}$  from Eq.(154). Finally, subtracting the proper combinations of the two- and one- spin susceptibilities one obtains the virial coefficient  $\chi_3(T)$  from Eq.(153).

## Appendix B. Virial expansion including single-occupied states

The Hilbert space we considered so far corresponded to each orbital  $i, j, k \dots$  occupied either by two electrons or empty. Now let us consider the same Hamiltonian, Eq.(145), but extend the Hilbert space to include possible single-electron occupancies of all orbitals. To avoid unnecessary complications we omit here the Hartree terms setting  $g_{\parallel} = 0$  in Eq.(145).

### Appendix B.1. One-orbital problem

The full Hilbert space in this case consists of

$$|0\rangle, |2\rangle, |\uparrow\rangle, |\downarrow\rangle.$$

The first two states contain even number of electrons (the "even" states) and the last two (the "odd" states) contain one electron each. Each "odd" state has extra energy  $\Delta_P$ .

It is important that the spin operator acting on the "odd" states  $|\uparrow\rangle$  or  $|\downarrow\rangle$  gives zero:

$$S^{+/-}|\downarrow\rangle = S^{+/-}|\uparrow\rangle = 0. \quad (\text{B.1})$$

The energies of the four states are (we count all energies with respect to  $-\varepsilon = -\xi + \Delta_P$ ):

$$-\varepsilon, \quad 2\xi - 2\Delta_P - \varepsilon = +\varepsilon, \quad \xi - \varepsilon = \Delta_P, \quad \Delta_P.$$

Eq.(B.1) suggests that the "partial susceptibilities"  $\gamma_{\text{odd}}$  given by Eq.(155) are zero for all the odd states. This is because the Hamiltonian Eq.(145) does not couple the even and odd sectors of the Hilbert space.

Thus all one has to do to compute the one-site susceptibility is to add  $2e^{-\Delta_P/T}$  to the partition function  $Z_0$ . The result is:

$$\chi^{(1)} = \left( \frac{1}{2\varepsilon} \right) F(\varepsilon, \Delta_P), \quad F(\varepsilon, \Delta_P) = \frac{\sinh\left(\frac{\varepsilon}{T}\right)}{\cosh\left(\frac{\varepsilon}{T}\right) + e^{-\Delta_P/T}}. \quad (\text{B.2})$$

Note that there is a nice property:

$$F(\varepsilon, \infty) = \tanh\left(\frac{\varepsilon}{T}\right), \quad F(\varepsilon, 0) = \tanh\left(\frac{\varepsilon}{2T}\right). \quad (\text{B.3})$$

### Appendix B.2. Two-orbital problem

The full Hilbert space for the 2-orbital problem consists of the *even sector*:

$$\psi_1 = |0, 0\rangle, \quad \psi_2 = |2, 2\rangle, \quad \psi_3 = |2, 0\rangle, \quad \psi_4 = |0, 2\rangle$$

an the *odd sector*:

$$\begin{aligned} \psi_{5,6} &= |\alpha, 0\rangle, & \psi_{7,8} &= |0, \alpha\rangle, & \psi_{9,10} &= |\alpha, 2\rangle, \\ \psi_{11,12} &= |2, \alpha\rangle, & \psi_{13-16} &= |\alpha, \alpha'\rangle, \end{aligned}$$

where  $\alpha = \uparrow$  or  $\downarrow$ .

Let us first find the eigenvalues in the odd sector (counted from  $-(\varepsilon_1 + \varepsilon_2)$ ):

$$\begin{aligned}\lambda_{5,6}^{(0)} &= \xi_1 - (\varepsilon_1 + \varepsilon_2) = -\varepsilon_2 + \Delta_P^{(1)}, \\ \lambda_{7,8}^{(0)} &= \xi_2 - (\varepsilon_1 + \varepsilon_2) = -\varepsilon_1 + \Delta_P^{(2)}, \\ \lambda_{9,10}^{(0)} &= \xi_1 + 2(\xi_2 - \Delta_P^{(2)}) - (\varepsilon_1 + \varepsilon_2) = \varepsilon_2 + \Delta_P^{(1)}, \\ \lambda_{11,12}^{(0)} &= 2(\xi_1 - \Delta_P^{(1)}) + \xi_2 - (\varepsilon_1 + \varepsilon_2) = \varepsilon_1 + \Delta_P^{(2)}.\end{aligned}$$

In all the above formulae

$$\varepsilon_i = \xi_i - \Delta_P^{(i)}, \quad (\text{B.4})$$

where  $\xi_i$  is a single-particle energy (eigenvalues of the state  $\psi_i(\mathbf{r})$ ) measured from the Fermi-energy, and  $\Delta_P^{(i)}$  is a pseudo-gap:

$$\Delta_P^{(i)} = \frac{g}{2} \sum_{\mathbf{r}} |\Psi_i(\mathbf{r})|^4. \quad (\text{B.5})$$

Note that Eq.(B.1) guarantees that the eigenvalues of the odd sector do not have any  $M_{ij}$ -dependent renormalization. However, not all the partial susceptibilities  $\gamma_{\text{odd}}$  are equal to zero. The reason is that the source terms  $\Delta S^+ + \Delta^* S^-$  contain only one  $S^{+(-)}$  operator whereas the number of sites is two. This operator may act on the site in an even state and then the result of action of the source term on a *semi-odd* state  $|\text{even}, \text{odd}\rangle$  will be non-zero. Thus we expect that the structure constants for the states  $\psi_i$ , ( $i = 5, 6, \dots, 12$ ) are non-zero. A simple calculation shows that

$$\begin{aligned}\gamma_5 &= \gamma_6 = -\gamma_9 = -\gamma_{10} = -\frac{1}{2\varepsilon_2}, \\ \gamma_7 &= \gamma_8 = -\gamma_{11} = -\gamma_{12} = -\frac{1}{2\varepsilon_1}.\end{aligned}$$

Now we are in a position to give an exact result for the 2-orbital susceptibility:

$$\chi_{12}^{(2)} = \frac{\frac{J_{12}^\perp}{2} \frac{\text{ssh}(\frac{E_+}{T}, \frac{E_-}{T})}{E_+ E_-} + \frac{\text{sch}(\frac{E_+}{T}, \frac{E_-}{T})}{2E_+} + \frac{\text{csh}(\frac{E_+}{T}, \frac{E_-}{T})}{2E_-} + \frac{\sinh(\frac{\varepsilon_1}{T}) e^{-\Delta_P^{(2)}/T}}{2\varepsilon_1} + \frac{\sinh(\frac{\varepsilon_2}{T}) e^{-\Delta_P^{(1)}/T}}{2\varepsilon_2}}{\text{cch}(\frac{E_+}{T}, \frac{E_-}{T}) + \cosh(\frac{\varepsilon_1}{T}) e^{-\Delta_P^{(2)}/T} + \cosh(\frac{\varepsilon_2}{T}) e^{-\Delta_P^{(1)}/T} + e^{-\Delta_P^{(1)}/T} e^{-\Delta_P^{(2)}/T}} \quad (\text{B.6})$$

where we denoted

$$\text{ssh}(x, y) = \sinh(x) \sinh(y), \quad \text{sch}(x, y) = \sinh(x) \cosh(y), \quad \text{cch}(x, y) = \cosh(x) \cosh(y)$$

If one neglects the renormalization of eigenvalues by interaction and sets  $E_+ = \varepsilon_1$ ,  $E_- = \varepsilon_2$ , the Eq.(B.6) is reduced to a simpler form

$$\begin{aligned}\chi_{12}^{(2)} &= \frac{J_{12}^\perp}{2\varepsilon_1 \varepsilon_2} F(\varepsilon_1, \Delta_P^{(1)}) F(\varepsilon_2, \Delta_P^{(2)}) + \\ &\quad \frac{F(\varepsilon_1, \Delta_P^{(1)})}{2\varepsilon_1} + \frac{F(\varepsilon_2, \Delta_P^{(2)})}{2\varepsilon_2},\end{aligned}$$

where  $F(\varepsilon, \Delta_P)$  is defined in Eq.(B.2). In this approximation the full susceptibility has the same form as Eq.(158) after one replaces  $\tanh(\varepsilon/T)$  by the function  $F(\varepsilon, \Delta_P)$ .

$$\chi^{(2)} = \sum_{i>j} \frac{J_{ij}^\perp}{2\varepsilon_i \varepsilon_j} F(\varepsilon_i, \Delta_P^{(i)}) F(\varepsilon_j, \Delta_P^{(j)}). \quad (\text{B.7})$$

However, when the renormalization of energy levels is taken into account, such simple replacement  $\tanh(E/T) \rightarrow F(E, \Delta_P)$  does not work any more.

### Appendix B.3. Three-orbital problem

In an absolutely similar way one can compute the exact susceptibility of a three-site problem, considering all 64 states of which 8 are even and 56 odd states are grouped as follows:

*group I:*

$$|\text{two-site even state}\rangle \otimes |\alpha\rangle$$

with  $\alpha = \uparrow (\downarrow)$  corresponding to the first, second or the third site. There are  $4 \times 2 \times 3 = 24$  such states.

*group II:*

$$|\text{one-site even state}\rangle \otimes |\alpha\rangle \otimes |\alpha'\rangle,$$

with an even state on the first, second, or the third site. There are  $2 \times 4 \times 3 = 24$  such states.

*group III:*

$$|\alpha, \alpha', \alpha''\rangle.$$

There are 8 such states.

The eigenvalues  $\lambda_\alpha^{(0)}$  can be found exactly like in the previous subsection; they are equal to (relative to the vacuum state  $-(\varepsilon_1 + \varepsilon_2 + \varepsilon_3)$ ) the eigenvalues of the corresponding even state plus the sum of  $\Delta_p^{(i)}$  of the singly occupied sites. For instance:

$$|0, 2, \alpha\rangle \rightarrow \lambda^{(0)} = -\text{sgn}(\varepsilon_1 - \varepsilon_2) \sqrt{(\varepsilon_1 - \varepsilon_2)^2 + |J_{12}|^2} + \Delta_p^{(3)},$$

$$|2, \alpha, \alpha'\rangle \rightarrow \lambda^{(0)} = \varepsilon_1 + \Delta_p^{(2)} + \Delta_p^{(3)},$$

$$|\alpha, \alpha', \alpha''\rangle \rightarrow \lambda^{(0)} = \Delta_p^{(1)} + \Delta_p^{(2)} + \Delta_p^{(3)}.$$

The three-orbital susceptibility  $\chi_{1,2,3}^{(3)}$  can be calculated using the general Eq.(154), in which the partition function  $Z_0 = Z_0(1, 2, 3)$  is equal to

$$\begin{aligned} Z_0(1, 2, 3) = & Z_0^{\text{even}} + 8 \cosh(\bar{E}_+^{(1,2)}) \cosh(\bar{E}_-^{(1,2)}) e^{-\bar{\Delta}_p^{(3)}} \\ & + 8 \cosh(\bar{E}_+^{(1,3)}) \cosh(\bar{E}_-^{(1,3)}) e^{-\bar{\Delta}_p^{(2)}} + 8 \cosh(\bar{E}_+^{(2,3)}) \cosh(\bar{E}_-^{(2,3)}) e^{-\bar{\Delta}_p^{(1)}} \quad (\text{B.8}) \\ & + 8 \cosh(\bar{\varepsilon}_1) e^{-\bar{\Delta}_p^{(2)}} e^{-\bar{\Delta}_p^{(3)}} + 8 \cosh(\bar{\varepsilon}_2) e^{-\bar{\Delta}_p^{(1)}} e^{-\bar{\Delta}_p^{(3)}} + 8 \cosh(\bar{\varepsilon}_3) e^{-\bar{\Delta}_p^{(1)}} e^{-\bar{\Delta}_p^{(2)}} \\ & + 8 e^{-\bar{\Delta}_p^{(1)}} e^{-\bar{\Delta}_p^{(2)}} e^{-\bar{\Delta}_p^{(3)}}. \quad (\text{B.9}) \end{aligned}$$

In Eq.(B.8) each line corresponds to the above group of states,  $E_\pm$  is given by Eq.(159), and  $\bar{E}, \bar{\Delta} = E/T, \Delta/T$ . The partition function of the even states  $Z_0^{\text{even}} = \sum_{\text{even states}} e^{-\lambda_\alpha^{(0)}/T}$  has been calculated above for the 3-spin case.

The numerator of Eq.(154)  $G(1, 2, 3) = -\sum_{\alpha} e^{-\lambda_{\alpha}^{(0)}/T} \gamma_{\alpha}$  is found to be the following:

$$G(1, 2, 3) = G^{\text{even}}(1, 2, 3) + 4 G_{12} e^{-\bar{\Delta}_p^{(3)}} + 4 G_{13} e^{-\bar{\Delta}_p^{(2)}} + 4 G_{23} e^{-\bar{\Delta}_p^{(1)}} \\ + 4 \frac{\sinh(\bar{\varepsilon}_1)}{\varepsilon_1} e^{-\bar{\Delta}_p^{(2)} - \bar{\Delta}_p^{(3)}} + 4 \frac{\sinh(\bar{\varepsilon}_2)}{\varepsilon_2} e^{-\bar{\Delta}_p^{(1)} - \bar{\Delta}_p^{(3)}} + 4 \frac{\sinh(\bar{\varepsilon}_3)}{\varepsilon_3} e^{-\bar{\Delta}_p^{(1)} - \bar{\Delta}_p^{(2)}} \quad (\text{B.10})$$

where

$$G_{ij} = \frac{J_{ij}^{\perp}}{E_+^{(i,j)} E_-^{(i,j)}} \sinh(\bar{E}_+^{(i,j)}) \sinh(\bar{E}_-^{(i,j)}) + \\ + \frac{\sinh(\bar{E}_+^{(i,j)})}{E_+^{(i,j)}} \cosh(\bar{E}_-^{(i,j)}) + \frac{\sinh(\bar{E}_-^{(i,j)})}{E_-^{(i,j)}} \cosh(\bar{E}_+^{(i,j)}) \quad (\text{B.11})$$

is (up to a constant factor) the numerator in Eq.(154) for the 2-spin problem. Note also that  $\sinh(\bar{\varepsilon}_i)/\varepsilon_i$  is (again up to a constant factor) the numerator of the one-spin problem. The quantity  $G^{\text{even}}(1, 2, 3) = -\sum_{\text{even states}} e^{-\lambda_{\alpha}^{(0)}/T} \gamma_{\alpha}$  has been calculated above for the 3-spin problem.

Using Eqs.(B.8),(B.10) one finds the 3-orbital susceptibility exactly:

$$\chi_{1,2,3}^{(3)} = \frac{G(1, 2, 3)}{Z_0(1, 2, 3)}. \quad (\text{B.12})$$

## References

- [1] P. W. Anderson, Phys. Rev. **109**, 492 (1958).
- [2] M. Ma and P. A. Lee, Phys. Rev. B **32**, 5658 (1985).
- [3] A. Kapitulnik and G. Kotliar, Phys. Rev. Lett. **54**, 473 (1985); G. Kotliar and A. Kapitulnik, Phys. Rev. B **33**, 3146 (1986).
- [4] L. N. Bulaevskii and M. V. Sadosvskii, Pisma ZhETF **39**, 524 (1984); L. N. Bulaevskii and M. V. Sadosvskii, J.Low Temp.Phys. **59**, 89 (1985); M. V. Sadosvskii, Phys. Rep, **282**, 225 (1997).
- [5] A. Ghosal, M. Randeria and N. Trivedi, Phys. Rev. B **65**, 014501 (2001).
- [6] S. Giorgini, L. P. Pitaevskii and S. Stringari, Rev. Mod. Phys. **80**, 1215 (2008).
- [7] A. Goldman and N. Markovic, Phys. Today **51**, 39 (1998).
- [8] A. M. Finkelstein, Physica B **197**, 636 (1994)
- [9] R. Fazio and H. van der Zant, Phys. Rep. **355**, 235 (2001); H. S. J. van der Zant, W. J. Elion, L. J. Geerlings and J. E. Mooij, Phys. Rev. B **54**, 10081 (1996).
- [10] A. I. Larkin, Ann. Phys. (Leipzig) **8**, 785 (1999).
- [11] K. B. Efetov, ZhETF **78**, 2017 (1980) [Sov.Phys.-JETP **51**, 1015 (1980)]
- [12] A. I. Larkin and Yu. N. Ovchinnikov, Phys. Rev. B **28**, 6281 (1983)
- [13] U. Eckern, G. Schoen and V. Ambegaokar, Phys. Rev.B **30**, 6419 (1984)
- [14] M. V. Feigel'man, S. E. Korshunov, and A. B. Pugachev, Pis'ma v ZhETF **65**, 541 (1997) [JETP Lett. **65**, 566 (1997).
- [15] B. G. Orr, J. M. Jaeger, A. Goldman and C. G. Kuper, Phys. Rev. Lett. **56**, 378 (1986).
- [16] M. P. A. Fisher, G. Grinstein and S. Girvin, Phys. Rev. Lett. **64**, 587 (1990).
- [17] M. P. A. Fisher, Phys. Rev. Lett. **65**, 923 (1990).
- [18] N. M. Zimmerman *et al*, J. Appl. Phys. **104**, 033710 (2008), N. M. Zimmerman and W. H. Huber, Phys. Rev. B **80**, 195304 (2009).
- [19] M. Mueller and L. B. Ioffe, arXiv:0711.2668
- [20] A. Gerber, A. Milner, G. Deutscher, M. Karpovsky, and A. Gladkikh, Phys. Rev. Lett. **78**, 4277 (1997).
- [21] V. F. Gantmakher *et al*, JETP **82**, 951 (1996).
- [22] I. S. Beloborodov, K. B. Efetov and A. I. Larkin Phys. Rev. B **61**, 9145 (2000).
- [23] I. S. Beloborodov, A. V. Lopatin, V. M. Vinokur, and K. B. Efetov, Rev. Mod. Phys. **79**, 469 (2007).
- [24] A. M. Finkelstein, Pis'ma ZhETF **45**, 37 (1987) [Sov. Phys. JETP Lett. **45**, 46 (1987)].
- [25] S. Maekawa and H. Fukuyama J. Phys. Soc. Jap. **51**, 1380 (1982); H. Takagi and Y. Kuroda, Sol. St. Comm. **41**, 643 (1982).
- [26] Yu. Oreg and A. M. Finkelstein, Phys. Rev. Lett. **83**, 191 (1999).
- [27] P. W. Anderson, K. A. Muttalib and T. V. Ramakrishnan Phys. Rev. B **23**, 117 (1983).
- [28] L. Coffey, K. A. Muttalib and K. Levin, Phys. Rev. Lett. **52**, 783 (1984).
- [29] M. E. Gershenson, Yu. B. Khavin, D. Reuter, P. Schafmeister, and A. D. Wieck, Phys. Rev. Lett. **85**, 1718 (2000).
- [30] D. Kowal and Z. Ovadyahu, Sol. St. Com. **90**, 783 (1994).
- [31] M. A. Skvortsov and M. V. Feigel'man, Phys. Rev. Lett. **95**, 057002 (2005).
- [32] B. Z. Spivak and F. Zhou, Phys. Rev. Lett. **74**, 2800 (1995).
- [33] V. M. Galitskii and A. I. Larkin, Phys. Rev. Lett. **87**, 087001 (2001).
- [34] M. V. Feigel'man, A. I. Larkin and M. A. Skvortsov, Phys. Rev. Lett. **86**, 1869 (2001); Uspekhi Fiz. Nauk **171**, 76 (2001).
- [35] A.A. Abrikosov and L.P. Gorkov, Sov. Phys. JETP **8**, (1958) 1090.
- [36] P.W. Anderson, J.Phys.Chem.Solids **11**, 26 (1959).
- [37] K. A. Matveev and A. I. Larkin, Phys. Rev. Lett. **78**, 3749 (1997).
- [38] B. Srinivasan, G. Benenti and D. L. Shepelyansky, Phys. Rev. B **66**, 172506 (2002); J. Lages and D. L. Shepelyansky Phys. Rev. B **64**, 094502 (2001).
- [39] C. Christiansen, L. M. Hernandez and A. M. Goldman, Phys. Rev. Lett. **88**, 037004 (2002); K. H. Sarma, B. Tan, K. A. Parendo and A. M. Goldman, arXiv:0704.0765
- [40] T. I. Baturina, A. Bilusic, A. Yu. Mironov, V. M. Vinokur, M. R. Baklanov and C. Strunk, Physics C **468**, 316 (2007).
- [41] S. P. Chockalingam, M. Chand, A. Kamlapure, J. Jesudasan, A. Mishra, V. Tripathi and P. Raychaudhuri, Phys. Rev. B **79**, 094509 (2009).
- [42] B. Sacepe, PhD Thesis, CEA Grenoble (2007).

- [43] B. Sacepe, C. Chapelier, T. I. Baturina, V. M. Vinokur, M. R. Baklanov, and M. Sanquer Phys. Rev. Lett. **101**, 157006 (2008).
- [44] G. Sambandamurthy, L. W. Engel, A. Johansson, and D. Shahar, Phys. Rev. Lett. **92**, 107005 (2004).
- [45] T. I. Baturina, A. Yu. Mironov, V. M. Vinokur and C. Strunk, Phys. Rev. Lett. **99**, 257003 (2007).
- [46] D. Shahar and Z. Ovadyahu, Phys. Rev. B **46**, 10917 (1992).
- [47] Z. Ovadyahu, private communication.
- [48] V. I. Anisimov, private communication.
- [49] T. I. Baturina, invited talks at Moriond Conference (2008) and NanoPiter Conference (2008).
- [50] E. Serret, Ph.D. Thesis, CNRS, Grenoble (2002).
- [51] W. Wu and E. Bielejec, cond-mat/0511121.
- [52] G. Sambandamurthy, L. W. Engel, A. Johansson, E. Peled, and D. Shahar, Phys. Rev. Lett. **94**, 017003 (2005).
- [53] M. A. Steiner and A. Kapitulnik, Physica C **422**, 16 (2005)
- [54] T. I. Baturina, Islamov D.R., Bentner J., Strunk C., Baklanov M.R., Satta A., JETP Letters **79** 337 (2004).
- [55] T. I. Baturina C. Strunk, M. R. Baklanov and A. Satta, Phys. Rev. Lett. **98**, 127003 (2007).
- [56] E. Bielejec, J. Ruan and W. Wu, Phys. Rev. Lett. **87**, 036801 (2001).
- [57] V. Yu. Butko and P. W. Adams, Nature, **409**, 161 (2001).
- [58] H. Q. Nguyen, S. M. Hollen, M. D. Stewart, Jr., J. Shainline, A. Yin, J. M. Xu and J. M. Valles, Phys. Rev. Lett. **103**, 157001 (2009)
- [59] E. Bielejec, J. Ruan and W. Wu, Phys. Rev. B **63**, 100502(R) (2001).
- [60] Y.M. Xiong, A.B. Karki, D.P. Young and P. W. Adams, arXiv:0901.1873.
- [61] V. F. Gantmakher, Golubkov M.V., Dolgoplov V.T., Tsydynzhapov G.E., Shashkin A.A., JETP Letters **68**, 363 (1998); V. F. Gantmakher, Physics-Uspekhi **41**, 214 (1998).
- [62] M. A. Steiner, N. P. Breznay and A. Kapitulnik Phys. Rev. B **77**, 212501 (2008).
- [63] Y. Dubi, Y. Meir and Y. Avishai, Phys. Rev. B **73**, 054509 (2006).
- [64] B. L. Altshuler, V. E. Kravtsov, I. V. Lerner and I. L. Aleiner, Phys. Rev. Lett. **102**, 176802 (2009).
- [65] M. Ovadia, B. Sacepe and D. Shahar, Phys. Rev. Lett. **102**, 176802 (2009).
- [66] F. Ladieu, M. Sanquer and J. P. Bouchaud, Phys. Rev. B **53**, 973 (1996).
- [67] A. I. Larkin, ZhETF **48**, 232 (1965) [Sov.Phys.JETP **21**, 153 (1965)].
- [68] M. D. Stewart Jr, Aijun Yin, J. M. Xu, J. M. Valles Jr, *Science*, **318**, 1273 (2007); arXiv:0712.1076
- [69] M. V. Feigel'man, L. B. Ioffe, V. E. Kravtsov and E. A. Yuzbashyan, Phys. Rev. Lett. **98**, 027001 (2007).
- [70] P. W. Anderson, Phys. Rev. **112**, 1900 (1958).
- [71] J. T. Chalker, Physica A, **167**, 253 (1990).
- [72] V. E. Kravtsov and K. A. Muttalib, Phys. Rev. Lett., **79** 1913 (1997).
- [73] A. D. Mirlin, Phys. Rep., **326**, 259 (2000).
- [74] Jan von Delft, Annalen der Physik (Leipzig), **10**, 219-276 (2001); cond-mat/0101021.
- [75] I. L. Kurland, I. L. Aleiner and B. L. Altshuler, Phys. Rev. B **62**, 14886 (2000).
- [76] A. MacKinnon. J.Phys.C **6**, 2511 (1994); T. Ohtsuki, K. Slevin and T. Kawarabayashi, Ann. Phys. (Leipzig), **8**, 655 (1999).
- [77] E. Cuevas and V. E. Kravtsov, Phys. Rev. B **76**, 235119 (2007).
- [78] F. Evers and A. D. Mirlin, *Anderson transitions*, Rev. Mod. Phys. **80**, 1355 (2008); arXiv:0707.4378.
- [79] A. Rodriguez, L. J. Vasquez and R. A. Roemer, private communication
- [80] L. B. Ioffe, I. R. Sagdeev and V. M. Vinokur, J. Phys. C, Solid State Phys. **18**, L641 (1985).
- [81] A. Mildenberger, F. Evers and A. D. Mirlin, Phys. Rev. B **66**, 033109 (2002).
- [82] A. D. Mirlin and Yan V. Fyodorov, Phys. Rev. B **56**, 13393 (1997).
- [83] Z. Ovadyahu and D. Shahar, private communications.
- [84] Z. Ovadyahu, J. Phys. C **19**, 5187 (1986)
- [85] L. B. Ioffe and M. V. Feigel'man, ZhETF **89**, 654 (1985) [Sov.Phys.JETP **62**, 376 (1985)]
- [86] Vik. S. Dotsenko, M. V. Feigel'man, and L. B. Ioffe, Sov. Sci. Rev. **15**, edited by I. M. Khalatnikov, Harwood Publishers, 1990.
- [87] L. B. Ioffe and A. I. Larkin, ZhETF **81**, 707 (1981) [Sov. Phys. JETP **54**, 378 (1981)].
- [88] P. De Gennes, "Superconductivity of metals and alloys", Westview Press (1999).
- [89] A. I. Larkin and A. A. Varlamov, in *Theory of Fluctuations in Superconductors*, Oxford University Press, New York, 2002.



- [90] A. I. Larkin and D. E. Khmel'nitsky, ZhETF **58**, 1789 (1970).
- [91] A. M. Tsvelik and M. V. Feigel'man, ZhETF **76**, 2249 (1979).
- [92] A. D. Mirlin, Y. V. Fyodorov, F. M. Dittes et al. Phys.Rev.E **54**, 3221 (1996).
- [93] L. B. Ioffe and M. Mézard, cond-mat arXiv:0909.2263 (2009).
- [94] M. V. Feigel'man, L. B. Ioffe and M. Mézard, to be published.
- [95] B. Sacepe, T. Dubouchet, C. Chapelier, M. Sanquer, M. Ovadia, D. Shahar, M. V. Feigel'man and L. B. Ioffe, to be published.
- [96] P. Nozieres and C. T. De Dominicis, Phys.Rev. **178**, 1097 (1969).
- [97] G. Deutscher, Rev. Mod. Phys. **77**, 109 (2005).
- [98] G. E. Blonder, M. Tinkham and T. M. Klapwijk, Phys. Rev. B **25**, 4515 (1982).
- [99] E. V. Bezuglyi, E. N. Bratus', V. S. Shumeiko, G. Wendin and H. Takayanagi, Phys. Rev. B **62**, 14439 (2000).
- [100] Y. Tanaka, A. A. Golubov, and S. Kashiwaya, Phys. Rev. B **68**, 054513 (2003).
- [101] T. Dubouchet, C. Chapelier, M. Sanquer, B. Sacepe, M. Ovadia and D. Shahar, to be published.
- [102] D. Basov, T. Timusk, B. Dabrowski and J.D.Jorgenson, Phys. Rev. B **50**, 3511 (1994).
- [103] L. B. Ioffe and A. J. Millis, *Science*, **285**, 1241 (1999).
- [104] J.K. Chin, D.E. Miller, Y. Liu, C. Stan, W. Setiawan, C. Sanner, K. Xu, and W. Ketterle, *Nature*, **443**, 961 (2006).
- [105] J. Billy, V. Josse, Z. Zuo, A. Bernard, B. Hambrecht, P. Lugan, D. Clament, L. Sanchez-Palencia, P. Bouyer and A. Aspect, *Nature* **453**, 891 (2008); G. Roati, C. D'Errico, L. Fallani, M. Fattori, C. Fort, M. Zaccanti, G. Modugno, M. Modugno and M. Inguscio *Nature* **453**, 895 (2008).
- [106] M. Mueller, cond-mat arXiv:0909.2260 (2009).
- [107] D. Kowal and Z. Ovadyahu, Physica C **468**, 322 (2008).
- [108] Z. A. Xu, N. P. Ong, Y. Wang, T. Kakeshita and S. Uchida, *Nature*, **406**, 486 (2000); Phys. Rev. Lett. **88**, 257003 (2002).
- [109] P. Spathis, H. Aubin, A. Pourret and K. Behnia, Europhys. Lett. **83**, 57005 (2008); A. Pourret, P. Spathis, H. Aubin and K. Behnia, arXiv:0902.2732
- [110] M. N. Serbin, M. A. Skvortsov, A. A. Varlamov and V. M. Galitskii, Phys. Rev. Lett. **102**, 067001 (2009).
- [111] K. Michaeli and A. M. Finkelstein, Europhys. Lett. **86**, 27007 (2009); arXiv:0912.4219.
- [112] A. Pourret, H. Aubin, J. Lesueur, C. A. Marrache-Kikuchi, L. Berge, L. Dumoulin and K. Behnia, *Nature Physics*, **2**, 683 (2006); Phys. Rev. B **76**, 214504 (2007).
- [113] D. Podolsky, S. Raghu and A. Vishwanath, Phys. Rev. Lett. **99**, 117004 (2007).
- [114] M. A. Steiner, G. Bobinger and A. Kapitulnik, Phys. Rev. Lett. **94**, 107008 (2005).
- [115] T. Timusk and B. Statt, Rep. Prog. Phys. **62**, 61 (1999)
- [116] C. Howald, P. Fournier and A. Kapitulnik, Phys. Rev. B **64**, 100504(R) (2001)
- [117] S. H. Pan, J. P. O'Neal, R. L. Badzey et al, *Nature* **413**, 282 (2001).
- [118] K. M. Lang, V. Madhavan, J. E. Hoffman, E. W. Hudson, H. Eisaki, S. Uchida and J. C. Davis, *Nature*, **415**, 412 (2002).
- [119] K. K. Gomes, A. N. Pasupathy, A. Pushp, S. Ono, Y. Ando and A Yazdani, *Nature* **447**, 569 (2007).
- [120] J. Corson, R. Mallozzi, J. Orenstein, J. N. Eckstein and I. Bozovic, *Nature* **398**, 221 (1999).
- [121] Y. Wang, L. Li and N. P. Ong, Phys. Rev. B **73**, 024510 (2006).
- [122] O. Yuli, I. Asulin, Y. Kalcheim, G. Koren, and O. Millo Phys. Rev. Lett. **103**, 197003 (2009).
- [123] V. B. Geshkenbein, L. B. Ioffe and A. I. Larkin, Phys. Rev. B **55**, 3173 (1997).
- [124] V. Galitski and S. Sachdev, Phys. Rev. Lett. **79**, 134512 (2009)